Applied Physics Reviews

Materials for optical fiber lasers: A review

Cite as: Appl. Phys. Rev. **5**, 041301 (2018); https://doi.org/10.1063/1.5048410
Submitted: 13 July 2018 • Accepted: 12 August 2018 • Published Online: 17 October 2018

P. D. Dragic, M. Cavillon and J. Ballato

APPLIED PHYSICS REVIEWS

Materials for optical fiber lasers: A review

P. D. Dragic,[1,a)] M. Cavillon,[2,b)] and J. Ballato[2]
[1]*Department of Electrical and Computer Engineering, University of Illinois at Urbana-Champaign, Urbana, Illinois 61801, USA*
[2]*Department of Materials Science and Engineering, Clemson University, Clemson, South Carolina 29631, USA*

(Received 13 July 2018; accepted 12 August 2018; published online 17 October 2018)

Over the past two decades, fiber laser technologies have matured to such an extent that they have captured a large portion of the commercial laser marketplace. Yet, there still is a seemingly unquenchable thirst for ever greater optical power to levels where certain deleterious light-matter interactions that limit continued power scaling become significant. In the past decade or so, the industry has focused mainly on waveguide engineering to overcome many of these hurdles. However, there is an emerging body of work emphasizing the enabling role of the material. In an effort to underpin these developments, this paper reviews the relevance of the material in high power fiber laser technologies. As the durable material-of-choice for the application, the discussion will mainly be limited to silicate host glasses. The discussion presented herein follows an outward path, starting with the trivalent rare earth ions and their spectroscopic properties. The ion then is placed into a host, whose impact on the spectroscopy is reviewed. Finally, adverse interactions between the laser lightwave and the host are discussed, and novel composition glass fiber design and fabrication methodologies are presented. With deference to the symbiosis required between material and waveguide engineering in active fiber development, this review will emphasize the former. Specifically, where appropriate, materials-based paths to the enhancement of laser performance will be underscored. https://doi.org/10.1063/1.5048410

TABLE OF CONTENTS

[a)]p-dragic@illinois.edu
[b)]Present address: Université Paris Sud, Orsay 91405, France.

I. INTRODUCTION

As of the writing of this review, fiber lasers exceeding 100 kW of optical power are commercially available.[1] In homage to the importance of fiber lasers, there are a number of excellent reviews that have emerged over the past decade or so.[2–9] Applications for them are wide-ranging, from weapons systems[10] to down-hole drilling,[11] and from medicine[12] to lidar.[13] Well-understood to those in the field is that continuous-wave (CW) high power fiber lasers serve mainly as brightness (power density) converters. Low brightness pump light from groups of semiconductor diode lasers may be coupled into the cladding region of an active fiber. Over some length of fiber, this pump light then is absorbed and converted to signal power propagating in the much higher brightness core. Coupled with high efficiency, this has enabled a plethora of manufacturing applications.[14] Fiber lasers can efficiently be pulsed, and for reasons unique to the amorphous host, enable gain at somewhat arbitrary (and well-controlled) wavelengths, as may be required, for example, in spectroscopic lidar systems.[13,15,16] That being said, it is not necessarily the goal of this paper to review fiber laser applications, configurations, or requirements. The reader is referred to the aforementioned review papers for more details.

Clearly, central to the growth of fiber laser power is the continued advancement of high brightness pump technology.[17–19] However, the scaling of optical power also has been influenced by a variety of other factors. For instance, the development of novel fiber architectures with enhanced mode areas has played a crucial role. In particular, such fibers can help to circumvent certain power-limiting interactions between the lightwave and the host. In many instances, one or more such deleterious interactions limit the scalability of a particular system. As reviewed herein, these can be related to, for example, nonlinear propagation effects, or even to structural changes in the glass or to the rare earth dopant. Common to all of them, however, is that the host material is complicit in, nay the leading perpetrator of, the limitation. To summarize, the rare earth is doped into a host material. The above-mentioned host then influences the spectroscopic properties of the dopant, such as upper state lifetime or emission and absorption cross sections. However, in a tragic irony, as the light from the rare earth becomes more and more intense, the host supporting it can no longer handle the power; the rare earth ion never sensing that something imminent is about to cause the host to yield.

Ultimately, many of these power-related issues are those linked to the material and its various properties. With this avowal, the purpose of this paper is to review and to reinforce the relevance of the material in high power fiber laser technologies. The discussion is limited mainly to silicate glasses as the refractory and high-quality host-of-choice for most applications. Historically, the development of optical fiber has been done with close collaboration between both waveguide and material engineering.[20] Indeed, in the past decade or so, the focus seems to have leaned towards novel waveguide designs. However, there is an emerging body of work emphasizing the enabling and fundamental role of the material. It is the purpose of this paper to buttress the importance of the latter, but with the acknowledgement that this does not necessarily come in lieu of the former. That being said, this review is meant to be approachable by those only somewhat familiar with the field or by graduate students starting out in the area.

The remainder of this paper is organized as follows. Fabrication of the active medium will be discussed in Sec. II, with a focus on the more conventional chemical vapor deposition methods. From this point, the active medium is treated progressively, beginning with the active ion and light generation, and ending with deleterious light matter interactions involving the host material. The discussion herein largely is limited to what (at least) these authors perceive to be the most common of the rare earth elements encountered in fiber laser applications: Yb^{3+}, Tm^{3+}, and Er^{3+}. Section III of this paper is dedicated to the origins of the excited states (energy level diagrams) of the rare earth elements. Then, in Sec. IV, the rare earth ions are placed into a host and the influences of the environment on the spectroscopic properties are reviewed. After briefly describing the optical waveguide, several material-related deleterious effects are presented in Sec. V. In the spirit of the theme of this review, a semi-empirical model is included that can be utilized to tailor the glass host to achieve specific desired outcomes, such as the suppression of nonlinear effects. The paper concludes with future perspectives, with a major emphasis on the fabrication of fibers with less conventional compositions.

II. OPTICAL FIBER FABRICATION

This section focuses on the fabrication of optical fibers. Though a remarkably broad and rich number of glass-forming compounds exist and have been made into fibers, comments here will be limited to silica-based optical fibers used for practical telecommunications and laser or amplifier applications.

A. Preform formation

All silica-based optical fibers of practical importance are drawn from glass fabricated using a chemical vapor deposition process. These methods are commercially known as either Outside Vapor Deposition (OVD), Modified Chemical Vapor Deposition (MCVD), Vapor Axial Deposition (VAD), or Plasma Enhanced Chemical Vapor Deposition (PECVD); all variations on a similar chemical scheme.

Each involves the high temperature oxidation of volatile halide compounds, thermophoretic deposition of glass particulate soot, and subsequent sintering and consolidation into a solid glass preform later drawn into fiber. The foundational reaction is $SiCl_4 + O_2 \rightarrow SiO_2 + 2Cl_2$. Of critical importance to the performance of the fiber is the fact that $SiCl_4$ exhibits a vapor pressure that is approximately 12 orders of magnitude higher than that of the most detrimental impurities; e.g., transition metal compounds like Fe_2Cl_6. This directly drives the remarkable purity, hence low intrinsic losses, of CVD-derived silica optical fibers.

In order to obtain waveguiding optical fibers, dopants must be added to the silica in order to raise or lower the

refractive index. Dopants also can be used to modify thermal and thermomechanical properties. The primary oxide compounds employed in CVD-derived optical fibers are GeO_2, P_2O_5, B_2O_3, and Al_2O_3. Fluorine, typically either as SF_6 or SiF_4, also is employed. Lanthanides (e.g., Er_2O_3, Yb_2O_3) are added for active fibers. Relative to the base SiO_2, GeO_2 dopants raise the linear and nonlinear refractive index and enhances photosensitivity and Raman gain; Al_2O_3 raises the linear and nonlinear refractive index and enhances the spectroscopic properties of lanthanide dopants up to their concentration quenching limit; P_2O_5 raises the refractive index and reduces viscosity, thermo-optic coefficient (TOC), and photo-darkening; B_2O_3 reduces the refractive index and thermo-optic coefficient; and F reduces both the linear and nonlinear refractive index and viscosity. Each of Al_2O_3, P_2O_5, B_2O_3, and F increase the thermal expansion coefficient when added to silica.

With the exception of Al_2O_3,[21] B_2O_3[22,23] and the lanthanide oxides,[24] there is a complete solid solution between SiO_2 and GeO_2[25] and P_2O_5,[26] such that glass stability (i.e., liquid-liquid or solid-solid immiscibility) is not such an issue and compositions generally are defined by the desired refractive index profile, stress state (via thermal expansion mismatch), and viscosity at the processing conditions. Additionally, while the SiO_2, GeO_2, and P_2O_5 compounds are formed through vapor phase reactions ($SiCl_4$, $GeCl_4$, and $POCl_3$), the B_2O_3 and F typically are added directly from gaseous precursors (SiF_4 and BCl_3), whereas the Al_2O_3 and lanthanide oxides typically are added via solution doping of dissolved salts (e.g., $AlCl_3$, $YbCl_3$, and $ErCl_3$). For all intents and purposes, it is these vapor phase transport and reactivity that give such processes their control over refractive index profiles and the derived glasses their very low attenuation values.

B. Compositional limitations in vapor deposition

Glass formation is dependent on chemical composition, scale (size/volume) of the sample, and its thermal and process history. Since each practitioner of the principal vapor deposition processes inevitably has a different purpose for their fiber, general trends and glass forming ranges are discussed herein and supported by the literature where available; though the Reader should not take such compositional limits as strict bounds on glass formation or allowable preform compositional ranges. Additionally, the advent and remarkable progress in microstructured and photonic crystal designs over the past decade mean that both material and geometric approaches can be symbiotically employed to obtain the desired performance specifications for a given application. Indeed, while this review advocates a unified materials approach to mitigating nonlinearities (to be discussed later), given the efficacy of the mitigation and the simplicity of the resultant fiber structure, a combined approach (e.g., intrinsically low nonlinearity glasses in a microstructured design) offers tantalizing benefits for a broad range of novel uses.

In addition to the conventional dopants noted above, a wide variety of less common additives to silica have been examined. Table I provides a compilation of vapor-deposited silicate compositional ranges for the stated dopant along with selected comments and the associated references.

While considerable time was spent reviewing the literature (publications and patents), it is foolhardy to assume that Table I is complete. For example, a patent search with terms "optical fiber," "MCVD," and "composition" returned nearly 2000 results.[49] Accordingly, it is offered as a best-effort analysis of additives thought potentially useful (or, at least, interesting) and compositional maxima reasonably

TABLE I. Best effort compilation of maximum dopant concentrations into silica using vapor deposition methods.

Dopant into SiO_2	Concentration (mol.%)				
GeO_2			97[27]		
Al_2O_3	9.5[28]	20 ($Al_2O_3 + P_2O_5$)[29]	6[30]	10[31,32]	
P_2O_5	10[29]				0.6 SnO_2 + 9 P_2O_5[33]
B_2O_3		17[34]			
Sesquioxides (other than B_2O_3, Al_2O_3, or rare-earth oxides, RE_2O_3)	20 Ga_2O_3 + 10 Ta_2O_5[35]	3 Ga_2O_3 + 1.4 BaO[36]		5[a] Ga_2O_3[37]	
Pentoxides (other than P_2O_5)					
RE_2O_3	11[38]				
Alkali oxides (AO)	>20 ppm[39]		<7[40]	0.2 AO + 0.2 AE[41,c]	
Alkaline earth (AE) oxides	<2 (BaO)[42]				
ZrO_2		>5[43]			
TiO_2		20[44,a]			
Transition metals		0.1[45b]			
Ta_2O_5		1.5[46]			
SnO_2		0.15[47]			
Sb_2O_5		2.8[48]			

[a]Note that these compositions are given in weight percent.
[b]Not a compositional limit; used for spectroscopic purposes.
[c]Estimated range based on extrema provided in Ref. 41. The actual ranges provided in the patent are "$3 < (n_1M+n_2H)/H < 20$," preferably <10, where n_1 and n_2 are the valences of the modifier and the homogenizer, respectively, and M and H are the concentration, in mol. %, of modifier and homogenizer, respectively, with modifiers chosen from Li, Na, K, Rb, Cs, Be, Mg, Ca, Sr, and Ba, and the 4f-type rare earths and homogenizers chosen from B, Al, Ga, In, P, As, and Sb.

permissible using vapor deposition methods possibly coupled with, for example, solution doping.

Further, by way of a few caveats, the data in Table I represent only (i) compositions given in peer-reviewed journal articles or issued patents, (ii) on all-glass optical fibers (i.e., not nanophase separated or glass-ceramics; though these will be discussed later), and (iii) without regard to a specific attenuation level.

C. Optical fiber formation

Because strength is of paramount importance for both telecommunication and laser/amplifier applications, the surface of the fiber cannot be contacted. Accordingly, the silica based preforms described above are formed into cylindrical (core/clad) optical fibers using a draw process on a vertical draw tower.

The preform is lowered into a high temperature, inert atmosphere furnace. The exact temperature for the draw will depend on the preform dimensions and desired draw tension, which helps maintain diameter control as well as slightly modifying the index or index profile. For silica-based preforms, the fiber draw temperature typically corresponds to a glass viscosity of about 10^6 poise (10^5 Pa·s), which is between about 1925 °C and 2000 °C.

Initially, the temperature is raised above the draw temperature in order to hasten softening of the preform and facilitates the formation of a "drop" or "gob" that defines the transition from bulk preform into (optical) fiber. The fiber then is pulled through a series of other instruments disposed on the draw tower to measure the bare and coated fiber diameters, apply and cure polymer coatings, ensure proper concentricity of the coating around the glass fiber, provide the tension for pulling the fiber, and ultimately collect the fiber onto a spool.

In order to preserve the near-intrinsic strength of the fiber, one or more (often two) polymer coatings are applied on-line once the fiber has sufficiently cooled. The first polymer layer, called the primary coating, is relatively soft and relieves some of the strain placed on the fiber during use. The second polymer layer, called the secondary coating, is harder and provides abrasion resistance.

The coatings are applied as liquids to the fiber during the draw using dies that do not directly contact the fiber surface. The coatings then are cured using on-line ultraviolet lamps. One variation on this theme includes double-clad laser fibers (more details later), which are constructed from an active glass core, passive glass clad (the first cladding), and a low refractive index polymer layer (the second cladding), which guides the pump light in the cladding.

Additional detail on CVD preform fabrication processes as well as fiber drawing is given in Refs. 50 and 51.

D. Other characteristics of drawn fiber

The process of drawing a preform into fiber can introduce changes to glass characteristics from those in the preform state. Two such examples are (1) frozen-in stresses and strains that may affect changes to the refractive index or other material properties, and (2) the formation of optically active (i.e., light absorbing or emitting) defects. Case #1 is treated in an excellent review by Yablon,[52] wherein such stresses (mechanical deformation) or strains (force per unit area) are classified as being either elastic or inelastic. Elastic stresses and strains are defined to be those resulting from mechanical equilibration among differing regions of the fiber, while inelastic ones are those frozen into the glass matrix. The former can arise from (a) thermal expansion and glass transition temperature (T_g) differences in the various doped (or undoped) regions of the fiber or (b) differences in the viscosities of the various regions. In the case of (a), for instance, consider a fiber being drawn that is in the cooling (quenching) phase, and that the cladding has a T_g that is higher than that of the core. The continued cooling of the core from the cladding T_g, and its concomitant contraction, will leave the cladding under tension.[53] In the case of (b),[54] regions of the fiber with higher viscosity will cool first during draw, rendering these regions under strain as the drawing tension remains applied. Residual stresses, therefore, are tensile in regions of relatively higher viscosity. This, in equilibrium (i.e., in the final drawn fiber), therefore, imparts compressive stress to the lower-viscosity regions in the drawn fiber.[55] Both processes, (a) and (b), ultimately result in changes in the refractive index profile.[56] Depending on the application, such stresses can therefore significantly impact the waveguiding characteristics of an optical fiber.[57]

Turning now to defects, a pristine pure silica glass will exhibit a network of interconnected SiO_4 tetrahedra. The process of fiber draw can lead to the cleavage of bonds or reforming of the network structure in ways rendering point defects (most generally "departures" from the continuous network of SiO_4 tetrahedra) that can act as color centers.[58–61] Skuja[62] provides a very detailed review of a number of oxygen deficiency- and excess-related defects. Non-bridging oxygen hole centers (NBOHCs)[63–65] are one type of color center, represented chemically as [≡ Si – O •]. Here, "≡" represents bonding to three oxygens and "•" represents an unpaired electron, i.e., a dangling bond. These centers are highly localized, are optically active, and have luminescence near 1.9 eV (thus otherwise known as *R*-centers or red centers), and absorption near 2.0 eV. The oxygen deficiency center (ODC), with absorption bands in the UV, is another type of point defect, two of which appear to be dominant.[62,66,67] The first of these, ODC(I), consists of an oxygen vacancy lying between two bonded silicon atoms and is represented chemically as [≡ Si – Si ≡]. The ODC(I) also is known as the "relaxed vacancy." The other prominent oxygen vacancy defect, ODC (II), has two plausible configurations.[62] One is the silylene-type defect (represented as [:Si =]) in which two oxygen vacancies reside at a single silicon atom, whereas the second is represented as an oxygen vacancy on two unbounded Si sites ([≡ Si…Si ≡] or the "unrelaxed" vacancy). While these ODCs are known to result in the photosensitivity of the germanosilicate glasses used in fiber Bragg grating fabrication,[62,66] they also may play a role in the photodarkening of high-power fiber lasers (to be discussed in more detail in Sec. V D). The reader is referred to

Skuja[62] for the basic spectroscopy and chemical nature of these and other point defects.

III. THE ACTIVE ION

A. Free ions

The lanthanides (more specifically trivalent lanthanides, Ln^{3+}, for the purposes of this paper) can be found on the periodic table with atomic numbers ranging from 57 (lanthanum) to 71 (lutetium) and are tremendously important in a number of applications due to their ability to produce light via 4f→4f transitions (excluding La^{3+} and Lu^{3+}). While there are a number of very good reviews detailing these applications,[68–74] the reader is reminded that the focus in this review is on materials for high power fiber lasers. Continuing, the Ln^{3+} ions are characterized by a partly filled 4f subshell, having the electronic configuration $4f^X5s^25p^6$, where X = 0 for La and increasing along the lanthanide series (with the 4f subshell being filled for Lu^{3+}).

This notation differs somewhat from the usual noble gas shorthand notation, which for neutral Yb, for example, would be $[Xe]4f^{14}6s^2$. Ionization preferentially removes both 6s electrons and one 4f electron rendering $[Xe]4f^{13}$ (triply ionized Yb^{3+}). The alternate ($4f^X5s^25p^6$) notation reflects the imperfect screening by the 4f electrons from the positively charged nucleus. This imperfect screening leads to an increasing effective nuclear charge, eZ_{eff}, (e is the electron charge, 1.6×10^{-19} C) as one traverses the lanthanide series towards Lu. An increased eZ_{eff} causes the 4f subshell to become more tightly bound, with electronic wavefunctions which, therefore, can lie *within* the 5s and 5p subshells.[75,76] This also leads to the observed decrease in atomic radii with the increase in the atomic number, well-known as the "lanthanide contraction."[77–81] The n = 5 subshells, in turn, shield the 4f subshell from the local environment, resulting in energy level diagrams that appear to be free ion-like and relatively insensitive to the host.[82,83]

The Hamiltonian describing the free ion 4f energy levels is given by[82,83]

$$H = -\frac{\hbar^2}{2m}\sum_{i=1}^{N}\Delta_i - \sum_{i=1}^{N}\frac{Z_{eff}e^2}{r_i} + \sum_{i<j}^{N}\frac{e^2}{r_{ij}} + \sum_{i=1}^{N}\zeta(r_i)\mathbf{s}_i\bullet\mathbf{l}_i$$
$$= H_{KE} + H_{N-4f} + H_{4fi-4fj} + H_{S-O}, \quad (1)$$

where N is the number of 4f electrons, m is the electron mass, r is the position of electron i relative to the nucleus, and Δ is the Laplacian operator. The first two terms are simply the kinetic energy of the 4f electrons (H_{KE}), and their Coulombic interactions with the nucleus ($H_{N\text{-}4f}$), respectively. These terms typically are negligible compared with the last two, which are the Coulombic interactions between the different 4f electrons ($H_{4fi\text{-}4fj}$) ($r_{ij} = |\mathbf{r}_j - \mathbf{r}_i|$) and the spin-orbit interactions ($H_{S\text{-}O}$), respectively. The spin-orbit coupling function is given by[82]

$$\zeta(r_i) = \frac{\hbar^2}{2m^2c^2r_i}\frac{dU(r_i)}{dr_i}, \quad (2)$$

where $U(r_i)$ is the potential in which the 4f electron i is moving. The case where $H_{4fi\text{-}4fj} \gg H_{S\text{-}O}$ is known as Russell-Saunders (LS) coupling,[82] which usually is adequate for calculations of the eigenfunctions of an isolated many-electron atom.[84] Methods to calculate the eigenfunctions involve using the Central Field Approximation. As Wybourne[83] points out, the key aspect of this approximation is that "each electron is assumed to move independently in the field of the nucleus and a central field made up of the spherically averaged potential field of each of the other electrons." In this way, each electron moves through a spherically symmetric potential. The solutions to the Schrödinger equation, therefore, are formed by a basis set of functions separable in the radial and angular directions.[82,83] More details can be found in a number of publications on the topic, as such calculations are beyond the scope of this review.[82,83,85,86]

The hierarchy in terms of the magnitude of energy splitting is 4f → Coulomb → Spin-Orbit, as illustrated in Fig. 1. In accordance with LS coupling, the Ln^{3+} energy levels typically are identified by three principle quantum numbers: L, S, and J. L gives the total orbital angular momentum, S the total spin angular momentum, and J the total angular

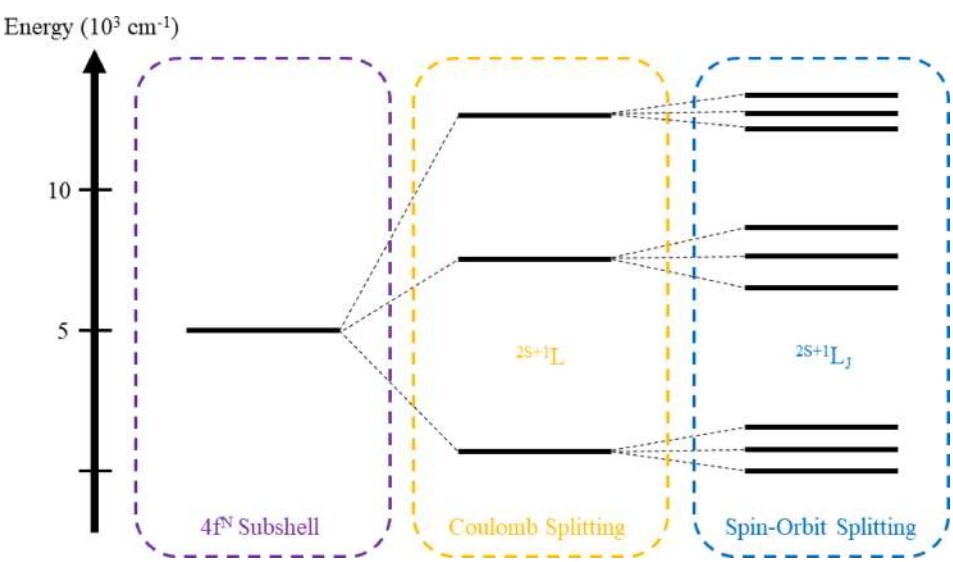

FIG. 1. Splitting hierarchy for the free Ln^{3+} ions. The $4f^N$ subshell splitting is strongest with the Coulombic interaction ($H_{4fi\text{-}4fj}$), and with the spin-orbit splitting ($H_{S\text{-}O}$) somewhat lesser in magnitude. An energy scale is provided which gives approximate magnitudes of the splitting.

TABLE II. Spin and orbital angular momentum chart for the electrons populating the 4f subshell in Yb^{3+} ground state ($^2F_{7/2}$).

m_l	−3	−2	−1	0	1	2	3
$^2F_{7/2}$	↑↓	↑↓	↑↓	↑↓	↑↓	↑↓	↑

momentum (taking on values between $|L-S|$ and $L+S$ in unit steps). The degeneracy of the LS splitting is given by $2J+1$, and fine splitting of this degeneracy will be discussed in Sec. IV. As an illustrative example, the Yb^{3+} ion ground state *term symbol* is determined in this context. The orbital angular momentum quantum number, l, takes on a value of 3 for the 4f subshell. Hence, the magnetic quantum number, m_l, can range from −3 to +3. A chart exhibiting this range of values is constructed and is shown in Table II. Of course, an electron may be spin up or spin down ($m_s=+1/2$ or $m_s=-1/2$, respectively). Hund's rules and the Pauli exclusion principle then can be invoked[87] to populate the orbitals. Hund's rules state that the lowest energy term (1) maximizes the spin multiplicity (2S + 1), (2) maximizes L, and (3) where, for a less than half filled shell, $J=|L-S|$ and $J=L+S$ for shells greater than half-full (with all possible excited values of J lying between those two endpoints in unit steps). Continuing with Yb^{3+}, since it has 13 electrons in the 4f subshell, Table II is populated from $m_l=-3$ to +3 with spin up, then with spin down starting again from $m_l=-3$. This leaves one unpaired spin at $m_l=+3$. The total spin, S, therefore, is 1/2 and the spin multiplicity is 2. Summing the m_l values for the electrons, L = 3 (L always is taken to be positive). Finally, since the Yb^{3+} subshell is more than half-full, $J=L+S=3+1/2=7/2$ for the ground state. The conventional notation for a term is $^{(2S+1)}L_J$. The L's are designated by letters S, P, D, F, G, H, I, K… corresponding to L = 0, 1, 2, 3, 4, 5, 6, 7… and therefore the ground state term is $^2F_{7/2}$. Since J can take on the values 7/2 ($L+S$) and 5/2 ($|L-S|$), the latter must be the excited state, therefore having the term $^2F_{5/2}$. Table III summarizes the ground state for the Ln^{3+} ions and a general energy level (or "Dieke") diagram is provided in Fig. 2.[88]

B. The "big-three"

In this section, some of the basic spectroscopic features of arguably the three most commonly used trivalent lanthanides are outlined. These are Yb^{3+}, Er^{3+}, and Tm^{3+} and Dieke diagrams are provided in Fig. 3, which include some of the common radiative transitions in silicate glasses. Common pumping wavelengths are shown as dashed lines in the figure.

1. Yb^{3+}

As with trivalent cerium,[88–90] the 4f Dieke diagram for Yb^{3+} is characterized by a two-level system. Absorption and emission in this ion occurs at a wavelength near 1.0 μm. In principle, this configuration should offer no gain (as a two-level system), and, as such, would not permit lasing. However, as will be discussed in Sec. IV, the degeneracy of the LS splitting is broken via interaction with the local environment (i.e., the host material). Since Yb^{3+} has half-integer spin, the $^2F_{5/2}$ and $^2F_{7/2}$ energy levels are Kramer's doublets, and therefore the degeneracy becomes $(2J+1)/2$.[91] Hence, the $^2F_{5/2}$ and $^2F_{7/2}$ levels are split into 3 and 4 sublevels (known as manifolds), respectively, with $3\times4=12$ transitions possible. The maximum splitting of the energy levels can be generalized using Kramer's Theorem, taking on values of 2J + 1 and J + 1/2 for ions with even and odd numbers of 4f electrons, respectively.[92] Tm^{3+} therefore is governed by the former, while Er^{3+} by the latter.

2. Tm^{3+}

The energy level diagram for Tm^{3+} is considerably more complex than it is for Yb^{3+}. In silicate glasses, 2.0 μm thulium lasers[93–96] ($^3F_4 \rightarrow {}^3H_6$) have found their way into a number of commercial applications. It should be noted that silicate-based glasses usually are sufficiently transparent at this wavelength[97] such that laser efficiency is not compromised in the fiber lengths typical of these lasers. Since there are a number of energy levels available, multiple pumping schemes are possible, but the most commonly used are $^3H_6 \rightarrow {}^3H_4$[93–96] (790 nm) and $^3H_6 \rightarrow {}^3F_4$[98,99] (1.7 μm, often referred to as "resonantly pumped"). The former affords the use of mature diode laser technologies for pumping, while the latter typically is realized through tandem pumping by another fiber laser,[99–101] although Newburgh *et al.*[98] have recently showed an efficient in-band (resonantly) diode laser pumped (1.62 μm) system operating at 1.93 μm. Research into the various pumping schemes has focused on optimization of the laser slope efficiency, which at a theoretical maximum approaches the ratio of the pumping (λ_p) to lasing (λ_s) wavelengths for 100% quantum conversion efficiency. This is formalized through the definition of the so called

TABLE III. Parameters utilized to designate the ground state terms for the Ln^{3+} ions.

Ion	Ce^{3+}	Pr^{3+}	Nd^{3+}	Pm^{3+}	Sm^{3+}	Eu^{3+}	Gd^{3+}	Tb^{3+}	Dy^{3+}	Ho^{3+}	Er^{3+}	Tm^{3+}	Yb^{3+}
Configuration	$4f^1$	$4f^2$	$4f^3$	$4f^4$	$4f^5$	$4f^6$	$4f^7$	$4f^8$	$4f^9$	$4f^{10}$	$4f^{11}$	$4f^{12}$	$4f^{13}$
Unpaired spins	1	2	3	4	5	6	7	6	5	4	3	2	1
S	1/2	1	3/2	2	5/2	3	7/2	3	5/2	2	3/2	1	1/2
2S + 1	2	3	4	5	6	7	8	7	6	5	4	3	2
L	3(F)	5(H)	6(I)	6(I)	5(H)	3(F)	0(S)	3(F)	5(H)	6(I)	6(I)	5(H)	3(F)
J	$\|L-S\|$	$\|L-S\|$	$\|L-S\|$	$\|L-S\|$	$\|L-S\|$	$\|L-S\|$	$\|L\pm S\|$	$\|L+S\|$	$\|L+S\|$	$\|L+S\|$	$\|L+S\|$	$\|L+S\|$	$\|L+S\|$
	5/2	4	9/2	4	5/2	0	7/2	6	15/2	8	15/2	6	7/2
Ground state	$^2F_{5/2}$	$^3H_4$	$^4I_{9/2}$	$^5I_4$	$^6H_{5/2}$	$^7F_0$	$^8S_{7/2}$	$^7F_6$	$^6H_{15/2}$	$^5I_8$	$^4I_{15/2}$	$^3H_6$	$^2F_{7/2}$

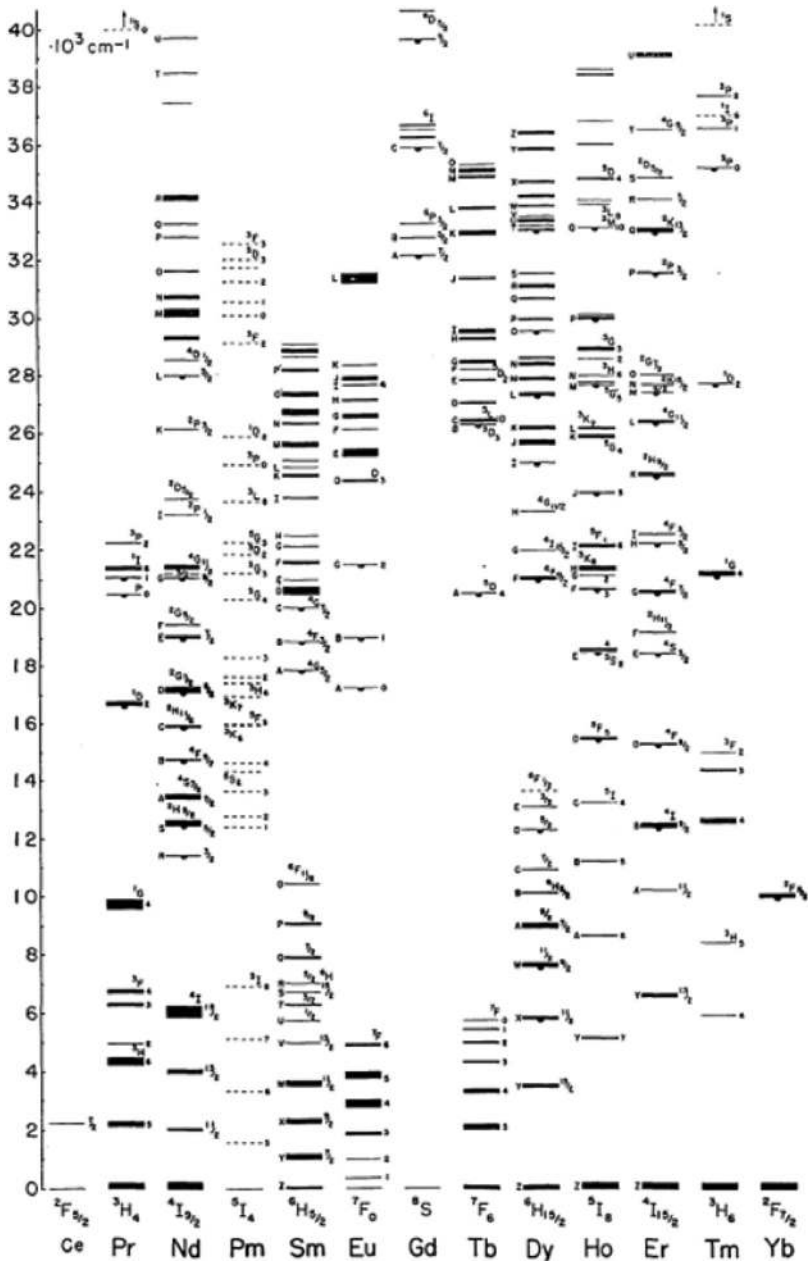

FIG. 2. Energy level diagrams for the Ln^{3+} ions (4f levels). Reproduced with permission from G. H. Dieke and H. M. Crosswhite, Appl. Opt. **2**, 675 (1963). Copyright 1963 OSA Publishing. Note that the ground state term for Gd is incompletely identified in the original publication (see Table III).

quantum defect (QD) parameter where $QD = 1 - \lambda_p/\lambda_s$. Optimization of the QD (for all lasing dopants, not just Tm) with regard to resonant pumping requires that the pump and signal wavelengths are as close together as possible, which, as will be discussed in Sec. IV, depends strongly on the magnitude and nature of LS degeneracy splitting by the host. While pumping at 790 nm seems that it would be rather inefficient (~40% maximum), a cross-relaxation process[102] enables one to obtain two signal photons from a single pump photon, thereby doubling the available efficiency. In short, the process begins with pumping from the ground state to the $^3H_4$ level of a first Tm ion. This level then becomes depopulated through the transfer of one photon to a neighboring Tm^{3+} ion, rendering both ions in the $^3F_4$ excited state, as illustrated in Fig. 4.

Finally, the presence of multiple energy levels may facilitate a process known as *upconversion*. Excitation to higher lying energy levels from a metastable or pumping level can occur through the absorption of a signal or pump photon (excited state absorption or ESA). Since this can lead to visible luminescence or nonradiative relaxation processes, upconversion typically is considered to be a deleterious, or parasitic, phenomenon. In the case of Tm^{3+}, upconversion from the $^3H_4$ level is unlikely, either through absorbing a pump or signal photon, since there are no corresponding energy levels present. For example, absorbing a pump photon from $^3H_4$ would lead to excitation lying someplace between $^1G_4$ and $^1D_2$. Should either of these levels have broadly split manifolds, then the upconversion process becomes more likely through interactions involving the edges of the bands. It is worth noting that upconversion-based lasers have been demonstrated in non-silicate glasses, for example producing blue,[103–107] red,[104,108] and NIR (~800 nm)[109,110] wavelengths. However, such sources have not yet entered the high power mainstream, in neither silicate glasses nor otherwise.

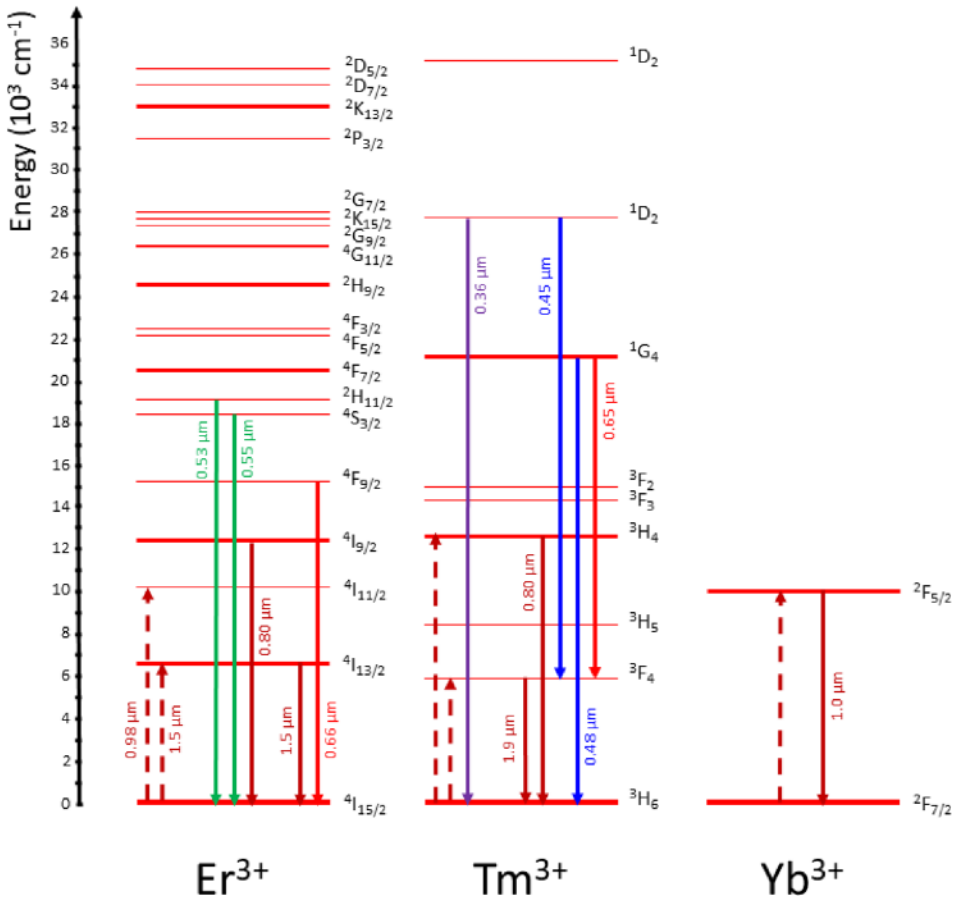

FIG. 3. f-f energy level diagrams for three Ln^{3+} ions, after Ref. 88. A few radiative transitions are identified with solid lines. Common pumping wavelengths are identified by the dashed lines.

3. Er^{3+}

Trivalent erbium is well known to be the workhorse of long-haul fiber amplifier technology. It is entirely serendipitous that it, via the $^4I_{13/2} \rightarrow {}^4I_{15/2}$ transition, efficiently produces light near 1.5 μm, spectrally overlapping precisely with the minimum attenuation wavelength region found in silica optical fibers. Telecommunications-grade erbium doped fiber amplifiers (EDFAs) are a mature technology and several very good books have been written on the subject.[111–113] Much as with the case of Tm^{3+}, pumping can be in-band (resonant) or not. For the latter, the common pumping path is via the $^4I_{15/2} \rightarrow {}^4I_{11/2}$ transition,[114,115] with excitation to the $^4I_{13/2}$ level obtained through a fast nonradiative decay process from the pumping level. Much of the early development of such EDFAs, therefore, relied heavily on the development of high-brightness diode lasers near 980 nm.[116,117] On the other hand, advantages to in-band pumping ($^4I_{15/2} \rightarrow {}^4I_{13/2}$)[118,119] for high power lasers is the possibility of a greatly reduced QD.[120,121] Clearly, the greater number and density of energy levels in the Er^{3+} system makes ESA more likely.[122–125] However, this has not proven to be an incapacitating problem for commercial EDFAs. Finally, upconversion lasers in Er^{3+} have mainly come in the form of emissions in the green.[126,127]

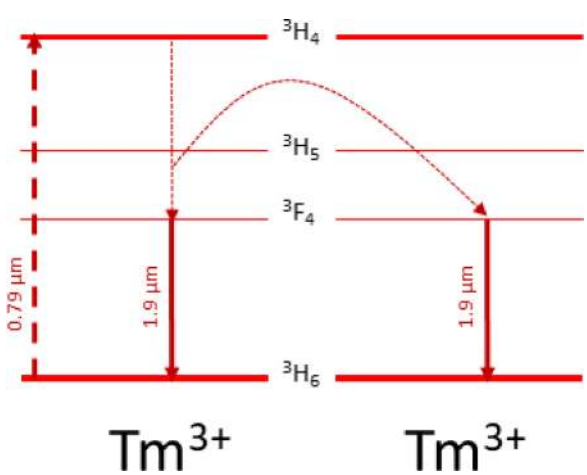

FIG. 4. Cross relaxation diagram for 790 nm pumping in Tm^{3+}. A first Tm ion absorbs a pump photon, transfers energy to another ion, rendering both ions in the $^3F_4$ excited state.

IV. THE ACTIVE ION IN A GLASS HOST

A. Stark splitting, radiative transitions, and Judd-Ofelt theory

As described in Sec. III, the degeneracy of the 4f energy levels can be generalized using Kramer's Theorem, taking on values of 2J + 1 and J + 1/2 for ions with even and odd numbers of 4f electrons, respectively. This degeneracy is broken when the ion is placed into a host, such as a glass or crystal. The host imparts an external electric field to which each degenerate electronic configuration for a given energy level will have a different response, leading to the splitting of the energy levels into *manifolds*. For example, the Yb^{3+} ground state $^2F_{7/2}$ is split into a manifold of up to 7/2 + 1/

2 = 4 sub-levels. This Stark splitting[128] typically is only of the order of a few hundred to a thousand cm^{-1}.[129–132] Transitions between the Stark components within a manifold, therefore, involves the creation or annihilation of phonons. This splitting is particularly important for Yb-doped lasers, since it can lead to effectively 3- or 4-level operation from what is nominally a 2-level system,[133] and enables in-band (resonant) pumping of both Tm^{3+} and Er^{3+} systems for reduced quantum defect lasers.[134]

In many single crystal solids, all rare earth sites are ideally identical to each other, giving rise to emission and absorption spectra that are homogeneous across all active ions. This gives rise to a spectrum that can have significant structure,[135–138] with resolvable peaks corresponding to the inter-Stark transitions. For example, the $^4I_{13/2} \rightarrow {}^4I_{15/2}$ transition in erbium has a maximum of $(13/2 + 1/2) \times (15/2 + 1/2) = 56$ possible inter-manifold transitions. In an amorphous material, however, each rare earth ion may experience a slightly different local field due to the amorphous glass structure, and therefore a slightly different distribution of the Stark components within each manifold. When taken aggregately, the transitions then appear broadened, possessing more continuum-like spectra. While this is an inhomogeneous spectral broadening process, efficient phonon interactions render the gain spectrum predominantly homogeneous in behavior.[139–141]

Clearly, a first requirement of a laser host is that it be optically transparent at the pump and emission wavelengths of interest. Next, it must permit the absorption and emission of photons by the active ions. Judd[142] and Ofelt[143] independently developed a theory to estimate the line-strengths of the optical transitions in solids. The Judd-Ofelt (J-O) theory provides a means to calculate stimulated emission cross sections from measured absorption spectra[144–147] and is nicely summarized by Krupke for Nd-doped laser glasses.[148] The J-O model states that the electric dipole line-strength S (not to be confused with the total spin S) may be written in terms of empirical parameters (the Judd-Ofelt parameters), Ω_i, as[144]

$$S = e^2 \sum_{i=2,4,6} \Omega_i \left| \langle [S,L]J \| U^{(i)} \| [S',L']J' \rangle \right|^2, \tag{3}$$

where the $\|U^{(i)}\|$ are the free-ion reduced matrix elements of the spherical tensor operators calculated using the intermediate coupling approximation,[142] with the $\langle \|U^{(i)}\| \rangle$ values being invariant of the host. In addition, $[S,L]J$ is the starting energy level (e.g., $^4F_{5/2}$ for Yb^{3+}), $[S',L']J'$ is the ending level (e.g., $^4F_{7/2}$ for Yb^{3+}), and e is the electron charge (paying careful attention to units). It has been shown that the J-O parameters can be relatively strong functions of the host material and rare earth environment. An analysis by Jørgensen and Reisfeld[149] suggested that covalent bonding strongly enhances Ω_2, while Ω_6 may be related to the rigidity of the host. Tanabe, *et al.*,[150] found that in a series of Er^{3+}-doped alkali-metal borate glasses Ω_2 increases with the increase in the local asymmetry,[151] and that Ω_4 and Ω_6 are related to the basicity of the glass. Takebe, *et al.*,[152] found that Ω_6 increases with ionic packing ratio of the host, and that both Ω_4 and Ω_6 decrease with the increase in the number of 4f electrons.

The connection of the Judd-Ofelt parameters to rare earth-ligand bond covalency also is relevant with respect to the nephelauxetic effect.[153] The nephelauxetic effect,[154] which is Greek for "cloud expanding," describes the expansion of electronic orbit radii with the increase in the bond covalency. This results from a decrease in the interelectronic repulsion[155] and leads to a red shift of the emission/absorption bands in the lanthanide ions (relative to the free or in-aqua-ions) since the electrons become more delocalized with the increase in the degree of covalency. The nephelauxetic ratio, as defined by Jørgensen,[154] is given by

$$\beta = \frac{F_k(complex)}{F_k(free\ ion)}, \tag{4}$$

where the F_k (k = 2, 4, 6) are the interelectronic repulsion parameters, or Slater integrals,[156] for the free or in-complex (i.e., in a host) ion. Often, the free ion values are not known, and those in aqua instead are assumed. Equation (4) can be used, to some extent, to estimate the degree of covalency via $b = (1 - \beta)/2$.[154,156] As described in Sec. III, the 4f electrons are effectively shielded by n = 5 subshells. However, the degree of covalency not only has an impact on the strength of the transitions, which Reisfeld identifies as increasing with the increase in the degree of covalency for Nd^{3+},[157] but it also can have an important impact on emission and absorption wavelengths via the nephelauxetic effect.

The values for the $\langle [S,L]J \| U^{(i)} \| [S',L']J' \rangle$ integrals can be found tabulated in the literature. These are transition-specific ($^{(2S+1)}L_J \rightarrow {}^{(2S'+1)}L'_{J'}$) and have been identified for a large number of transitions covering the trivalent lanthanide ions.[158–160] The line-strength is connected to the absorption spectrum via[148]

$$\int_{\lambda_1}^{\lambda_2} \rho \sigma_a(\lambda) d\lambda = \rho \frac{8\pi^3 \overline{\lambda}}{3ch(2J+1)} \frac{1}{n} \frac{(n^2+2)^2}{9} S, \tag{5}$$

where λ_1 and λ_2 represent the start and end of an absorption band (such as $^4I_{15/2} \rightarrow {}^4I_{11/2}$ in Er^{3+}). In Eq. (5), n is the host refractive index at the mean wavelength ($\overline{\lambda} = \int_{\lambda_1}^{\lambda_2} \lambda \sigma_a(\lambda) d\lambda / \int_{\lambda_1}^{\lambda_2} \sigma_a(\lambda) d\lambda$) of the absorption band, σ_a is the absorption cross section, (2J + 1) is the degeneracy of the beginning (i.e., ground) state, ρ is the active ion number density (m^{-3}), and the factor $(n^2+2)^2/9$ is the local field correction for an ion in the dielectric medium under the tight binding approximation.[161] Evaluating Eq. (5) for a single transition gives rise to one equation with three unknowns: the J-O parameters. This is insufficient to determine the Ω_i values, and it must therefore be applied to multiple absorption or emission features. For this reason, due to its having only a single transition, J-O data for Yb^{3+} doped glasses are not found in the literature.[162]

In the case of the emission spectra, the transition probability (Einstein A coefficient) is found from the line-strength with

$$A([S',L']J';[S'',L'']J'') = \frac{64\pi^4}{3h(2J'+1)\overline{\lambda}^3} n \frac{(n^2+2)^2}{9} e^2 \times \sum_{i=2,4,6} \Omega_i \left| \langle [S,L]J \| U^{(i)} \| [S',L']J' \rangle \right|^2, \tag{6}$$

where a single prime (S') denotes the starting and a double prime (S'') the ending levels. In this case, $\bar{\lambda}$ is the mean wavelength of a fluorescence band g(λ) ($\bar{\lambda} = \int_{\lambda_1}^{\lambda_2} \lambda g(\lambda) d\lambda / \int_{\lambda_1}^{\lambda_2} g(\lambda) d\lambda$). Should more than one terminal level be present (such as is the case with pumping Nd^{3+} into the $^4F_{5/2}$ level), the branching ratios, or relative emission strength, can be invoked. The branching ratio is defined to as[148]

$$R\left([S',L']J';[S^n,L^n]J^n\right) = \frac{A\left([S',L']J';[S^n,L^n]J^n\right)}{\sum_n A\left([S',L']J';[S^n,L^n]J^n\right)}, \quad (7)$$

where the prime denotes the starting level (excited state) and the superscript n denotes the terminal levels. Equation (7) gives the proportion of luminescence starting from the upper state and ending on level n. Hence, should luminescence from an excited state possess 3 or more luminescence bands, the J-O quantities can be determined.[15,148] Finally, the denominator in Eq. (7) gives the inverse of the total radiative lifetime (τ_{rad}) from the upper (starting) state. From the Einstein A coefficients, the induced emission cross sections then can be calculated.[148,163]

In the case of resonant pumping (absorption and emission between two manifolds only), the equations above may be combined to give the Füchtbauer-Ladenburg equation.[148] In its most well-known form, it is given by[164,165]

$$\sigma_e(\lambda) = \frac{1}{\tau_{rad}} \frac{\lambda^5}{8\pi c n^2} \frac{I(\lambda)}{\int_{\lambda_1}^{\lambda_2} I(\lambda)\lambda d\lambda} \approx \frac{1}{\tau_{rad}} \frac{\bar{\lambda}^4}{8\pi c n^2} \frac{I(\lambda)}{\int_{\lambda_1}^{\lambda_2} I(\lambda) d\lambda}, \quad (8)$$

where I is the spectral intensity and the approximate expression is applicable to cases of narrow spectrum. Equation (8) conveniently provides a means to calculate the emission cross section spectrum from measurements of τ_{rad} and a fluorescence spectrum. Another useful formulation given by McCumber[166] relates the emission to the absorption cross-sections[138]

$$\sigma_e(\nu) = \sigma_a(\nu) \frac{Z_{lower}}{Z_{upper}} \exp\left(\frac{E_{ZL} - h\nu}{kT}\right), \quad (9)$$

where E_{ZL} is the zero-phonon line energy, ν is the frequency, and the Z's are the partition functions[166] for the upper and lower energy levels, given by

$$Z = \sum_k d_k \exp\left(-\frac{E_k}{kT}\right), \quad (10)$$

where d_k is the degeneracy of each level within a manifold. E_k is the energy of a level within a manifold relative to the lowest level within that manifold.

B. Magnetic dipole transitions

While the f-f transitions in the trivalent rare earth ions are predominantly electric dipole (ED) in nature,[167] the active ion also may respond to the presence of a magnetic field,[168,169] leading to magnetic dipole (MD) contributions. This leads to a corrected form of Eqn. (6) given by[165,170]

$$\begin{aligned} A([S',L']J';[S'',L'']J'') &= \frac{64\pi^4}{3h(2J'+1)\bar{\lambda}^3} \Bigg[n \frac{(n^2+2)^2}{9} e^2 \sum_{i=2,4,6} \Omega_i \\ &\times \left| \langle [S,L]J \| U^{(i)} \| [S',L']J' \rangle \right|^2 + e^2 \frac{h^2}{16\pi^2 m^2 c^2} \\ &\times \left| \langle [S,L]J \| \mathbf{L} + 2\mathbf{S} \| [S',L']J' \rangle \right|^2 \Bigg], \end{aligned} \quad (11)$$

where m is the electron mass. In order to deduce the J-O parameters from spectroscopic data, the MD part usually is subtracted from the total observed $A([S',L']J';[S'',L'']J'')$ or line-strength[152,168,171] using the literature data. This is justified since the MD line-strengths are not strongly affected by the host, unlike the ED line-strength through the J-O parameters.[172] Carnall *et al.*[168] and, more recently, Dodson *et al.*[173] have compiled a list of the relative contributions by the MD (in particular, the dimensionless oscillator strengths) for a large number of transitions across the lanthanides. The relationships between oscillator strength and line-strength or emission probability can be found elsewhere.[170,173]

C. Non-radiative (multiphonon) transitions

The absolute upper state decay rate is a combination of both radiative and other processes, including those that generate phonons, or heat. These non-radiative (NR) processes give rise to an observed ("obs") upper state lifetime that is described by

$$\frac{1}{\tau_{obs}} = \frac{1}{\tau_{rad}} + \frac{1}{\tau_{NR}}. \quad (12)$$

NR processes require thermal transfer with the environment, and in the case of fiber lasers, this energy is deposited into the glass host. Radiative and NR de-excitation are competing processes, with the latter becoming more likely as the number of phonons required to cross a transition decreases. This is a strong function of the host and its maximum phonon energy. Layne *et al.*[174] give an expression for the NR decay rate

$$\frac{1}{\tau_{NR}} = C(n(T)+1)^p \exp(-\alpha \Delta E), \quad (13)$$

where C and α are semi-empirical parameters that depend on the host. In Eq. (13), $\alpha = -\ln(\varepsilon)/h\nu_T$, where ε is a (electron-phonon) coupling coefficient, and $h\nu_T$ is the maximum phonon energy (of the host). In addition, ΔE is the energy gap and p ($= \Delta E/h\nu_T$) is the number of phonons required to traverse the transition. Finally, $n(T) = \left(\exp\left(\frac{h\nu_T}{kT}\right) - 1\right)^{-1}$. Reisfeld *et al.*[175,176] have compiled several values pertinent to Eq. (13) and these are reproduced in Table IV. In summary, for the relevant transitions identified in Sec. III for Yb^{3+}, Er^{3+}, and Tm^{3+}, the NR component is much smaller than the radiative one.

TABLE IV. Empirical parameters for evaluating Eq. (13).

Glass family	C (s^{-1})	α (10^{-3} cm)	$h\nu_T$ (cm^{-1})
Phosphate	5.4×10^{12}	4.7	1200
Borate	2.9×10^{12}	3.8	1400
Silicate	1.4×10^{12}	4.7	1100
Tellurite	6.3×10^{10}	4.7	700
Germanate	3.4×10^{10}	4.9	900
ZBLA	1.6×10^{10}	5.2	500

D. Yb^{3+}, Er^{3+}, and Tm^{3+}

This subsection provides a discussion of the spectroscopy of the three relevant transitions identified in Sec. III, in the context of the host glass. As previously noted, each ion has a maximum number of possible inter-manifold transitions, all of which can be influenced by the local environment. It has long been known that co-dopants, such as Al_2O_3 or P_2O_5, for example,[177] can modify not only the position of absorption and emission bands but also the relative branching ratios where relevant. Depending on the strength and nature of this ion-host interaction, emission and absorption spectra can therefore be compositionally tailored, to at least some extent, in an effort to improve laser system performance. Next, this is illustrated, conceptually, with two example Yb^{3+}-doped silicates.

1. Yb^{3+}

The $^2F_{5/2} \leftrightarrow {}^2F_{7/2}$ path in trivalent ytterbium is allowed a maximum of 12 inter-manifold transitions. An archetypal example of the effect of the host on the shape of the emission spectrum is given in Fig. 5. Two glass hosts are compared: (1) a commercial Yb-doped aluminosilicate core fiber[178] (blue curve, Liekki Oy, Finland) and (2) a Yb-doped multicomponent strontium aluminum fluorosilicate core fiber[179] (orange curve). Common to most Yb-doped glasses is the presence of an essentially host-invariant and relatively strong, zero-phonon line near 976 nm. As an aside, in order to prevent reabsorption from influencing the measured spectra, which usually is manifested as apparently weaker zero-phonon emission strength, these spectra should be collected from the side of the fiber to minimize optical path-length, hence reabsorption. Clearly, the same consideration is required for analysis of bulk glass materials.

In the case of Yb^{3+}, the key change in the shape of the spectrum is the position of the longer-wavelength portion, which is blue-shifted in the fluorosilicate glasses. The magnitude of this wavelength shift can be quantified by calculating the average emission wavelength for the transition, given by

$$\lambda_{ave} = \frac{\int_{\lambda_1}^{\lambda_2} \lambda I(\lambda) d\lambda}{\int_{\lambda_1}^{\lambda_2} I(\lambda) d\lambda}, \tag{14}$$

where $I(\lambda)$ is the emission spectrum and the integration limits are restricted to the emission band of interest. With respect to Fig. 5, they are 1004.1 nm and 999.5 nm for the aluminosilicate and fluorosilicate fibers, respectively. Cavillon *et al.*[179] attributed the reduction in the average emission wavelength in the fluorosilicates to the addition of F to the host. Most interestingly, the emission spectra from these fibers very closely resembled those of fluoride (ZBLAN) fibers,[180] with the average emission wavelength reaching an asymptotic value with as little as 5 at. % of F. This suggests that only small amounts of additive are needed to completely change the shape of the emission spectrum. From a practical perspective, this means that fluoride-like spectroscopic properties can be garnered in a mostly silica glass, which also then brings the physical robustness (strength, ability to be spliced, etc.) required for the high power fiber laser application. However, this comes at the expense of reduced absolute emission and absorption cross sections. Yu *et al.*[181] have recently shown that such glasses may be useful for efficient low-quantum-defect laser operation. Based on the discussion above, it is tempting to ascribe the change in spectroscopy to decreased covalence (or increased glass ionicity) with the introduction of F to the host, at least in the vicinity of the Yb^{3+} ion.

Similarly, an evolution also is observed in the absorption spectra. The normalized absorption spectra for the same two fibers in Fig. 5 are shown in Fig. 6. In both cases, the zero phonon line appears at the same wavelength, but the short-wavelength portions differ somewhat, with the fluorosilicate glass exhibiting a much flatter spectrum. When

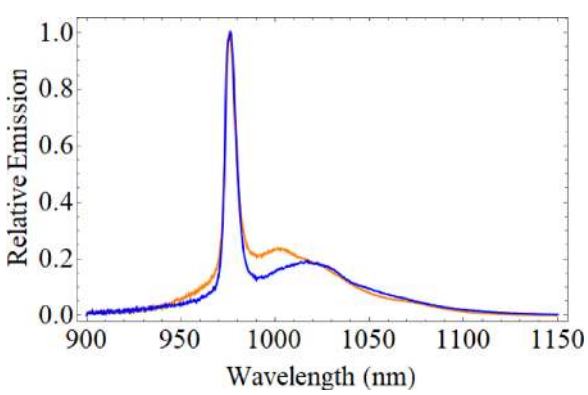

FIG. 5. Normalized emission spectra for Yb^{3+} in commercial aluminosilicate glass (blue) and multicomponent fluorosilicate glass (orange).

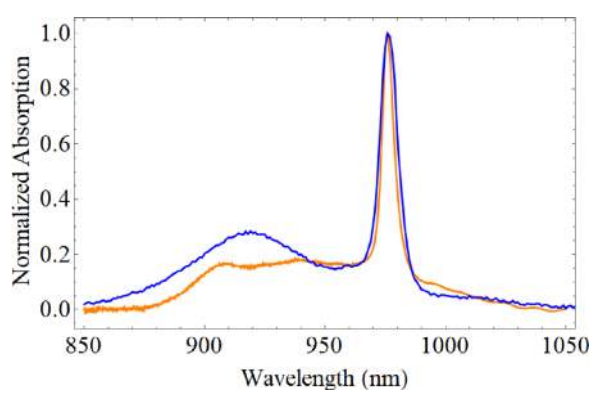

FIG. 6. Normalized absorption spectra for Yb^{3+} in commercial aluminosilicate (blue) and strontium-aluminum fluorosilicate glasses (orange).

pumped near 920 nm, the flat spectrum suggests that laser output power can be less susceptible to changes or fluctuations in pumping wavelength. The host also impacts the fluorescence lifetime, with data for the same two fibers shown in Fig. 7. As with the fluoride glasses, the fluorosilicates exhibit longer upper state lifetimes than their aluminosilicate counterparts. However, with an increased upper state lifetime comes the concomitant reduction in emission cross section [via Eq. (8)]. The 1/e- decay time (often called the "1/e folding time," which is the time it takes for the emission intensity to reach 1/e its original value) are approximately 778 μs and 1257 μs for the aluminosilicate and fluorosilicate fibers, respectively. It is important to point out that the single-exponential decay observed in both fibers suggests that the Yb^{3+} sites likely are all similar throughout the doped region. Applying Eq. (8), one arrives at peak emission cross section values of 2.54×10^{-24} m^2 and 1.75×10^{-24} m^2, for the aluminosilicate and fluorosilicate fibers, respectively.

Particularly interesting in the spectroscopic data from the various Yb-doped silicate (and even non-silicate) glasses (either in bulk or fiber form) found in the literature is that they usually resemble one or the other of the two types presented above. For instance, Yb-doped phosphosilicate glasses tend to exhibit flatter absorption spectra in the range of 900 nm to 950 nm, possess a local emission maximum closer to 1000 nm, and have a relatively long (1.5 ms)[182] upper state lifetime (and therefore reduced cross sections).[182–185] These are all characteristics similar to those found in zero-silica phosphate glasses,[186] and also those attained with the introduction of F in the case above. However, it is worth pointing out that P_2O_5 should promote covalent bonding in silica. Other hosts with similar properties include those possessing heavy metal additives, such as lead germanate[187] and lead bismuth gallate[188] glasses. Borate and fluoroborate glasses[189] are somewhat more similar to phosphate glasses, though the addition of Na_2O was shown[189] to alter the spectroscopy more towards the aluminosilicates. Glasses with properties more closely resembling the aluminosilicates[190] include lanthanum aluminosilicates,[191] yttrium aluminosilicates,[192] Mg- and Li-doped aluminosilicates,[193,194] and pure[195] and lightly doped silica.[196] For completeness, Fig. 8 gives the emission and absorption cross section spectra for Yb-doped yttrium aluminosilicate glass.[192]

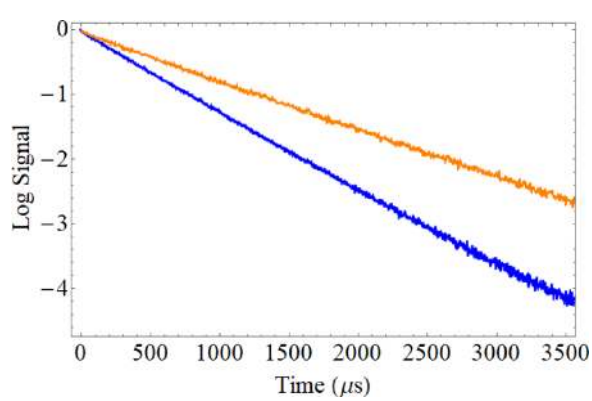

FIG. 7. Lifetime measurements for Yb^{3+} in commercial aluminosilicate (blue) and strontium-aluminum fluorosilicate glasses (orange).

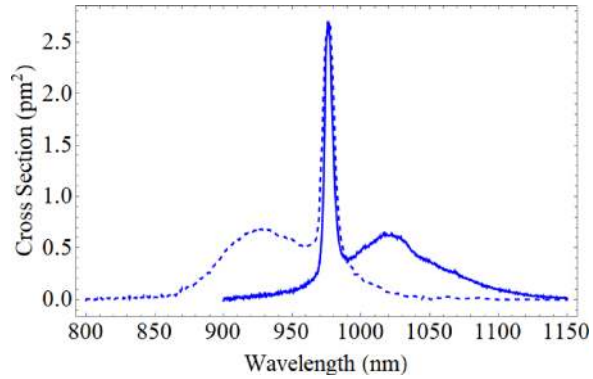

FIG. 8. Emission (solid line) and absorption (dashed line) cross section spectra for Yb-doped yttrium aluminosilicate glass.[192]

2. Er^{3+}

Comparing erbium emission spectra ($^4I_{13/2} \rightarrow {}^4I_{15/2}$) from the same two families of glasses presented above, shown in Fig. 9, also unveils interesting characteristics. In this case, the average emission wavelengths are quite similar (1539.4 nm and 1539.1 nm for the aluminosilicate and strontium-alumino fluorosilicate glasses, respectively). However, the fluorosilicate glass has a spectrum that is narrower than that of the aluminosilicate glass. The full-width-at-half-maximum spectral widths are roughly 43 and 24 nm for the aluminosilicate and fluorosilicate glasses, respectively. In the case of high power operation, a narrower spectral width suggests the availability of larger emission cross section values, while broader spectra are advantageous for communications amplifier applications. Considerable work has been done characterizing host glasses for the latter and a number of reviews/summaries can be found in the literature for both silicate and non-silicate glasses, including absorption, emission, radiative lifetime, and J-O parameters.[197–201] In a recent summary, Linganna *et al.*,[199] tabulates literature data for ten different glass families. To conclude this subsection, the emission and absorption cross section data for an aluminosilicate core fiber with 9.4 ms upper state radiative lifetime are provided in Fig. 10.

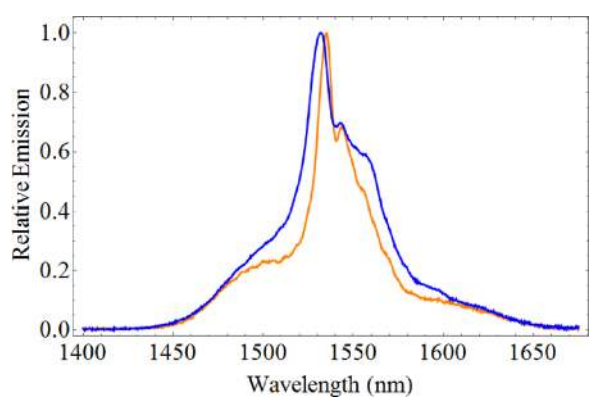

FIG. 9. Normalized emission spectra for Er^{3+} in aluminosilicate (blue) and strontium-aluminum fluorosilicate glasses (orange).

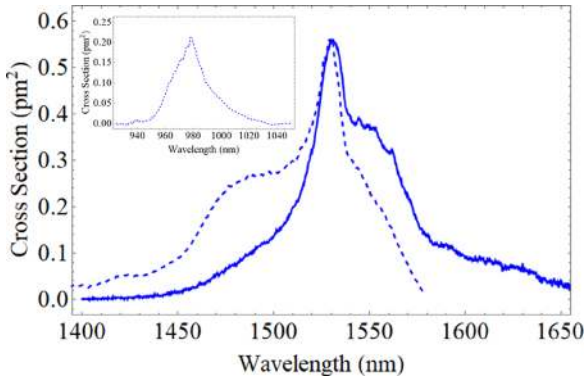

FIG. 10. Emission (solid line) and absorption (dashed line) cross section spectra for Er-doped aluminosilicate glass ($^4I_{13/2}\leftrightarrow{}^4I_{15/2}$ path). The inset gives the $^4I_{15/2}\rightarrow{}^4I_{11/2}$ cross sections.

3. Tm^{3+}

Figure 11 provides the absorption and emission cross section data for a commercial (Coherent|Nufern, East Granby, CT) Tm-doped fiber.[101] Typical lifetimes are 1.16 ms and 1.54 ms for lightly (14.5×10^{25} ions/m^3) and heavily (28.5×10^{25} ions/m^3) doped fibers, respectively.[101] The transition of interest ($^3F_4\rightarrow{}^3H_6$), peaking near 1.85 μm, is quite broad. Therefore, the host does not influence this transition as significantly as with the relevant transitions in Yb^{3+} or Er^{3+}. However, some work has been done in this area. For instance, Dhar *et al.*[202] have shown that relative to pure silica, the addition of GeO_2 and P_2O_5 blue- and red-shift the $^3H_6\rightarrow{}^3F_4$ band, respectively. However, the shift is largely insignificant when compared with the spectral width of the absorption band. Wen *et al.* observed blue-shifted spectra in a barium-gallium germanate glass.[203] A slightly different trend was reported by Turri *et al.*,[204] where spectra were somewhat red-shifted in germanate glasses relative to silica and mainly only were narrower in the phosphate glasses, but this likely is attributable to variations in the glass compositions. Turri *et al.*[204] also summarize literature data for Tm-doped silica, borophosphate, fluorophosphate, and phosphate glasses. The data for other glass systems also are available, including germanate-tellurite glasses,[205] ZBLAN,[206] and soda lime silicates,[207] to name a few.

E. Nanoparticle doping

The introduction of rare earth ions into the glass matrix also can be realized through the use of nanoparticle (NP) doping, whereby the rare earth ion is incorporated into the nanoparticle, which then is doped into the glass. This enables one to tailor both the distribution of the rare earth ions and their local chemical environment. In the context of distribution, it primarily serves the purpose of minimizing the ion-ion interactions that result in lifetime quenching. Early on, Liekki Oy of Finland developed a direct nanoparticle deposition method for Yb-doped fibers.[208] In this process, individual NPs can be incorporated while maximizing the physical separation of the Yb atoms. They showed that this led to a reduction of inversion-related optical damage ("photodarkening" discussed in Sec. V D) and more efficient laser operation. A simple gauge that has been used to estimate Yb-Yb clustering levels is the physical observation of the level of cooperative luminescence visible from the fiber when pumped.[209] A spectrum is provided in Fig. 12 below for an aluminosilicate glass. Essentially, it is a self-convolution, or more or less a frequency-doubled version of the $^4F_{5/2}\rightarrow{}^2F_{7/2}$ IR luminescence, believed to result from the simultaneous emission by Yb-Yb pairs. While potentially useful for some applications,[187,210,211] in principle, stronger cooperative luminescence suggests more Yb clustering (or at least ion pairs), and more significant quenching, which deleteriously impacts high power laser performance. Many groups have studied concentration quenching in Yb-doped fibers,[212–217] and while quenching limits the Yb_2O_3 concentration to about 1 to 2 wt. % in a mostly silica glass, it is higher in phosphate glasses.[218,219] Due to the presence of multiple upconversion paths, Er^{3+}- and Tm^{3+}-doped materials have lower concentration quenching limits.[220] Lin *et al.*[221] recently showed that, through a NP doping process, high Er^{3+} concentrations (4×10^{25} ions/m^3) can be realized without reductions in the upper state lifetime. Such enhancements to the doping concentration are particularly important considering the low absorption cross sections of Er^{3+} when compared with Yb^{3+}. Finally, for reasons of pumping into the $^3H_4$ level described in Sec. III B 3, some ion-ion interaction is preferred for Tm^{3+}. NP doping will be revisited in "Future Perspectives."

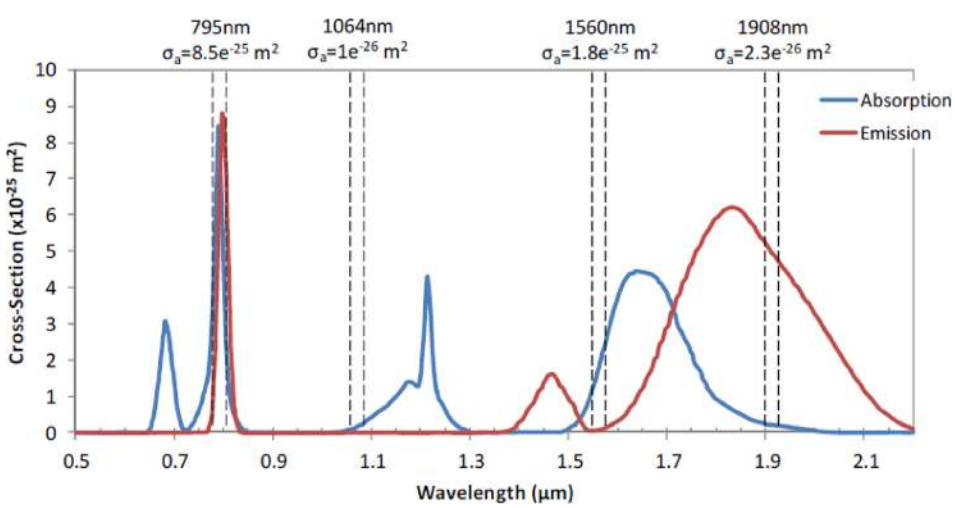

FIG. 11. Emission and absorption cross section spectra for a commercial Tm-doped fiber. Reproduced with permission from D. Creeden *et al.*, Opt. Express **22**, 29067 (2014). Copyright 2014 OSA Publishing.

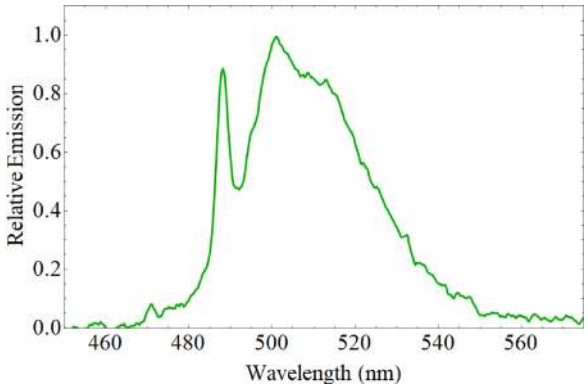

FIG. 12. Cooperative luminescence spectrum produced from Yb-Yb ion pairs in an aluminosilicate glass fiber.

While the use of NPs offers a means to reduce the effects of concentration quenching, they also offer a means to tailor the local environment of the rare earth ion. In the context of the discussion in Sec. IV D above, silica's fairly refractory and high strength attributes have rendered it highly agreeable for use in high-power fiber laser technologies. However, spectral or other features characteristic of other glasses may be preferable for a given application. In this case, the rare earth is embedded into a NP of desired composition, which, in turn, is doped into the silica host. For example, this provides a means to introduce heavy metal ions for the reduction of phonon energy (near the active ion),[222] but in a relatively small quantity still enabling a relatively low fiber NA.[223] Recent work on Yb_2O_3-doped NP-doped glass fibers[224] includes Y_2O_3 NPs,[225,226] Y_2O_3-Al_2O_3 NPs,[227] and zirconia-germano aluminosilicate NPs,[228] to name a few. Similarly, some Er^{3+} NP work includes Al_2O_3 NPs,[221,229] alkaline earth metal oxide NPs,[230,231] and LaF_3[232] and Lu_2O_3 NPs.[232] For Tm^{3+}, they include LaF_3[223] and Al_2O_3[233] NPs. Brief reviews have been offered by Kasik *et al.*[234] and Ballato *et al.*[235]

F. Sensitization

This section is concluded with a brief discussion of sensitization, which is the co-doping of multiple, interacting active ions into the same glass host. The idea behind sensitization is to pump one active ion, and to have that excitation transferred to a different active ion. This can serve both to extend the available emission wavelength range and to enhance pump absorption in an optical fiber. Numerous examples of co-doped fibers can be found in the literature, including Tm-Ho,[236] Tm-Bi,[237] Ho-Pr,[238] Tm-Tb,[239] among many others. However, in the present context (Er^{3+} and Tm^{3+}) sensitization by Yb^{3+} often is used to enhance the net absorption coefficient of an active fiber. As discussed above, the absorption cross sections for both Er^{3+} and Tm^{3+} are somewhat lower than that of Yb^{3+}. Therefore, one conceivably can take advantage of the high ytterbium absorption cross section, and through efficient energy transfer, lase on erbium or thulium. Much more work has been done on the former,[240–244] than the latter,[202,245–249] with power mainly limited by parasitic lasing by the Yb^{3+} ions.[250] It is useful to point out that Er-Yb co-doped fibers are now commercially ubiquitous.

V. THE OPTICAL FIELD AND LIGHT-MATTER INTERACTIONS

A. The optical waveguide

While the main focus of this review is the material from which an active fiber is made, the waveguide defines the properties of the propagating optical modes that interact with it. Therefore, it is prudent to briefly review some active optical fiber (waveguide) configurations and their formation. The richness of the literature focusing on waveguide design is many orders of magnitude greater than the discussion offered herein. As such, and with apologies to those concepts not mentioned here, only a few examples are provided to help set up context for Sec. V B.

The simplest and arguably most intuitive configuration for the optical fiber is known as a step-index fiber, wherein a core (which usually is where the active ion can be found) of uniform refractive index n_{core} is surrounded by a cladding region of lower index, satisfying $n_{clad} < n_{core}$. This gives rise to the well-known total internal reflection phenomenon and the simple guided-ray picture of wave-guidance.[251] This refractive index distribution is visualized through the refractive index profile (RIP), which provides refractive index values relative, typically, to the outermost cladding region. Figure 13 displays such a RIP for the simple step-index structure, but near the fiber core. The refractive index difference between the core and cladding ($\Delta n = n_{core} - n_{clad}$) and core diameter, 2a, together normally set the propagation characteristics of a fiber. Therefore, the selected absolute refractive index value does not usually significantly impact any simple waveguide analysis. The numerical aperture (NA) is given by $NA = \sqrt{n_{core}^2 - n_{clad}^2}$ and the V-number by $V = 2\pi aNA/\lambda$, where a is the core radius and λ is the vacuum optical wavelength. For V values less than 2.405 (the first zero of the zeroth-order Bessel function), the (azimuthally symmetric, cylindrical) fiber supports a single guided mode at a wavelength of λ. For $V > 2.405$, the fiber is considered to be multimode (MM).

The small core diameter and low NA of the fiber core represents a "high-brightness" region.[252] Typical erbium doped fiber amplifiers (EDFAs) are core-pumped, meaning

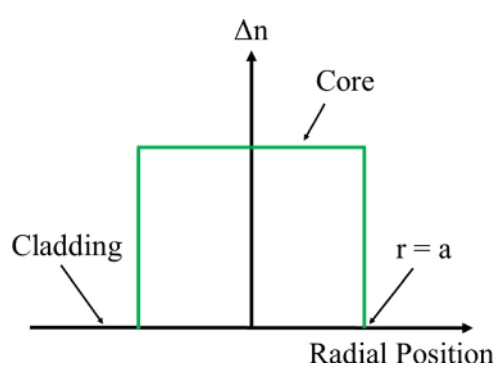

FIG. 13. Refractive index profile typical of a step index optical fiber.

that pump light is coupled directly into the core of the fiber. Currently, commercial single mode fiber-coupled pump lasers are limited to about 1 W of optical power.[253] While polarization or wavelength multiplexing techniques may be possible, significant power scaling, even to the 10s of Watts level using such pump lasers is not feasible. In response, and nearly three decades ago, double clad fibers were developed.[254,255] In principle, a typical fiber possesses a core and a cladding, as shown in Fig. 13. For reasons of mechanical strength and the removal of unwanted light from the cladding, the fiber has an outer polymer coating, usually a UV-curable acrylate. Rather than to configure the buffer to couple light away from the cladding (buffer index larger than the cladding index) as in a telecommunications fiber, it may be configured such that light is confined to the cladding (requiring the index of the buffer to be less than that of the cladding). The cladding then can serve as a low-brightness waveguide for the pump light, allowing the coupling of light from diode stacks, or MM fiber-coupled pumps, into the fiber. Typical low-index polymer coated fibers give an outer cladding NA of ~0.46.[256] Furthermore, there may instead be a low-index glass region between the cladding and polymer/buffer for high power operation.[257] Ultimately, while guiding the pump in the cladding reduces the effective small signal absorption coefficient at the pumping wavelengths (due to the reduced overlap between the pump spatial distribution and rare earth doped core), complete pump absorption is possible and highly efficient laser operation can therefore result. This was facilitated by the realization that such a structure, if azimuthally symmetric about the fiber axis, can support higher order modes (HOMs) that propagate in a helix in a space to the outside of the core region. Such modes then would experience diminished absorption. Shaped cladding geometries,[258,259] therefore, were developed to overcome this issue. Further details on fiber geometries, pump delivery, etc., can be found in any one of a number of reviews previously mentioned on high power fiber lasers.[2,3,5,8]

The RIP need not be strictly step-index (i.e., rectangular) in shape. The index profile may be graded (graded index profile or GRIN) to more closely resemble a Gaussian or other function. Generally, GRIN fibers possess fewer modes than step index fibers of the same core radius and peak value of Δn. Coupled with depressed inner cladding regions (or "trenches") situated between the core and outer cladding, such structures form the basis for the design of next-generation high-bandwidth MM communications fibers.[260,261] While such MM fiber structures may not be directly useful in high power fiber laser applications, elements of this waveguide design can be. For example, Yoo *et al.*[262] have shown that with proper design, the W-type fiber[263,264] shown in Fig. 14 possesses a fundamental mode cutoff wavelength which can be used to wavelength-filter deleterious amplified spontaneous emission (ASE) in Nd-doped fiber lasers for efficient operation on the 3-level transition. The following year, researchers from the same group showed that this fiber structure also can be used to filter Raman (Stokes') scattered light (discussed in Sec. V B 2), thereby suppressing the stimulated form of this process.[265] Careful design of these structures also permits the tailoring

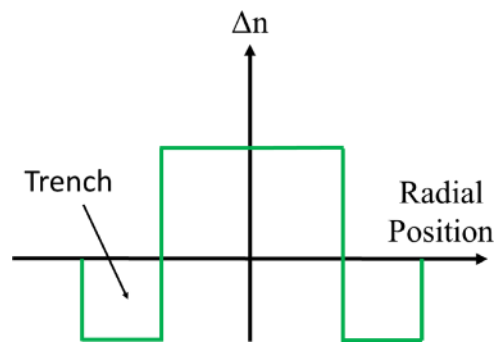

FIG. 14. Refractive index profile typical of a W-type step index optical fiber. The "trench" region often is referred to as a depressed cladding layer.

of the dispersion characteristics important for mode locked lasers[266–268] and supercontinuum generation.[269–271]

While single mode or few-moded fibers are most desirable from the standpoint of beam quality, requisite dopant concentrations and subsequent refractive index values may not afford this behavior. In response, triple-cladding, or pedestal, fibers have been developed,[272] illustrated in Fig. 15. The structure is similar to the W-type fiber (in that it is also a three-layered structure), but the inner cladding region has a refractive index much more similar to, but still less than, that of the core. In this structure, the central region and adjacent inner cladding cooperate to form an effective fiber with refractive index difference Δn_1, with the caveat that the distance (b – a) be large enough that the r = b boundary does not somehow result in coupling of light into the inner cladding region. This design has proved to be particularly useful in Yb^{3+}:Er^{3+} co-doped fiber amplifiers due to the large ytterbium concentrations required for efficient high-power operation.[273–275] Such fibers also can benefit from selective transverse doping of the rare earth. Laperle *et al.* showed that with careful control of the mode properties and distribution of rare earth within the core (such that the fundamental mode has the highest spatial overlap with the active rare earth), effectively single mode operation in a few-moded pedestal structure can be facilitated.[276]

Leaning now towards the counter-intuitive, an optical fiber need not be strictly index guiding to facilitate efficient laser operation. Siegman showed that with a sufficiently large gain coefficient, robust single spatial mode operation from a fiber configured to be *anti-guiding* ($n_{clad} > n_{core}$) is

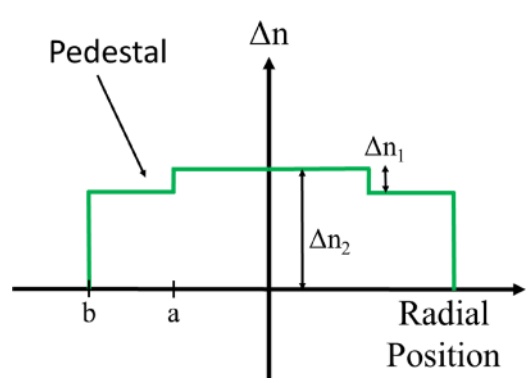

FIG. 15. Refractive index profile typical of a triple cladding fiber.

possible.[277] Ultimately, these fibers are leaky even for the fundamental mode, but with enough gain, loss can be compensated for and greatly exceeded.[278,279] Several groups have continued development of this technology,[280–282] but it has not yet entered the commercial mainstream.

From a manufacturing perspective, the aforementioned waveguide configurations are relatively straightforward. However, as will be discussed in Sec. V B, there has been a push to expand the mode size in optical fiber in order to raise the thresholds for the onset of nonlinear parasitic phenomena. While increasing the core radius, a, is an obvious response to this problem, it also typically increases the number of modes propagating in the active fiber core, rendering an achievable high beam quality is very challenging. Adjusting the NA in such "Large Mode Area," or LMA, fibers to compensate are difficult given that typical[283] core NA values of 0.06 result from a refractive index difference, Δn_1, of merely 1.3×10^{-3}. This greatly tightens the tolerances on dopant concentrations and core composition,[284,285] making the fiber more challenging to fabricate with decreasing refractive index difference. An early approach to effective single mode operation in an intrinsically MM fiber was the use of selective mode filtering; i.e., fibers with built-in propagation loss to higher-order modes (HOMs). Early in the development of high-power fibers lasers, Koplow *et al.* showed that with proper mode launch conditions and coiling the active fiber to an appropriate radius effectively single mode operation could be achieved.[286] Li *et al.* later identified some practical limitations to scaling this approach.[287] These included limited differential loss between the fundamental (LP_{01}) mode and the HOMs, mode distortion and squeezing due to bending, and mechanical reliability of a large-diameter, tightly bent fiber. An alternative approach, introduced by Galvanauskas *et al.*, is the so-called "Chirally Coupled Core," or CCC, fiber.[288] In this structure, a satellite core orbits the central core in a helical path along the axial direction. HOMs couple to this satellite core and are then subsequently shed into the cladding, rendering effectively single mode behavior. Such effectively single mode behavior in fibers with core diameters greater than 50 μm has been demonstrated.[289]

More complex, microstructured fibers also have garnered significant research efforts over the past 15 years or so. Russell first proposed photonic crystal fibers in the early 1990s. As stated in their groundbreaking paper, photonic crystals are "materials that have a periodic modulation of the refractive index on the scale of a wavelength."[290] The first such fiber was passive, with a core being clad in a periodic structure of air holes embedded in pure silica (hence the moniker "holey fiber"). However, the concept has since been broadly applied to active fibers and fiber laser technologies.[291] One of the primary applications of the photonic crystal structure was the air-clad fiber,[292] whereby an outer layer of holes acted to confine pump light to the cladding. In this way, the NA of the pump guide could be increased (> 0.75) enabling the coupling of more low-brightness pump power into the fiber. The use of air-clad fibers has been a proven path towards power scaling of fiber lasers.[293–295] An early example of such a fiber is shown in Fig. 16. Generally, the use of microstructuring has had the goal of enhancing the mode size to elevate the turn-on thresholds of nonlinear parasitics (to be discussed in Sec. V B). Using such microstructured fiber methodologies, Schmidt *et al.* demonstrated mode areas on the order of 2300 μm^2 in a high power fiber laser.[296] Leakage channel fibers, designed to have selective losses to unwanted modes, are yet another type of microstructured fiber. Dong *et al.* showed that such fibers are capable of producing mode areas up to 3160 μm^2.[297] Dong[298] provides an excellent review of these and other approaches not discussed here, microstructured or otherwise, including HOM-based fiber amplifiers that offer enhanced mode diameter and stability.[299]

The purpose of the aforementioned brief fiber review was to place the optical mode in the context of important light-matter interactions with the material comprising the fiber. The high-intensity guided wave has a relatively long propagation length (i.e., the fiber length) that can give rise to significant power scaling limitations and, hence, the push towards ever-increasing mode areas. Moving forward, an important modal characteristic includes the effective mode index, n_{eff}, which defines phase matching conditions in a number of nonlinear processes. This value can be determined by computing the propagation constant in the fiber.[300] The mode area also is an important parameter, defining an effective intensity of the mode. The effective mode area (μm^2) is defined to as

$$A_{eff} = \frac{\left(\int_0^{2\pi}\int_0^{\infty} \boldsymbol{E}(r,\theta)\boldsymbol{E}^*(r,\theta) r dr d\theta\right)^2}{\int_0^{2\pi}\int_0^{\infty} (\boldsymbol{E}(r,\theta)\boldsymbol{E}^*(r,\theta))^2 r dr d\theta}, \quad (15)$$

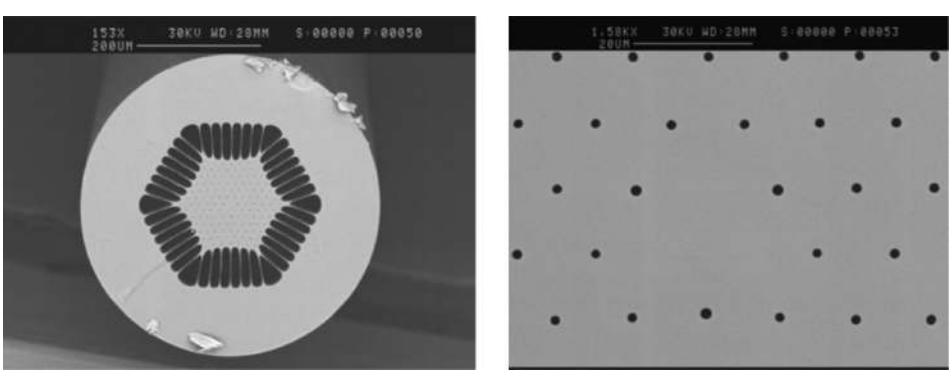

FIG. 16. (a) Scanning electron micrograph of the air-clad fiber from Ref. 295. (b) Close-up of the core region, showing a large-pitch microstructure. Reproduced with permission from J. Limpert, Opt. Express **11**, 818 (2003). Copyright 2003 OSA Publishing.

where $\mathbf{E}(r,\theta)$ is the electric field distribution of the optical mode in all fiber regions. Calculation of this value therefore requires determination of the optical mode profile, $\mathbf{E}(r,\theta)$. Furthermore, measurements of those fiber characteristics relevant to fiber lasers generally are not made directly on the material itself. Rather, the waveguide and the material comprising it cooperate to define measureable optical *mode* properties, from which *material* parameters can be inferred.

To illustrate this, Fig. 17 shows a fictitious RIP for a slightly graded index, high-NA core-clad fiber, along with the calculated intensity distributions for the LP_{01} and LP_{04} modes at 1030 nm. The GRIN structure of the core clearly indicates that the composition varies in the radial direction. As such, the mode itself does not reside in a homogeneous material, but instead overlapping regions of differing properties. In the case of the LP_{01} mode, ~88% of the total power is confined to the region between the two vertical dashed lines (integrated in two dimensions). Since this region has a relatively "flat" profile (a horizontal line is added as a guide for the eye), the mode characteristics will closely resemble the property of the material there. Hence, more generally, if the mode is tightly confined to the core center, it may be a good simplifying approximation to take any measured mode properties as simply those of the material. Turning now to the LP_{04} mode, it may seem that with the high central intensity a similar conclusion could be drawn. However, in this case only ~32% of the optical power lies in the defined region. Therefore, the overlap of the mode itself with the compositional profile must be included in any analysis.

Figure 18 provides another illustration of the importance of the compositional profile and an inhomogeneous distribution of glass constituents. It shows the RIP of a fictitious fiber with relatively low NA, along with the corresponding LP_{01} mode intensity profile (solid curves). The core is taken to be a binary silicate, possessing an index-raising, *but dn/dT-lowering*, constituent. Logically, the central part of the core should have the lowest SiO_2 content, thereby the highest index and lowest value of dn/dT. With the increase in T, the index of the central region increases at a rate lower than the surrounding glass, resulting in a non-uniform reduction in the fiber Δn. This is shown as the "High T" RIP in Fig. 18

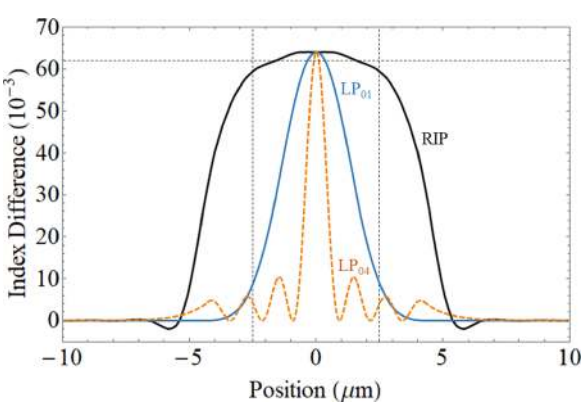

FIG. 17. RIP for a fictitious fiber with relatively high NA along with the LP_{01} and LP_{04} mode intensity profiles. 88% of the power in the LP_{01} mode lies within the region bounded by the vertical dashed lines. That value is 32% for the LP_{04} mode.

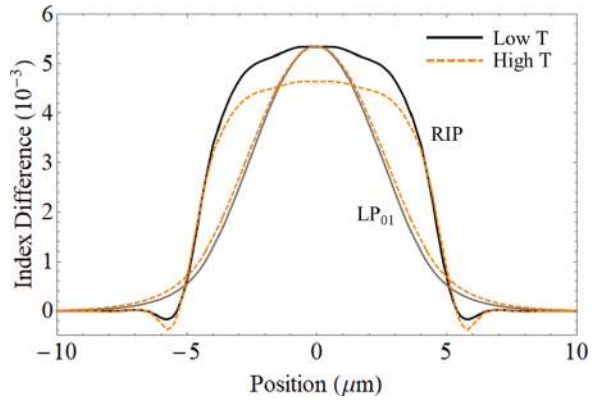

FIG. 18. RIP for a fictitious fiber at room temperature with relatively low NA shown with the corresponding LP_{01} mode intensity profile (solid curves) at 1534 nm. To illustrate the effect of inhomogeneous dn/dT, the RIP and mode are shown at an elevated temperature (orange dashed curves).

(orange dashed curve). Accurate calculations of the modal properties at elevated temperatures, therefore, may require that this inhomogeneous relative change in index be taken into account.

We conclude this section with a brief discussion of the refractive index. The composition of the glass comprising the fiber drives its refractive index, which in-turn defines the RIP. Key to the design of a fiber RIP, therefore, is to know the index of a given material and how it depends upon the optical wavelength. Cauchy[301,302] was the first to identify a simple empirical dispersion equation (nearly 200 years ago!) which has the general form

$$n(\lambda) = \sum_{i=0}^{\infty} \frac{A_i}{\lambda_i^2}, \tag{16}$$

where the A's are empirical parameters that can be found from fittings to data. Clearly, Eq. (16) does neither account for resonance-like absorption peaks nor processes involving gain, and therefore can be construed to be valid for transparent materials. Starting here, Sellmeier[303] proposed what was to become a widely used empirical relationship

$$n^2(\lambda) = 1 + \sum_{i=1}^{\infty} \frac{A_i \lambda^2}{\lambda^2 - \lambda_i^2}, \tag{17}$$

where A_i and λ_i are fitting parameters. Most typically, only two or three terms of the summation are sufficient to describe the refractive index of a material across a meaningful wavelength range. While the Sellmeier equation possesses obvious singularities (resonances), it does nicely account for the tails of absorption features that may be found in the ultraviolet or mid-infrared regions of the optical spectrum. A drawback to this equation is that it covers a single, homogeneous material and does not directly facilitate glass design for achieving particular target values. Regardless, the literature is rich with Sellmeier coefficients for a number of different glasses,[304–309] and even includes a very nice web-based database.[310] For an arbitrary composition, a "mixed" Sellmeier equation may be used.[23,311] In the case of a binary glass

possessing constituents a and b, Fleming[312] provides the following simplified expression:

$$n^2(\lambda) = 1 + \sum_{i=1}^{N} \frac{\left(A_i^a + X\left(A_i^b - A_i^a\right)\right)\lambda^2}{\lambda^2 - \left(\lambda_i^a + X\left(\lambda_i^b - \lambda_i^a\right)\right)^2}, \quad (18)$$

where X is the mole fraction of constituent b. In this way, a glass can be designed for a specific application. Of course this requires that one have knowledge of the Sellmeier coefficients of any (pure) potential glass constituent. This can be challenging, especially as many materials, such as Al_2O_3, do not form pure glasses and therefore these data must be inferred from mixtures. Regardless, limited literature data can be found for pure "glassy" silica additives, such as for SiO_2,[312] GeO_2,[312] Al_2O_3,[313] although most of the literature is dedicated to multicomponent glasses. The Sellmeier coefficients can be identified from these multicomponent glasses using a procedure to be discussed in Sec. V C.

Sometimes, what qualifies as a silicate constituent can have very surprising properties. A well-known case-in-point is often referred to as the $AlPO_4$ join. Both Al_2O_3 and P_2O_5 raise the refractive index when added to silica. However, when present together, they form the bond ≡Al-O-P≡, preserving the tetrahedral network.[314] In contrast to alumina and P_2O_5, the $AlPO_4$ unit actually *decreases* the refractive index when added to silica.[315] It is believed that in fiber, $AlPO_4$ formation is complete, and should the starting concentrations of Al and P not be equimolar, the glass will be rich in either Al_2O_3 or P_2O_5. Likhachev *et al.*[316] showed that this phenomenon imprints upon Er^{3+} emission spectra, as P-rich fibers possessing $AlPO_4$ have emission spectra resembling those from phosphosilicate glass. The same was found to be true of Al.

Finally, a brief discussion of the dispersion characteristics of the RIP is useful. Using the data in Fleming,[312] Fig. 19 shows the refractive index difference for a pure SiO_2-clad germanosilicate core fiber for three different GeO_2 concentrations. While the refractive index does indeed change across this wavelength range (it decreases with the increase in the wavelength), Δn is not a strong function of wavelength. This is interesting from a practical perspective, as a measurement of the refractive index *difference* at one convenient wavelength in the near IR can cover a much broader wavelength range.[317]

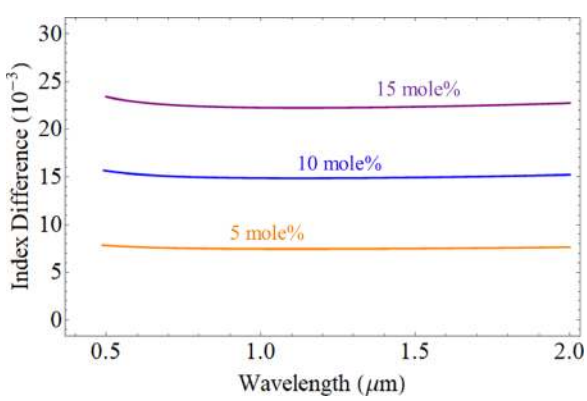

FIG. 19. Refractive index difference for a GeO_2-doped silica core clad in pure silica for three different GeO_2 concentrations using the data from Fleming.[312] Δn is very uniform, especially in the range from about 900 nm to 2000 nm.

B. Nonlinear interactions

In Secs. II–IV, the glass was treated simply as a host for the laser active rare earth ions. Its impact on rare earth (RE) spectroscopy was outlined and the importance of avoiding concentration quenching effects was discussed. These RE doped glasses then are used in fiber laser or amplifier systems, usually in applications requiring the continued scaling of optical power. Power scaling is not indefinite and oftentimes is limited by the appearance of strong interactions between the light wave and host medium. This section will briefly review nonlinear optical phenomena as one such example of deleterious light-matter interactions in high power fiber laser systems. Specifically treated are stimulated Brillouin scattering (SBS), stimulated Raman scattering (SRS), processes connected to the nonlinear refractive index (n_2), and, finally, thermally driven transverse mode instability (TMI), in that order. While it is conceded that nonlinear processes can be harnessed and beneficially utilized in fiber-based applications, here the perception is that which renders them undesirable.

1. Stimulated Brillouin scattering (SBS)

Brillouin light scattering is an acousto-optic process involving hypersonic (~10 GHz) sound waves and the light wave in the fiber.[318–320] From a bath of acoustic phonons (i.e., in the material),[321] a forward-going optical field will select and scatter from those acoustic waves that are Bragg-matched to it, or where $\lambda_a = \lambda_o/2n_{eff}$. The subscripts "a" and "o" denote the acoustic and optical wavelengths, respectively, and n_{eff} is the modal effective area. The acoustic wave is a longitudinal pressure wave, and it is the spatially modulated refractive index, resulting from the photoelastic effect, from which the optical wave scatters. The forward-going optical and acoustic fields are co-propagating, and therefore the scattered wave is Stokes' shifted by the acoustic (or Brillouin) frequency ($\nu_B = \frac{V_a}{\lambda_a}$, where V_a is the acoustic velocity). This process is the spontaneous form of Brillouin scattering (spBS). With the increase in the optical power, the scattered and forward-going optical waves interfere, strengthening the acoustic wave through the process of electrostriction. This positive feedback cycle (illustrated in Fig. 20) and subsequent growth of the scattered wave intensity with the increase in the power is governed by the Brillouin gain coefficient (g_B or, interchangeably, BGC), given by[318]

$$g_B = \frac{2\pi n^7 p_{12}^2}{c\lambda_0^2 V_a \rho \Delta\nu_B}. \quad (19)$$

Here, n is the linear refractive index, p_{12} is the transverse photoelastic (Pockels) coefficient, c is the velocity of light in vacuum, ρ is the glass density, and $\Delta\nu_B$ is the Brillouin linewidth. Owing mainly to the strong dampening, or attenuation (material coefficient γ_m), of such hypersonic acoustic waves

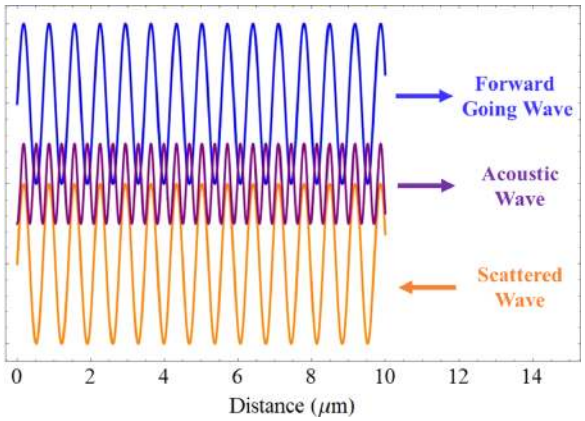

FIG. 20. Illustration of the SBS process. A forward-going optical wave (blue) propagates in the medium. This wave scatters from an acoustic wave (purple) that is Bragg-matched to it. With the increase in the optical power, the scattered (orange) and forward waves interfere, strengthening the acoustic wave, thereby enhancing the reflectivity. This positive feedback cycle continues with the increase in the power, resulting in the stimulated form of Brillouin scattering.

in the glass (~100 dB/mm[322]), Brillouin scattering has a finite bandwidth ($\Delta\nu_B$ ~10s to 100s of MHz[323]) and possesses a natural (Lorentzian) line-shape. $\Delta\nu_B$ must clearly therefore be proportional to γ_m.

In the transition from spBS to SBS, the acoustic wave becomes a highly efficient reflector, limiting the optical power available at the output end of a fiber laser system. Defining a threshold for the onset of SBS depends on the specific system, i.e., by answering the question "when does Brillouin scattering start doing bad things?" In a simplified mathematical way, one can begin with the equation for the evolution of the Stokes' power (P_s) in the fiber[318,324]

$$\frac{d}{dz}P_s(z) = -g_B P_s(z)\frac{P_p(z)}{A_{eff}^p} + \alpha_B(z)P_s(z), \tag{20}$$

where α_B is the amplifier gain coefficient at the Stokes' frequency and P_p is the pump power. P_p is the laser or amplifier signal power and not the pump that was used to excite the laser medium (e.g., 976 nm for either Yb^{3+} or Er^{3+}). Usually, a practical system will require that $P_s/P_p \ll 1$ (such as arbitrarily selected to be 0.1% at the fiber input). In that limit, $P_p(z)$ and $\alpha_B(z)$ can easily be calculated for a laser or amplifier,[325–327] with commercial software packages being readily available.[328,329] With an assumption of an effective Stokes' input power [$P_s(z = L)$],[324] subsequently solving Eq. (20) gives $P_s(z)$. Finally, the user then must decide on the maximum tolerable Stokes' power at some position along the fiber, such as $P_s(z = 0)$.

Based on some values for optical fibers typical of the time, Smith[324] famously derived a generalized "back-of-the-envelope" equation for the threshold for the onset of the stimulated form of Brillouin scattering as

$$P_{th}^{SBS} = 21\frac{A_{eff}}{g_B L_{eff}}. \tag{21}$$

Here, A_{eff} is the effective area of the optical mode and L_{eff} is the effective length, given by $L_{eff} = \frac{1}{\alpha}(1 - \exp(-\alpha L))$, which accounts for a non-uniform axial power distribution resulting from fiber loss (α is the optical attenuation coefficient in units of m^{-1}). In the limit where the fiber length, L, is very long, $L_{eff} \rightarrow 1/\alpha$. The physical threshold condition embodied in Eq. (21) is the power at which the pump power (P_p) is equal to the Stokes' power (P_s) at the fiber input end. From a practical standpoint, this threshold condition may indeed be somewhat generous. Additionally, the coefficient "21" depends on a variety of parameters that can vary from fiber-to-fiber. Regardless, Eq. (21) seems to have been generally accepted as a reasonable starting point in designing a system.

The fiber, while acting as an optical waveguide, also acts as an acoustic waveguide. Jen *et al.*[330–333] performed much early work analyzing the hypersonic acoustic guidance properties of optical fibers, including the impact of dopants. They found that, analogous to the optical case, the fiber can be either guiding or anti-guiding to longitudinal acoustic waves. The former case requires that the acoustic velocity of the core be less than that of the cladding.[331] To complete the analogy, one also may define a local acoustic index as the cladding acoustic velocity divided by the value at positions in the radial direction.[334] An acoustically guiding fiber, therefore, has an acoustic index in the core that is greater than that of the cladding. Interestingly, such acoustically guiding fibers generally also are acoustically multimode. Shibata *et al.*[335,336] first experimentally identified higher order longitudinal acoustic modes (HOAMs) in such an optical fiber. Since these modes also must have an associated transverse profile, Eq. (19) can be corrected with a scaling factor $\Gamma = \int E(r,\phi)^* u(r,\phi)E(r,\phi)\, dA \leq 1$, i.e., with an acoustic-optic overlap integral, where E is the normalized electric field (optical mode) and u is the power-normalized acoustic displacement field (acoustic mode).[320] Figure 21 gives an example BGS for an acoustically guiding fiber that exhibits HOAM interactions. Stronger peaks clearly belong to acoustic modes that have increased overlap with the optical field. Dragic *et al.*[337] recently provided evidence of HOAMs in an acoustically anti-guiding fiber.

Due to its spectral bandwidth, SBS has the strongest impact on laser signals that have a narrow linewidth ($\Delta\nu_L \ll \Delta\nu_B$). Where this is not the case, Eq. (19), with good approximation,

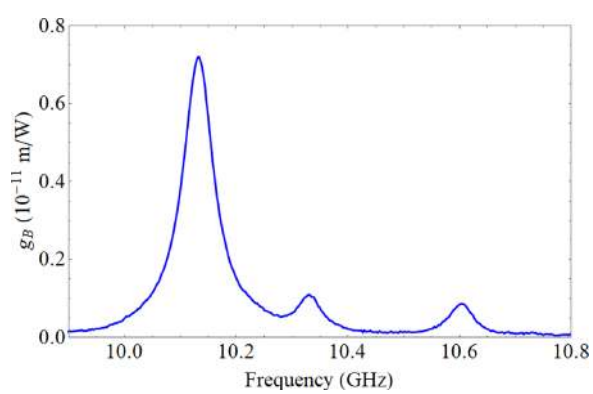

FIG. 21. Example of a BGS exhibiting HOAM interactions (in a P_2O_5 doped silica core fiber taken at a wavelength of 1534 nm). The azimuthally symmetric L_{om} modes have the highest overlap with the single mode optical field. The spectrum exhibits several Lorentzian lineshape features that can be assigned individually to the L_{01}, L_{02}, etc., acoustic modes.

can be scaled by the quantity $\Delta\nu_B/(\Delta\nu_L + \Delta\nu_B)$.[318] Therefore, when allowed by system constraints, broadening the laser spectrum appears to be the most effective means to avoiding SBS.[338] For example, assuming that $\Delta\nu_B = 58$ MHz[339,340] at 1050 nm in an Yb-doped fiber, operating with $\Delta\nu_L = 5.8$ GHz can offer a 100-fold increase in the SBS threshold power. Indeed, this has been a key to recent power scaling efforts.[341–345] White *et al.*[346] recently demonstrated 1.6 kW CW operation by employing a chirped modulation (laser linewidth broadening) scheme. Since $\Delta\nu_B$ usually is proportional to the square of the acoustic frequency[318,347–349] (which is inversely proportional to the optical wavelength), g_B has no dependence on wavelength aside from any chromatic dispersion in n or p_{12}.[350] However, since longer-wavelength lasers (such as 2.0 μm in Tm^{3+}) have Brillouin frequency shifts at lower frequencies, they possess lower intrinsic $\Delta\nu_B$ values. This enhances the relative effectiveness of broadening the laser spectrum in order to suppress SBS. For instance, the same $\Delta\nu_B = 58$ MHz at 1050 nm is ~16 MHz at a wavelength of 2 μm, but with roughly the same g_B. To conclude, short pulses with wide spectra and short interactions lengths also can be configured to avoid SBS.[351,352]

The review of Eq. (21) further suggests that by increasing A_{eff} and/or decreasing L_{eff} the SBS threshold can be elevated. The former is achieved with the LMA fibers discussed in Sec. V A. To shorten the requisite length of active fiber, an increase in the strength of pump absorption is necessary. This can be done by increasing the RE concentration (but while avoiding other deleterious effects such as lifetime quenching), sensitization by Yb^{3+} (where appropriate, as discussed previously), or by increasing the core size relative to the cladding (pump guide). All this being said, maximum power levels in narrow linewidth fiber systems still hover around the 1 kW mark.[353]

Several other methods have been proposed to suppress SBS with varying degrees of success. Most serve to somehow broaden the apparent Brillouin spectrum, $\Delta\nu_B$ (rather than $\Delta\nu_L$), thereby decreasing the peak Brillouin gain, g_B. First, axial gradients that cause the local Brillouin frequency to vary along the fiber can be implemented. For example, the fiber can be engineered to possess an axially varying core size[354,355] or composition.[356,357] One also can actively apply temperature[358,359] or stress and/or strain[360–362] distributions along the fiber length. The active techniques rely specifically on the responses of the host material's refractive index and acoustic velocity to temperature changes or applied strain.

Figure 21 hints at another way to suppress SBS. If the relative acousto-optic overlap integrals (i.e., interaction strengths) of the various acoustic modes could somehow be equalized, the maximum g_B may be reduced. For instance, a fiber possessing two Brillouin lines of equal strength would have half the g_B value of a fiber exhibiting a single line (assuming all have the same spectral width). Additionally, acoustic anti-guidance could potentially be built into the structure to further broaden $\Delta\nu_B$, since in the presence of acoustic waveguide-based attenuation (γ_{wg}), $\Delta\nu_B \propto (\gamma_m + \gamma_{wg})$.[363] A properly configured acoustically anti-guiding fiber, therefore, will have a γ_{wg} that is at least comparable to γ_m.[363] Acoustic anti-guidance requires that some region of the core has an acoustic velocity greater than that of an outer region. For pure silica claddings, this can be accomplished by adding Al_2O_3,[331] MgO,[364] or Li_2O[317] to the glass as they raise the acoustic velocity.

The preceding paragraph gave examples of Brillouin characteristics that can be realized through engineering of the fiber's transverse direction. Several groups have developed fibers incorporating those features for the suppression of SBS.[363,365–368] However, it seems that these fiber designs become increasingly challenging to implement and especially are more complicated from a manufacturing standpoint, as the core diameter becomes larger.[363,369]

Aside from the use of laser line-width broadening, each of the aforementioned SBS suppression techniques relies on the broadening of $\Delta\nu_B$ via some modification of one or more properties of the waveguide (either in the transverse or axial directions). However, Eq. (19) for g_B, at its most basic, is entirely material-based. Another approach, therefore, to mitigating SBS is the selection and use of materials that possess intrinsically low g_B.[370–373] In principle, this approach appears to be relatively straight forward: make use of fiber dopants that increase the values in the denominator while decreasing those in the numerator. Particularly interesting of the latter is that the p_{12} photoelastic constant can take either positive or negative values. Hence, by combining materials of positive and negative photoelasticity, it may be possible to achieve a glass composition where $p_{12} = 0$, and therefore $g_B = 0$.[374] So, the suppression method is simplified further yet: use a host that exhibits no SBS. This condition can be explained as one where the presence of the acoustic pressure wave does not impart a change in the relevant refractive index component, thereby precluding the occurrence of an interaction.

Ballato and Dragic *et al.* have shown that the use of the following dopants can bring significant reductions to the values of p_{12}: Al_2O_3,[374] La_2O_3,[375] BaO,[376] SrO,[377] MgO,[363] and Li_2O and Na_2O.[378] It turns out that fibers with the compositions required to realize significant reductions in g_B (>10 dB) are not those that currently can be fabricated using conventional CVD techniques. Instead, the molten core approach was used in fabrication; more details can be found in the literature.[371,379] With a reduction in g_B by almost 20 dB in an aluminosilicate fiber (relative to a typical telecoms single mode fiber having $g_B \sim 2.5 \times 10^{-11}$ m/W),[374] this appears to be a very promising approach to greatly suppress SBS in both CW and pulsed systems.

2. Stimulated Raman scattering (SRS)

Similar to Brillouin scattering, Raman scattering also is an acousto-optic interaction, but with phonons instead at optical frequencies (~10s THz). Unlike Brillouin scattering, however, there is no well-defined acoustic wave associated with Raman scattering. The simplest classical model for Raman scattering requires that the polarizability of the material not be fixed, but rather be a function of the interatomic spacing. A vibrating molecule, treated as a classical harmonic oscillator, therefore will have time-varying interatomic distances and hence polarizability. This results in a phase modulation of the optical wave and thus also the

associated frequency shift encountered in the Raman scattering process.[323] The Raman gain coefficient, g_R (or interchangeably RGC), is roughly 100 times lower than that of Brillouin scattering[324] and a Raman gain spectrum typical of fused silica is shown in Fig. 22. The spectrum is rather broad, and therefore, for the most part, SRS usually is not dependent on the laser spectral width.

A number of features are visible in the spectrum. The so-called defect lines at 490 cm^{-1} (D_1) and 600 cm^{-1} (D_2) are attributable to "breathing" modes of four- and three-membered rings, respectively.[381] The peak near 800 cm^{-1} (ω_3) is attributed to bending of the Si-O bond. The ω_4 bands (1065 cm^{-1} and 1200 cm^{-1}) are attributable to transverse-optical (TO) and longitudinal-optical (LO) modes.[382,383] However, regardless of the structure in the spectrum, the SRS process will be most efficient near the peak of the gain curve. Smith[324] gives the critical power for SRS to be $P_{th}^{SRS} = 20A_{eff}/g_R L_{eff}$. SRS, therefore, most often is currently encountered in long transport fibers or where the intracavity intensity is high and is expected to become more significant as CW fiber lasers continue scaling in power.[384]

The suppression of SRS typically is accomplished by adding a significant amount of propagation loss to the Stokes' wave. This can be done via fiber design or the addition of grating filters to the fiber. Since the pump and Stokes' waves have considerable spectral separation (10s of nm, depending on wavelength), this can be done with little added loss to the signal wavelength. There are numerous examples available in the literature, including filtering transmission gratings,[384,385] W-type fibers with fundamental mode cut-off,[265] fibers with cladding ring layers,[386] rods,[387] or satellite cores,[388] fibers with enhanced bending loss,[389] and photonic bandgap fibers,[390] to name a few. Going in the other direction, SRS can be used to construct lasers or amplifiers with reasonable efficiency and with potential for low quantum defect.[391–394]

The Raman gain spectrum also is a strong function of the material.[395] Many common fiber-forming dopants, such as GeO_2 and P_2O_5 (the latter when in sufficient quantity), enhance g_R when added to silica.[396] However, in some cases, g_R can be reduced with appropriate choice of material. One such case is the use of Al_2O_3, or more generally aluminosilicate glasses.[372,397] A roughly 3 dB reduction in g_R in an

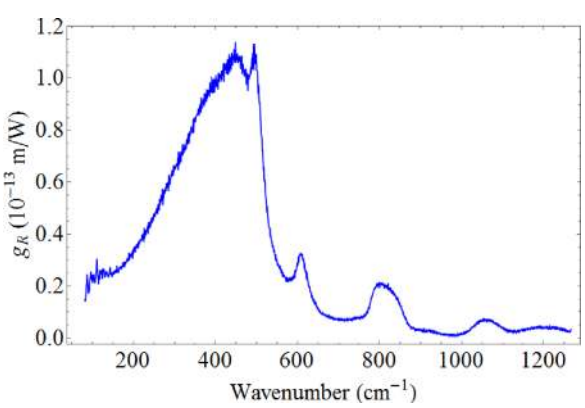

FIG. 22. Typical Raman gain spectrum from pure silica glass. Peak g_R value after Lines at a wavelength of 1050 nm.[380]

yttrium aluminosilicate core fiber was attributed to a combination of (1) increased glass disorder leading to a broader Raman spectrum, (2) using materials with reduced g_R (spread over a wide spectrum), and (3) low overlap with the Raman spectrum of SiO_2. Selection of low-Raman-gain materials may also be guided by the search for low molar volume and bond compressibility parameter materials.[373] Unlike with g_B, it does not appear likely that g_R can be made to be zero.[373]

3. n_2 related phenomena

The Kerr [$\chi^{(3)}$] nonlinearities are represented by a number of various phenomena.[318,323] These include wave-mixing interactions such as four-wave mixing (FWM) and phase modulation processes. The latter group appears to be most significant in the high power, single frequency regime. In short, the refractive index may be written

$$n(I) = n_0 + n_2 I, \tag{22}$$

where n_0 is the zero-intensity refractive index, n_2 is the nonlinear index, I is the optical intensity, and n_2 is on the order of 3×10^{-20} m^2/W for a conventional (silica) single mode fiber.[398] Those Kerr processes influencing the spectral quality of the laser source typically originate from temporal variations in I, leading to phase modulation of the laser signal. These include self- and cross-phase modulation (SPM and XPM, respectively).

Clearly, SPM is a potential obstacle in high power, pulsed, single frequency fiber laser systems. In these configurations, the laser pulse [I(t)] modulates the refractive index [n(I(t))] yielding a self-phase modulated signal. Depending on the application, the resulting spectral broadening may or may not be tolerable in a system. The accumulated nonlinear phase shift is given by $\phi_{nl} = k_o n_2 I L_{eff}$, where k_o is the optical wavenumber ($2\pi/\lambda_o$). Several methods may be used to suppress the effects of SPM. First, the intensity may be decreased by increasing the mode size through LMA fiber design, as previously discussed. Second, the fiber length (L_{eff} considers the non-uniform axial distribution of power) may be kept very short. Zhao *et al.*[399] recently showed that by shortening the gain fiber and increasing the pump power, the influence of SPM could be limited. However, such configurations come at the expense of laser efficiency.[400] Munroe *et al.*[401] pre-compensated for SPM by externally phase-modulating a seed source[402] such that it cancels ϕ_{nl}. Using this methodology, Su *et al.*[403] recently demonstrated a peak power of 1.47 kW in a spectral bandwidth of 185 MHz in a 3.5 m length of 10 μm core diameter ytterbium doped fiber.

SPM need not only appear in pulsed systems but also anywhere where I → I(t). In CW systems, this includes the presence of relative intensity noise (RIN), usually originating at the system seed[404] source. In the context of the previous observations,[405] McNaught *et al.*[406] recently analyzed the effect of RIN on SPM and beam combining efficiency in multi-kW systems and showed that it can be adequately controlled for the application. Zunoubi *et al.*[407] recently described a process by which group velocity induced relative

intensity noise (RIN) resulted in spectral broadening of a two-tone amplifier designed for the suppression of SBS. This was attributed to XPM and group velocity dispersion in a phase modulated signal. Lastly, Anderson *et al.*[408] recently confirmed this with measurements but concluded that it would not be a significant impairment to beam combining efficiency in coherently combined phase fiber laser arrays.

The nonlinear phase shift also possesses a material path towards suppression of Kerr nonlinearities: the utilization of materials with low n_2. Generally, there is a trend of increasing n_2 as n_0 increases.[409] Given that SiO_2 has a relatively low refractive index, its n_2 already is relatively low.[373] However, the use of F[410] or P_2O_5[411] co-doping can further reduce n_2 values. Unfortunately, investigations of high power lasers based on such glass materials (specifically tailored for the reduction in n_2) appear to be lacking in the literature.

Finally, it is important to point out that the Kerr nonlinearity also can result in catastrophic optical damage to an optical fiber operating at high power.[412] In short, high optical intensity leads to an increased refractive index, effectively increasing the core-cladding Δn. This results in a reduction in the mode diameter, and therefore an increase in the mode intensity. As the power grows along a segment of gain, the mode therefore decreases in size, eventually to a point where the glass can no longer support the power density and optical damage results. In the case of silica, the optical power would need to approach the order of ~MW in a tightly focused spot.[413,414] Such power levels were successfully reached by several fiber-based configurations.[415–417]

4. Transverse mode instability (TMI)

Owing to the importance of the problem, there are number of excellent papers and reviews in the literature dedicated to TMI.[418–422] Therefore, this section will be kept brief, and mainly within the spirit of the paper generally, with the focus mainly on the material. TMI is known to be a nonlinear process that causes a beam of relatively high quality to become multimode and dynamic.[423] Ironically, TMI appears to be a problem largely brought about by the waveguide. Efforts to enhance A_{eff} for the suppression of the aforementioned nonlinear interactions usually led to LMA fibers that were at least few moded. As discussed in Sec. V A, this has led to a number of waveguide designs that achieve effective single mode operation. In TMI, the weak HOMs interfere with the fundamental (or the desired) mode, resulting in an intensity pattern that interacts with the gain dynamics of the laser. Depopulation of the excited upper state is strongest where the intensity is greatest, and therefore a thermal pattern is generated through quantum defect heating. This thermal pattern obviously then must be driven by the aggregate modal interference intensity pattern. Via the thermo-optic effect, this thermal distribution becomes a refractive index pattern (or grating) and thereby a potential path for mode coupling. For more details on the various models for this process, the reader is directed to the reviews identified above.[418–422]

Dong[424] provides a derivation of the TMI threshold in the context of stimulated thermal Rayleigh scattering (STRS), such that

$$P_{th}^{TMI} \propto \frac{\rho c_p}{dn/dT}\left(\frac{\lambda_s}{\lambda_p} - 1\right)\mathcal{F}, \tag{23}$$

where ρ is the mass density, c_p is the specific heat, and $\mathcal{F}$ is a function that accounts for the mode overlap and frequency distributions. The parenthetic term is the quantum defect (QD; discussed previously), where the subscripts "s" and "p" refer to the signal and pump wavelengths, respectively. Several recent proposals for the enhancement of the TMI threshold have focused on increasing $\mathcal{F}$. These include carefully controlled fiber tapers,[425] low-NA fibers to limit mode content,[342] fibers with engineered RIPs to reduce spatial overlap between modes,[426] optimized pumping direction relative to the signal,[427] and fibers that have enhanced HOM loss,[428,429] to name a few.

Considering once again the material parameters in Eq. (23), a fiber with $dn/dT = 0$ should not have a TMI limitation.[372] Although suggested, this has not yet been widely studied in the literature. Indeed, such a fiber can be achieved with appropriate combination of materials possessing positive (e.g., SiO_2) and negative (e.g., P_2O_5[430]) dn/dT values.[431] The use of a strictly single mode fiber also should obviate the need for TMI suppression. However, in light of the nonlinear parasitics described above, this may not be feasible without the consideration of less conventional glasses for high-power fiber laser applications.

Finally, to conclude this section, a dn/dT-associated damage limit is briefly discussed: thermal lensing. With the increase in the temperature, where $dn/dT > 0$, there will be an increasing refractive index. Should the refractive index difference between the core and cladding increase due to such an increase in fiber temperature, this will lead to a reduction in the mode size.[432] This is fully analogous to the case of self-focusing. Brown *et al.*[433] defines a critical power for the onset of thermal lensing effects to be where the heat induced index change is equal to the starting core-cladding Δn. This critical power is proportional to the inverse of dn/dT, and with its reduction (or even $dn/dT = 0$), damage thresholds can therefore be significantly elevated. Under typical circumstances, however, it seems that thermal lensing is not the most significant power scaling limitation to high power operation.[2]

C. First principles to model glass properties

This section summarizes semi-empirical equations that enable the investigation, prediction, and calculation of typical properties (e.g., refractive index, mass density) in multicomponent glasses, using only a few experimental data points. The presented tools are of interest as they offer simple, yet efficient and effective, ways to interrogate any given glass system and predict, within a certain degree of accuracy, their properties.[434,435] This section is not intended to provide a review of all the models found in the literature that can be used to calculate typical glass characteristics. Indeed, a very

nice review on glass modeling has been provided by Volf.[436] Instead, this section will focus on the set of models developed by the authors, as they have uniquely been applied to optical fibers of interest for fiber laser applications. The simple computational tools described herein can be utilized to engineer multicomponent hosts with tailored properties, specifically geared towards the improvement of fiber laser performance, such as through a deliberate reduction of one or more nonlinear gain coefficients.[437]

The additive models presented herein treat the glass as a homogeneous (or well mixed) one (i.e., no heterogeneities, phase separation, and crystallization) in which its constituent species are considered to be fully independent. This is illustrated in Fig. 23, wherein a homogeneous glass composed of a mixture of compounds A and B, (1) can be considered as the sum of two *independent* glass segments comprised of compounds A and B, respectively (2). To exemplify the additivity approach, consider one of the most fundamental glass properties, the refractive index, in a well-mixed binary glass (e.g., $SiO_2 + GeO_2$ or A + B) comparable to situation (1) in Fig. 23. The time-of-flight for the light to travel the distance L is

$$t = \frac{Ln}{c}, \tag{24}$$

where n is the glass refractive index and c is the speed of light in vacuum. Now, considering situation (2) in Fig. 23, in which the light would propagate successively in compound A for the distance L_A and in compound B for the distance L_B, the above equation can be re-written as follows:

$$t = \frac{L_A n_A}{c} + \frac{L_B n_B}{c}. \tag{25}$$

Setting Eqs. (24) and (25) equal to each other yields

$$n = \frac{1}{L}(L_A n_A + L_B n_B). \tag{26}$$

Through inspection of Fig. 23, it is clear that the terms L_A/L and L_B/L give the volume proportion of constituents A and B in the binary glass. These volume fractions are now defined to be m_A and m_B, respectively. Written in terms of the mole fraction of the constituents [C], m_A is given to be[438]

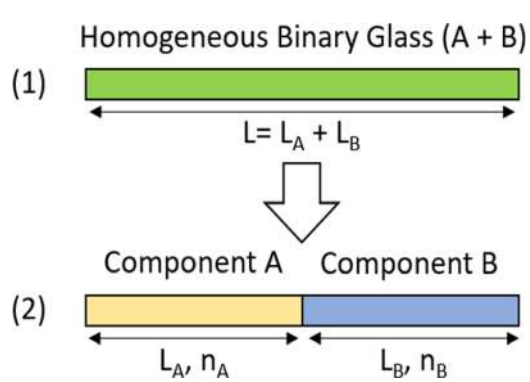

FIG. 23. (1) Illustration of a homogeneous binary glass composed of compounds A and B and (2) the same glass, in which compounds A and B are considered to be independent of each other.

$$m_A = \frac{\frac{M_A}{\rho_A}[C_A]}{\frac{M_A}{\rho_A}[C_A] + \frac{M_B}{\rho_B}[C_B]}, \tag{27}$$

where M_A, ρ_A, and M_B, ρ_B are the molar masses (kg/mol) and mass densities (kg/m^3) of components A and B, respectively. In the case of a binary material $m_B = 1 - m_A$. Dragic[370] provides equations for the case of a ternary glass, which, through symmetry arguments, can be expanded to any arbitrary multicomponent system, leading to a generalized expression for the refractive index

$$n = \sum_i m_i n_i. \tag{28}$$

Equation (28) can be further generalized to consider a variety of other glass properties via[439]

$$G = \sum_i g_i x_i, \tag{29}$$

where G is the aggregate glass [homogeneous, like in (1) of Fig. 23] property, g_i is the property of each individual compound that makes up the glass, and x_i is the additivity parameter (e.g., volume, mole, or weight fraction). The choice of the latter is a strong function of the glass property. As was shown for the case of the aggregate refractive index, g is the constituent refractive index n, and x is the *volume fraction* m of that constituent. As the additivity parameter, the volume fraction has been shown to be very good for the refractive index,[440] mass density,[370] acoustic velocity,[439] thermo-optic coefficient (dn/dT),[430] and nonlinear refractive index (n_2).[313]

At this point, it is important to state that the additive model does not necessarily give any insights into the structure of the glass. It mainly serves the purpose to efficiently determine parameters useful in the design of glass optical fibers. Furthermore, the assumption that the glass is separable into its constituents is reasonable for network-forming additives (such as GeO_2 and B_2O_3). For network modifiers (such as BaO or Li_2O) or intermediates (such as Al_2O_3), the additive models are best construed to be more a portrayal of how the non-silica constituent changes the properties of SiO_2. Moreover, one must be careful using these models and the choice of compound species. One well-known example is the co-addition of Al_2O_3 and P_2O_5 into silica glass. As described in Sec. II A, when added independently into silica, Al_2O_3 and P_2O_5 both raise the linear refractive index; however, co-doping of both species together usually results in the formation of $AlPO_4$, which is known to instead lower the refractive index.[241,314] Therefore, in this case, $AlPO_4$ should be considered as the independent glass species.

Other relevant glass properties do not add directly through Eq. (29), but instead are carried through the calculation by another parameter. Two such examples are the longitudinal and transverse Pockels coefficients, p_{11} and p_{12}, respectively. In this case, the following were proposed to be additive:[378,441]

$$C_1 = \frac{1}{2}n^3[p_{11} - 2\nu p_{12}], \tag{30}$$

$$C_2 = \frac{1}{2}n^3[p_{12} - \nu(p_{11} - p_{12})], \tag{31}$$

with Eq. (31) often referred to as the strain-optic coefficient.[442] In Eqs. (7) and (8), the photoelastic constants and Poisson ratio (ν) are those of the individual constituents (e.g., SiO_2 or GeO_2). The right-hand-side of Eq. (29) contains the summation of the individual C's of the constituents, while the left-hand-side gives the aggregate values. Assuming that ν is additive through the volume fraction (although this has not yet been verified), Eqs. (30) and (31) can be recast for the mixed glass, leading to a system of two equations that can be solved for the two unknowns (p_{11} and p_{12} of the multicomponent glass). In the case of p_{12}, one arrives at

$$p_{12} = \frac{2}{n^3}\frac{C_2 + \nu C_1}{(1-2\nu)(1+\nu)}, \tag{32}$$

where n, C_1, C_2, and ν are for the aggregate glass [using Eq. (29)].

Other materials parameters require corrected models in order to well-match observed experimental data. The Brillouin linewidth ($\Delta\nu_B$, which is linearly proportional to the acoustic attenuation coefficient α, m^{-1}) is one such example. This spectral width ultimately gives the lifetime of the phonons involved in the Brillouin scattering process. While this is a strong function of the material, it also is a strong function of the frequency of the interacting acoustic wave(s).[318] Considering the former, adding a material with greater acoustic loss to silica will obviously render broader spectra with the decrease in the silica content. However, if that additive also influences the acoustic velocity, resulting in a change in the interaction frequency, this, in-turn, also will affect $\Delta\nu_B$. Consideration of the latter effect, therefore, requires a correction to the simple additivity formula. Generally, $\Delta\nu_B$ has a square dependency on the acoustic frequency ν_B. However, it was shown that this dependence varies depending on the nature of the glass dopant. For example, B_2O_3-containing silicate glasses exhibit different dynamic viscoelastic damping processes whereby the acoustic attenuation ultimately is not proportional to ${\nu_B}^2$.[349] Most generally, therefore

$$\Delta\nu_B = \frac{V_a}{\pi}\sum_i x_i F_i(\nu_B/\nu_{ref})\alpha_i(\nu_{ref}), \tag{33}$$

where V_a is the acoustic velocity of the aggregate glass, and ν_{ref} is some reference frequency where α_i is tabulated. For the most common materials, $F(\nu_B/\nu_{ref}) = (\nu_B/\nu_{ref})^2$. In Eq. (33), the acoustic frequency is determined by the Bragg condition, $\nu_B = 2V_{a,eff}n_{eff}/\lambda$, where V_a is the phase velocity of the acoustic mode and n_{eff} is the effective index of the optical mode.

In some cases, the volume fraction is not the appropriate additivity parameter. For instance, molar fraction is used for heat capacity.[443] In other cases, mass density serves as a more appropriate additivity parameter. A case in point is the coefficient of thermal expansion (CTE). Indeed, there exist many semi-empirical models to predict CTE in glasses.[444–448] However, Cavillon *et al.*[449] recently developed a simple additive model for the CTE, based on a derivation of the volume expansion in isotropic solids such as glasses. As will be discussed shortly, knowledge of the CTE in an optical fiber can be particularly important where a change in temperature is experienced. The CTE model is summarized as[449]

$$CTE = \sum_i \frac{CTE_i \rho_i y_i}{\rho}, \tag{34}$$

where for a binary system

$$y_A = \frac{\left(\frac{[C_A]M_A}{\rho_A T_A}\right)}{\left(\frac{[C_A]M_A}{\rho_A T_A} + \frac{[C_B]M_B}{\rho_B T_B}\right)}, \tag{35}$$

in which T represents the number of structural units per compound (T_{SiO_2}, $T_{P_2O_5} = 1$ while $T_{B_2O_3} = 2$) and $y_B = 1 - y_A$. Figure 24 shows the result of this additive modeling plotted with CTE data found in the literature. This example helps demonstrate the potential of using simple additivity principles of one property to predict others that are functions of it.

Optical fiber is distinct from bulk glass in that the core may be clad in a material with very different physical properties, including differing CTE values. One of the most common applications that utilizes a differential in CTE is in the fabrication of polarization maintaining (PM) fibers that utilize stress-applying-parts (SAPs) added to the fiber cladding.[450] The SAP regions typically have a larger CTE than the core, and their inclusion results in a frozen-in birefringence after the fiber is drawn. In the case where an inner region has a CTE greater than that of the surrounding cladding, an increasing temperature can result in a change in the strain field.[451] This can impact certain fiber characteristics, including both the refractive index and acoustic velocity. In

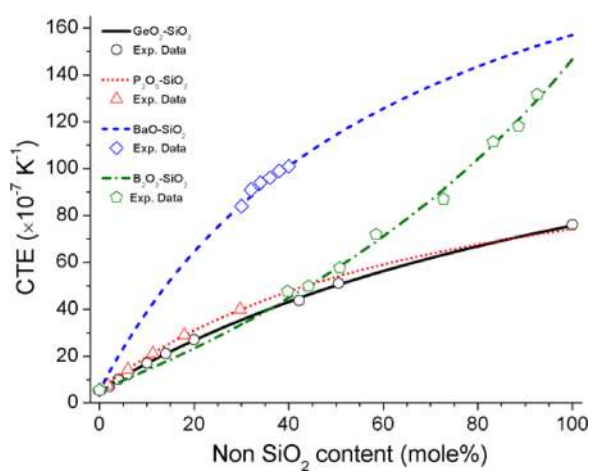

FIG. 24. Coefficient of thermal expansion (CTE) model derived from additivity of density for a variety of binary silicate glasses. Adapted from Cavillon *et al.*[449]

the case of the refractive index, the complete temperature-dependent refractive index (the g term) is given by[452]

$$g_i = n_i = n_{0,i} + \frac{dn_i}{dT}(T - T_0) + \frac{dn_i}{d\varepsilon}\frac{d\varepsilon}{dT}(T - T_0), \quad (36)$$

where n_0 is the room-temperature (T_0) refractive index and dn_i/dT is the bulk TOC. The strain (ε) terms are given by

$$\frac{dn_i}{d\varepsilon} = -\frac{1}{2}n_{0,i}^3\left[2(p_{12,i} - \nu_i(p_{11,i} + p_{12,i})) + (p_{11,i} - 2p_{12,i})\right] \quad (37)$$

and

$$\frac{d\varepsilon}{dT} = -(CTE_{core} - CTE_{clad}), \quad (38)$$

where the CTEs (linear) are for the aggregate core or cladding glass. Equation (37) accounts for strain in all three primary orthogonal directions. For materials that bring a negative dn/dT to silica and also an increase in CTE, cladding the fiber in SiO_2 acts to lessen the effectiveness of dn/dT reduction.[430] This is particularly important to consider when designing a fiber with reduced thermo-optic effect. Dragic *et al.*[453] provide a similar expression for the thermo-acoustic coefficient (TAC, or the change in acoustic velocity with temperature). This also is important as a large TAC enables the suppression of Brillouin scattering through axial thermal gradients.[359,454]

This section is concluded with a brief discussion of the "bulk" values utilized in the aforementioned models. In principle, the determination of the pure constituent parameters (e.g., refractive index, acoustic velocity, photoelastic coefficients, etc.) requires measurements on drawn fibers. However, a new thrust to calculate them from their bulk precursors has recently been initiated.[455,456] These properties usually will differ significantly from their bulk, and often crystalline, counterparts.[376] In these cases, the models provided above are fit to experimental data with the g_i values taken as the fitting parameters. Usually, this requires the presumption of those values for pure silica,[457] although with enough experimental samples, this need not be strictly required. Armed with the g_i values for the constituents, one then can extrapolate to compositions lying outside of the measurement range for the application-specific optimization of any of one or more of the relevant glass characteristics. In the case of one property, it may be dn/dT alone, whereas, for example, multiple properties (V_a, $\Delta\nu_B$, n, ρ, and p_{12}) are required to calculate the Brillouin gain coefficient of a glass host.[318] Dragic *et al.*[435] provided a relatively detailed compilation of these values for a number of co-constituents. Since the additive model is largely empirical, extrapolation should be exercised with caution as any changes to glass structure in extrapolated compositional ranges will likely cause the model to break down.

D. Photodarkening

Many optical glasses are known to be photochromic; that is, possess a transmission spectrum that (or whose apparent color) can change significantly with optical irradiation.[458] This often results from color center (CC) formation via some type of structural change (such as the formation of defects) in the glass which may or may not be reversible. With the goal of applying this to optical fiber, Papunashvili *et al.*[459] studied "the possibility of obtaining an optical fiber with a photochromatic core…" As is now known, this indeed is readily possible, and most often is referred to (as a process) as "photodarkening." This deleterious effect causes a steady decline in fiber laser output power due to the formation of CCs possessing absorption tails extending into the near IR.[460] Limiting the discussion to silicates, early observations of this phenomenon were made in both thulium[461,462] and terbium-doped[463] glasses. Soon thereafter, a form of (unassigned) unsaturable absorption was observed in Yb-doped fibers,[464] possessing similarity with the observed excess optically induced loss spectrum noted in Millar *et al.*[461] Paschotta *et al.*[464] showed that the magnitude of this excess loss is a strong function of Yb_2O_3 concentration.

In the late 1990s and early 2000s, as Yb-doped fiber laser power began to scale, photodarkening (PD) represented a potential hurdle to commercial viability. It is therefore no surprise that early work in trying to understand, and suppress, PD came through the commercial sector. Liekki Oy[465] of Finland (now nLight) and their collaborators did extensive characterization,[465] including identification of a measurement methodology,[466] determination of the PD rate as a function of inversion,[467] studying the distribution of PD in the context of mode spatial distribution in the core,[468] and investigations of thermal bleaching[469] and the effect of pumping wavelength.[470] While much work was subsequently done by these and other groups, a consensus on the causes of PD is still lacking, although most of its effects are widely recognized and well known.

A generalized apparatus used to characterize PD is shown in Fig. 25.[466,467] The fiber under test may be a small-core single mode fiber, or an LMA fiber. In the case of the former, single mode pumps and a wavelength-division multiplexer (WDM) can be used, while in the latter the fiber may be cladding-pumped via fiber-combined MM pumps. A water bath may serve as thermal control, as necessary,

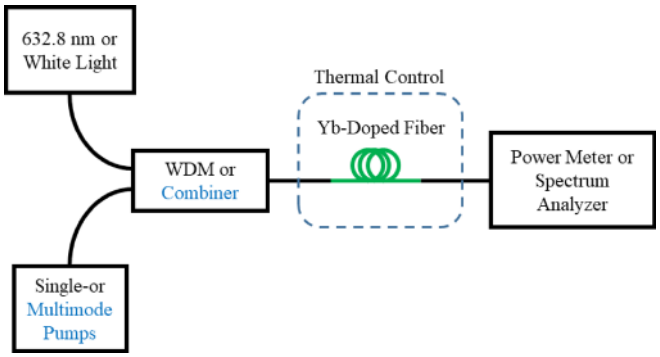

FIG. 25. Measurement apparatus for the characterization of PD in a Yb-doped fiber. Uniform inversion is required throughout the test fiber. For LMA fibers, cladding pumping short segments of fiber through a combiner may therefore be required. This is an accelerated PD procedure, as inversion is not depleted through stimulated emission.

depending on how much heat is deposited into the glass via the quantum defect or other non-radiative processes. Ultimately, with pump power present, the transmittance of light in the visible (using either a white light source or perhaps a single frequency laser such as a HeNe) is measured as a function of any of time, pump power (inversion), and pumping wavelength. Inversion should be as uniform as possible in the fiber to ensure that the PD rate is the same throughout, and this typically requires the use of short lengths of Yb-doped fiber. This way, inversion remains saturated through the fiber length.[467,471] In a real fiber amplifier configuration, due to the requirement of near-complete pump absorption for efficient operation, inversion cannot be length-wise uniform. As such, since PD increases with the increase in the inversion,[467] PD-induced losses in a real system will, therefore, not be axially uniform.[472]

Presumably, the PD process results in the formation of CCs whose number density increases over time. Proportional to this CC concentration, an absorption coefficient may also be determined, or measured. It has been shown that the temporal evolution of the photo-induced loss coefficient (m^{-1}) can be modeled by the widely used stretched exponential function given by[473]

$$\alpha(t) = \alpha_\infty \left[1 - \exp\left(-(t/\tau)^\beta\right)\right], \tag{39}$$

where α_∞ is a steady-state (or saturated) attenuation (for $t \to \infty$), τ is the rate constant, and β is the stretching parameter. The value of β was found to vary from 0.4 to 0.7.[474] The assumption also is usually made that the starting attenuation for the pristine sample $\alpha(t=0)=0$. With regard to units, the total loss expressed in decibels is linearly proportional to α (m^{-1}) and therefore, the stretched exponential function often is fitted to logarithmic data.[475–477] Figure 26 provides an example plot of Eq. (39) (adapted from Jetschke *et al.*[478]). Increasing inversion has the effect of accelerating the PD process with a larger α_∞ also resulting. Jetschke *et al.* provide an expression for the inversion[478] (pumped but not lasing)

$$I = \frac{\sigma_a}{\sigma_a + \sigma_e} \frac{1}{1 + P_s/P_p}, \tag{40}$$

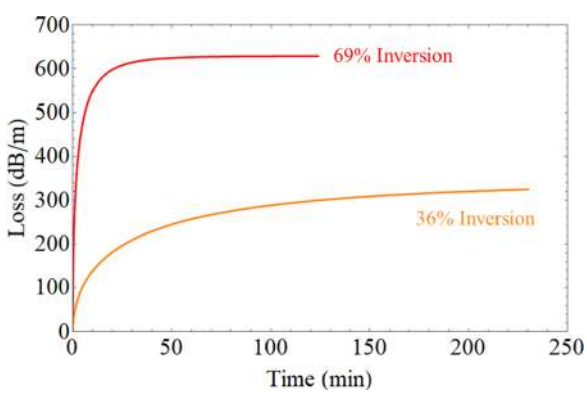

FIG. 26. Plot of the stretched exponential function for two different inversion levels. Adapted from Jetschke *et al.*[478]

where the saturation power $P_s = Ah\nu_p/\tau_s(\sigma_a + \sigma_e)$. Here, $\sigma_{a,e}$ are the absorption and emission cross sections at the pumping wavelength, respectively. Further, P_p is the pump power, A is the fiber cross section, $h\nu_p$ is the pump photon energy, and τ_s is the upper state lifetime. Clearly since $\sigma \to \sigma(\lambda)$, Eq. (40) provides insight into the dependence of PD with changing pump wavelength. Finally, PD is less significant in continuous-wave (CW) than pulsed lasers due to relatively lower steady state inversion in the former. In the latter, inversion can be very high in the time between pulses.

The values of τ measured as a function of inversion can provide some insight into the process by which PD occurs. Specifically, it was found that there is a power-law dependence of the inverse of τ on inversion, I.[470,478] More specifically, this can be represented by $\tau^{-1} \propto I^q$, where I is the fraction of Yb ions that are inverted. Plotting this on a log-log graph results in a line with slope q. The significance of this slope is that it suggests the number of Yb^{3+} ions that may be cooperating in the PD process. While seemingly impactful from the standpoint of understanding the origins of PD, the value for q varies considerably in the literature, ranging from 2.5 to just above 7.[467,470,471,474,477–480] This makes the task of identifying an activation energy quite daunting, as it potentially ranges from around 3 to 9 eV, which can encompass any number of known silica damage processes. Jetschke *et al.*[478] point out that some discrepancy between groups could include uncertainties in fittings-to-data, launched pump power, and realized versus modeled inversion levels.

Regardless of the number of Yb^{3+} ions cooperating in the PD process, it seems clear that there is a physical change to the glass that is facilitated by the creation and subsequent absorption of multiple photons. In Tm-doped silicates, upconversion to higher-lying levels can be very efficient, thereby enabling the emission of potentially damaging UV light.[462] Yb^{3+}, on the other hand, has only one excited state. As such, Tm^{3+} *impurities* have been eyed as a possible intermediary.[481–483] In principle, cooperative energy transfer from a group of Yb^{3+} atoms (and perhaps pump photons) to a local Tm^{3+} ion in the glass may lead to UV photon generation.[246] Jetschke *et al.*[484] analyzed a series of Yb-doped fibers, each roughly equimolar in Yb_2O_3, Al_2O_3, and P_2O_5 content but with varying Tm_2O_3 concentration. These constituents were present in a molar proportion of roughly $10Al_2O_3$:$1Yb_2O_3$:$1P_2O_5$, so largely aluminosilicates. They concluded that the presence of Tm with a concentration of greater than 10 mol-ppm can accelerate and strengthen PD. In contrast, for Tm impurity levels below 1 mole-ppm, there was no observed impact on what they dubbed the "intrinsic" PD. This was recently corroborated by Li *et al.*[485] where PD was still observed in fibers with minimal trace levels of Tm_2O_3 impurity. Jetschke *et al.*[486] extended their work to include fibers of $1Yb_2O_3$:$17P_2O_5$ core composition (a low PD composition, as will be discussed shortly) with varying Tm_2O_3 concentration and obtained similar results. So, indeed Tm appears to have a relatively strong impact on PD, but only when present in sufficient quantity. It is interesting to point out that Jetschke *et al.*[484] found that the addition of Er^{3+} actually reduced PD, but this was attributed to its

reducing the Yb^{3+} inversion and absence of strong upconversion.

The mechanism by which this "intrinsic" PD occurs is still under debate. It is known that it results in the formation of a broad absorption band with a tail that extends well into the near IR. An example of such an induced spectrum is provided in Fig. 27.[466] Excess absorptive (and non-radiative) losses at both the pump and signal wavelengths, even at the ∼ dB/m level are clearly sufficient to result in considerable degradation of fiber laser performance. Jasapara *et al.*[487] suggested that PD may be facilitated by a reduction of trivalent Yb (Yb^{3+}) to divalent Yb (Yb^{2+}) through a process of electron capture. Along those lines, Engholm, *et al.,* proposed that Yb-doped fibers possess a charge-transfer (CT) band near 230 nm.[488,489] Excitation into this band would then result in the formation of divalent Yb (the electron trap) along with a hole bound to a local anion, preserving charge neutrality. Engholm *et al.* therefore proposed the co-doping of Ce into the glass, since it might offer a means to trap electrons ($Ce^{3++} + e^- \rightarrow Ce^{3+}$) or holes ($Ce^{3+} + h^+ \rightarrow Ce^{3++}$) before permanent color centers are formed.[490] Indeed, they showed that the cerium atom can exist in both the 3+ and 4+ valence states in a fiber produced under oxidizing conditions. Others have confirmed the PD-suppressing qualities of cerium,[491–493] including observations of a self-photo-bleaching process that saw a photo-darkened fiber recover somewhat after a period of time.[494] The formation of divalent Yb is supported by additional evidence provided by both Rydberg *et al.*[495] and Wang *et al.*,[496] however, not all groups have observed its presence. Notably, Jetschke *et al.*[493] did not observe Yb^{2+} spectroscopic signatures in Yb-doped aluminosilicates, but did confirm the capability of cerium co-doping to suppress PD. They recommended a Ce/Yb ratio of between 0.5 and 0.7 to be ideal, but has the drawback of influencing (raising) the refractive index.

The REs have an electronic configuration of $4f^N5s^25p^6$ or $4f^{N-1}5s^25p^6$ in their divalent or trivalent phases, respectively. While the $4f^N \rightarrow 4f^{N'}$ transitions are normally those relevant for fiber laser applications, $4f^N \rightarrow 4f^{N-1}5d$ transitions also are possible. The latter are not parity forbidden, and as such can be many orders of magnitude stronger than the

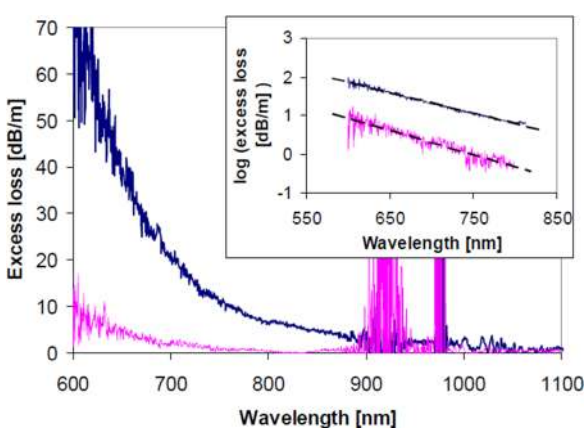

FIG. 27. Typical absorption center produced by the PD process. Reproduced with permission from J. J. Koponen *et al.*, Opt. Express **14**, 11539 (2006). Copyright 2006 OSA Publishing.

former.[82] As these transitions occur at energies in the range of 50 000 to 100 000 cm^{-1},[82] they usually are not observed in Yb^{3+}-doped silicates. In the case of the Yb^{2+}, however, these transitions are at lower energies, about 30 000 to 40 000 cm^{-1} [82,88] and therefore absorption features can be observed extending into the visible wavelength range.[497] These spectroscopic features make the Yb^{2+} identifiable from absorption (or even emission) spectra. Not unexpectedly, the excess absorption in the visible spectral range (see Fig. 27) was therefore assigned by Guzman Chávez, *et al.*, to absorption by Yb^{2+}.[498] Currently, however, there appears to be some consensus that the excess loss instead results from the formation of an aluminum oxygen hole center (AlOHC),[493,495,496,499–501] which possesses considerable absorption/emission activity in the VIS wavelength range. However, the precursor to the formation of the aforementioned hole center is still not yet fully agreed upon.

Another path to color center formation was suggested by Yoo *et al.*,[502] in which they proposed that Yb-ODCs are possible PD precursors. They showed the presence of a broad absorption peak near 220 nm in a pristine preform slice, with irradiation at 488 nm significantly enhancing absorption. They postulated the existence of a Yb-Yb (or Yb-Al) oxygen vacancy defect that may act in a way similar to the Ge-Ge [ODC(I)] oxygen vacancy. In the case of the latter, cleavage of the Ge-Ge bond is known to result in an E' center (≡Ge•) and a free electron, thereby preserving charge neutrality.[503,504] Should the free electron become trapped [Ge(1) and Ge(2) centers[503]], this leads to UV absorption bands that potentially may extend into the IR.[505]

Carlson *et al.*[506] postulated that ODC(II) may act as a precursor through the observation of energy downconversion from ODC(II)→Yb^{3+}. Upon extended exposure at 250 nm, a relative drop in both SiODC(II) and Yb^{3+} luminescence were observed. Further confirmation was later provided by Liu *et al.*[507] through measurements of absorption near 5 eV as a function of Yb and Er number density, observing a linear relationship between the two. Interestingly, they found that this loss in Er doped fiber grew at a much slower rate. They postulated that ODC(II) may act as a precursor through the interconversion of defects, namely, ODC(II)→E',[62] facilitated by upconversion from excited Yb^{3+} ions, and that the fiber draw itself may influence the observed distribution of defect phases. It is worth noting that Dragic *et al.*[508] showed that rare earth doped fibers seem also to possess a preponderance of oxygen hole centers, which can be excited through a two photon process starting in the infrared.[509] This suggests that the defect distribution in the glass can be rather complex. In a very thorough study, Mattsson[510] considered ODC(II) as instead playing a role in PD through a complex energy transfer process involving Tm^{3+} or Er^{3+} trace impurities.

Regardless of the physical mechanism, great strides have been made in suppressing PD. As described above, cerium co-doping has proven to be very effective. Early on it also was shown that the use of alumina[477,511] can reduce the strength of PD. Through an analysis of fibers with a range of Al/Yb ratios, Jetschke *et al.*[512] concluded that the absolute quantity of alumina in the glass, rather than the Al/Yb ratio,

drives PD, suggesting that Yb_2O_3 clusters are probably not completely removed via alumina doping. Nevertheless, it was soon found that the phosphosilicates possess much more resistance to PD than aluminosilicates.[480,513] Suzuki *et al.*[514] demonstrated a highly Yb-doped P_2O_5 co-doped, low-PD fiber which exhibited some loss recovery after the pump was switched off. Jetschke *et al.*[515] observed a similar recovery behavior in earlier work.

Jetschke *et al.*[516] showed that very low PD behavior can be obtained for an Al-P co-doped fiber, and a low NA simultaneously achieved due to the formation of low-index $AlPO_4$. They suggested an Al-to-P ratio of 1 (molar) may be optimal. An additional observation was made in that there was a reduction in Yb-Yb cooperative luminescence in fibers exhibiting reduced PD. This was corroborated by Deschamps *et al.*[517] who suggested that this results from the complete dissolution of Yb^{3+} clusters[518] by P_2O_5, thereby suppressing PD. Additionally, Deschamps *et al.*[501] showed that since P and Al tend to form the $AlPO_4$ join (discussed in Sec. V C), P/Al ratios of greater than one can effectively prevent the formation of AlOHCs (in a radiodarkened glass). They also found that Al-O-P linkages were in the vicinity of Yb^{3+} when P > Al and not vice versa. More recently, similar conclusions were drawn in sol-gel derived glasses.[496] An extensive study of the various P-associated diamagnetic centers was recently carried out by Giacomazzi *et al.*[519] Needless to say, there are considerable advantages to the co-doping of alumina and P_2O_5, enabling low-NA and low-PD fiber, both cooperating to make this material system very popular in state-of-the-art Yb-doped silicate-based high power fiber laser applications.[520–523] Management of PD is quite important, as it also has recently been found that it may influence TMI in high power fiber lasers due to the heating caused by the excess absorptive loss.[524–526]

The use of the Al-O-P-based glasses to suppress PD is quite restricting from the perspective of compositional flexibility. Zhao *et al.*[527] recently showed that the addition of Na^+ can offer reduced PD in aluminosilicate glasses. They suggested that the introduction of Na_2O brings oxygen into the network and helps to prevent the formation of ODC(I) defects. Another team reported on the ability of group II elements to reduce PD when added to highly Yb-doped aluminosilicate glasses fabricated using the zeolite method.[528–530] They showed that calcium, in particular, enabled PD levels rivaling those in commercially developed fibers. They hypothesized that the Ca^{2+} acts as an ytterbium stabilizer, preventing the formation of Yb^{2+}. Finally, Schuster *et al.*[531] showed that the fluorination of Yb-doped aluminosilicate glasses may also suppress PD relative to non-fluorinated ones. From the perspective of utilizing materials that can offer advantages such as reduction of Brillouin or Raman scattering, all of these results are quite exciting.

To conclude the discussion on PD in Yb-doped fibers, photo-bleaching also has been used as a method to "undo" PD in a Yb-doped fiber. Manek-Hönninger *et al.* showed that the exposure of photo-darkened fiber to 355 nm can return the fiber to a nearly pristine state.[532] Picolli *et al.*[533] using light at 550 nm and Gebavi *et al.*[534] using light at 633 nm showed that visible light has a similar effect. Jolly *et al.*[535] also recently published a model describing the continuous competition between photo-darkening and photo-bleaching in a Yb-doped fiber as it undergoes the aging process, shedding light on the kinetics of the process.

Finally, and coming full-circle, so to speak, a brief discussion of PD in high-power Tm-doped fiber lasers[536] is provided. Brocklesby *et al.*[537] studied the defects that can form via illumination with blue light (476 nm). They provided evidence that blue photons are sufficient to cause structural changes to the glass network. Frith *et al.*[538] provided evidence that pumping at 790 nm gives rise to a loss similar to that observed with blue irradiation. By optimization of the composition of the core and Tm^{3+} content (> 4 wt. %), the lifetime of the $^3H_4$ level can be reduced by enhancing the cross relaxation process to the $^3F_4$ level (~0.65 eV above the $^3H_6$ ground state, compared with ~1.25 eV for the $^2F_{5/2} \rightarrow {}^2F_{7/2}$ transition in Yb^{3+}), resulting in less population of the $^1G_4$ level. This reduces the relative abundance of blue light originating from the $^1G_4 \rightarrow {}^3H_6$ transition. They showed that long-lived lifetimes, exceeding 10 000 h, are feasible. As a result, PD in high power Tm-doped fiber lasers pumped at 790 nm does not seem to pose a major obstacle at this point.[539] On the other hand, longer-wave pumping, near 1.07 μm, for access to wavelengths other than the 2 μm band may prove to be problematic.[540,541]

VI. CONCLUSION AND FUTURE PERSPECTIVES

The purpose of this review was to highlight the importance of materials engineering for high power fiber laser applications. As strong and durable, refractory, and inexpensive, the focus has mainly been on silicate glasses. However, the narrow focus is not meant to rule out other glass families from filling performance gaps currently found in these laser types. The review began with a summary of fiber fabrication, and afterward the rare earth ion was introduced. A discussion of the impact of environment (i.e., "the host") on the rare earth was next provided. Finally, several deleterious, power-limiting light-matter interactions were described and reviewed. An emphasis was made on the availability of a materials-based solution to each of these. Of course, this approach requires tailoring the glass composition in order to suppress any one or more of these unwanted phenomena. Unfortunately, in many cases (e.g., low-g_B or low-g_R fibers), the suppression of parasitic effects requires compositions that are not attainable with current vapor deposition technologies.

Given the discussion in Secs. II–V, several desirable fiber characteristics can be identified justifying continued efforts in glass optimization. For instance, utilizing a longer fiber with lower rare earth concentration can help to reduce the thermal load (per length) and alleviate some of those associated problems. In addition, the use of fewer-moded cores can further help to manage TMI and support a robust single mode. The drawback, however, to the use of a smaller A_{eff} (should this be a result of fiber design) and longer fiber length is the consequent exacerbation of the problems associated with nonlinearities. While to date this has represented a performance trade-off in fiber (cores) made mostly from

silica, the use of less conventional materials, as an additional design knob, can help tilt the scales towards significantly improved fiber laser performance. It is an assertion of these authors that the development of novel, high-performance fibers will require the maturation of new ways to make them.

A. Approaches to novel compositions and fiber material microstructures

Vapor deposition methods have been extremely successful in enabling remarkably high volumes of ultra-low loss optical fibers. Indeed, there would be no Internet or related technologies as we know them, if not for vapor deposition-derived optical fibers. As discussed in Sec. II, however, there are limits to both the range of dopants and dopant concentrations. Provided below is a brief discussion of less conventional processing routes, still compatible with vapor deposition methods that could be used in more specialized occasions in order to achieve novel fiber compositions.

1. Sol-gel methods

The most common non-vapor approach to doping silica preforms is through the use of solutions.[542] Conventionally, soluble salts, such as metal chlorides, are dissolved in water and/or alcohol and infused into the porous silica soot prior to sintering of the preform. A variation on solution doping is the use of a sol-gel or, perhaps more broadly defined, metal-organic solution doping. Advantages include the possibility for more uniform doping and a wider range of materials and gelation characteristics than are available with vapor-phase doping or conventional dissolved salt solution doping. Important contributions include those from Bell Labs and Rutgers University and were focused on dopants such as Al_2O_3, GeO_2, P_2O_5, ZrO_2, and TiO_2[543] as well as Er- and Nd-doped aluminosilicate fibers and fiber lasers.[544,545]

Though not employed much at present, significant advancements in sol-gel chemistry, range of compositions, and gelation condition have occurred over the past 25 years. Accordingly, sol-gel or metal-organic solution doping of vapor-deposited silica preforms may be useful for non-conventional dopants and enhanced preform doping homogeneity.

2. Nanoparticle "doping"

The doped glasses from which commercial optical fibers have historically been made are chemically homogeneous in order to minimize attenuation due to scattering. However, there is a growing body of literature on the use of heterogeneous systems. These fall into two general categories: (1) nucleation or phase separation of nanocrystals and (2) solution doping with nanoparticles. This topic was introduced in Sec. IV E.

Though not vapor-phase derived, the benefits of nanoscale secondary phases in optical fibers were first studied in detail in pioneering work by Corning. Specifically, glasses were formed using melt-quenching techniques and subsequently heat-treated (subsequently termed "ceramming;" i.e., making into a ceramic) to nucleate small secondary crystalline phases inside the glass host. This secondary nanophase often was a heavy metal fluoride into which lanthanide dopants would partition yielding a low phonon energy environment from which efficient emissions could result that were not possible in conventional oxide glasses. The seminal examples of this were glass-ceramics, including ones formed into fiber amplifiers and lasers, which contained rare earth or transition metal doped PbF_2, CdF_2, and/or LaF_3.[546–550]

A growing body of literature now exists with respect to vapor deposited, phase separated (glass ceramic) optical fibers. Representative examples include nano-phase separated yttria-alumino-silica (YAS) glass optical fibers doped with bismuth[551] or Yb_2O_3,[227] Yb- and Er-doped zirconia-silicate optical fibers[228,552] and multicomponent silicates[553] and titanates.[554]

A second approach to "nanoparticle" doping involves the suspension of nanoparticles into a solution that subsequently is solution doped into the porous silica preform soot per convention.[542] In other words, the nanoparticles are formed first and then doped into the glass rather than, in the previously discussed case, the nanophases are formed from an unstable glass. Though the nanoparticle's composition, and occasionally morphology,[555] change with preform and fiber processing, it is known that (rare earth) dopants remain in an environment dominated by the nanoparticle. This permits isolation of dopant species to control energy transfer[556] and enhanced spectroscopic performance due to this locally modified chemical environment.[223,557] Recently, low loss and efficient ($\sim$ 80% slope efficiency) 2 μm fiber lasers have been realized using this form of nanoparticle doping.[232]

B. Compositional comparison of fiber fabrication processes

Next, three methods for making preforms and fibers are compared: (1) vapor deposition, (2) powder sintering (REPUSIL),[558] and (3) molten core[371] (which was introduced in Sec. V B). This is because each process has its own representative combination of time and temperature profiles and each composition has kinetic and thermodynamic driving forces.

The vapor deposition fabrication of optical fiber preforms has been described above and well-documented in the literature (see Sec. II). In the most general case, the process stages include core deposition, sintering, consolidation, and collapse to a solid rod that is then drawn. While the earlier stages are performed at temperatures below 2000 °C, the latter stages typically occur at temperatures of about 2400 °C.

The REPUSIL powder sintering process is a solution-based approach to make doped powders that are then fashioned into a cylindrical rod and, typically, clad in pure silica.[560] This preform is then placed back on an MCVD lathe for consolidation into the final solid rod. As such, the same general temperature extremes ($\geq$2200 °C) are experienced by the glass.[558]

The molten core method, originally developed for the fabrication of fibers with high rare earth concentrations,[561] has subsequently been extended to a much wider range of glass[371,372] (and References therein) and crystalline[562] core optical fibers, including semiconductors.[563,564] Since

TABLE V. Best effort comparison of maximum (selective) dopant concentrations into silica using selected fiber fabrication methods.

	Maximum concentration by fabrication method (mol. %)		
Dopant into SiO_2	*Vapor deposition*	*Powder sintering*	*Molten core*
Al_2O_3	8	8[558]	54[374]
Fluorine	2	2[558]	8[559]
Rare earth oxide	2	6 (Yb_2O_3)[558]	10 (Yb_2O_3)[a]
Alkaline earth oxides	<2 (BaO)[42]		18[376] (BaO)
Ta_2O_5	<1[46]		7 (+8 mol. % Al_2O_3)[a]
Li_2O	0.2[41]		6.5[317]

[a]Unpublished results by the authors.

the highest temperature experienced by the preform is the fiber draw temperature (≤2000 °C), it is necessarily a "lower temperature" process than vapor deposition methods which require a soot sintering and preform consolidation/collapse stage. This enables a greater concentration of volatile species to remain in the glass. Further, the direct quenching of the core melt into a glassy solid, as the fiber draws and cools quickly, yields a rapid (vertical) traversing of the phase diagram and kinetically expands the compositional ranges over which all-glass fibers can be formed (see Table V).

One also can include more "specialized" dopants, such as the alkali and alkaline earth oxides, as well as various metal dioxides (e.g., TiO_2, ZrO_2, SnO_2), sesquioxides (e.g., Ga_2O_3 and the lanthanide oxides, Ln_2O_3), and pentoxides (e.g., Ta_2O_5, Sb_2O_5). Bismuth oxide also has grown in interest as a compound for broadband telecomm amplifiers (at low concentrations) and for nonlinear fiber devices (at high concentrations). However, this will not be further discussed here due to lingering uncertainty as to the valency state(s) of the bismuth in various glass systems and how that influences performance. Recent Refs. 565 and 566 are suggested to the interested reader.

ACKNOWLEDGMENTS

The authors gratefully acknowledge the financial support from the Directed Energy Joint Transition Office (DE JTO) through sustained support over many years including Contract Nos. W911NF-05-1-0517, FA9550-07-1-0566, W911NF-12-1-0602, FA9451-15-D-0009/0001 and 0002, and N00014-17-1-2546. The authors also gratefully acknowledge the Air Force Office of Scientific Research (AFOSR) under Contract No. FA9550-16–1-0383.

[1]See https://www.ipgphotonics.com/en/products/lasers/high-power-cw-fiber-lasers for high power fiber laser product offerings from IPG Photonics, Oxford, MA, USA.
[2]J. W. Dawson, M. J. Messerly, R. J. Beach, M. Y. Shverdin, E. A. Stappaerts, A. K. Sridharan, P. H. Pax, J. E. Heebner, C. W. Siders, and C. P. J. Barty, "Analysis of the scalability of diffraction-limited fibre lasers and amplifiers to high average power," Opt. Express **16**, 13240 (2008).
[3]D. J. Richardson, J. Nilsson, and W. A. Clarkson, "High power fibre lasers: Current status and future perspectives," J. Opt. Soc. Am. B **27**, B63 (2010).
[4]P. Zhou, X. Wang, Y. Ma, H. Lü, and Z. Liu, Laser Phys. **22**, 1744 (2012).
[5]C. Jauregui, J. Limpert, and A. Tünnermann, "High-power fibre lasers," Nat. Photonics **7**, 861 (2013).
[6]M. E. Fermann and I. Hartl, Nat. Photonics **7**, 868 (2013).
[7]M. N. Zervas, Int. J. Mod. Phys. B **28**, 1442009 (2014).
[8]M. Zervas and C. Codemard, "High Power Fiber Lasers: A Review," IEEE J. Sel. Top. Quantum Electron. **20**, 219 (2014).
[9]S. Fu, W. Shi, Y. Feng, L. Zhang, Z. Yang, S. Xu, X. Zhu, R. A. Norwood, and N. Peyghambarian, J. Opt. Soc. Am. B **34**, A49 (2017).
[10]E. Honea, R. S. Afzal, M. Savage-Leuchs, N. Gitkind, R. Humphreys, J. Henrie, K. Brar, and D. Jander, Proc. SPIE **8601**, 860115 (2013).
[11]J. Hecht, "High-Power Lasers: Fibre lasers drill for oil," Laser Focus World **12**, 27 (2012).
[12]S. Taccheo, Proc. SPIE **10058**, 1005808 (2017).
[13]R. J. De Young and N. P. Barnes, Appl. Opt. **49**, 562 (2010).
[14]See https://www.ipgphotonics.com/en_uploads/widget/widget_item_pdf_704.pdf?_=751132596 for Industrial Laser Solutions, Fiber Lasers Technical Digest.
[15]P. D. Dragic and G. C. Papen, IEEE Photonics Technol. Lett. **11**, 1593 (1999).
[16]C. G. Carlson, P. D. Dragic, R. K. Price, J. J. Coleman, and G. R. Swenson, IEEE Sel. Top. Quantum Electron. **15**, 451 (2009).
[17]M. Hemenway, W. Urbanek, D. Dawson, Z. Chen, L. Bao, M. Kanskar, M. DeVito, D. Kliner, and R. Martinsen, Proc. SPIE **10086**, 1008605 (2017).
[18]Y. Kasai, S. Sakamoto, Y. Takahashi, K. Katagiri, and A. Sakamoto, Fujikura Tech. Rev. **2016**, 42.
[19]J. Biesenbach, "High brightness fiber coupled modular diode laser platform," in *2012 IEEE Photonics Society Summer Topical Meeting Series* (IEEE, 2012), Paper No. MA4.3.
[20]K. C. Kao and G. A. Hockham, Proc. IEE **113**, 1151 (1966).
[21]S. Risbud and J. Pask, J. Am. Ceram. Soc. **60**, 418 (1977).
[22]J. Rockett and W. Foster, J. Am. Ceram. Soc. **48**, 75 (1965).
[23]S. H. Wemple, D. A. Pinnow, T. C. Rich, R. E. Jaeger, and L. G. Van Uitert, J. Appl. Phys. **44**, 5432 (1973).
[24]H. Yamamoto, K. Akiyama, T. Hirata, and Y. Murakami, J. Ceram. Soc. Jpn. **113**, 325 (2005).
[25]G. Baret, R. Madar, and C. Bernard, J. Electrochem. Soc. **138**, 2830 (1991).
[26]T.-Y. Tien and F. Hummel, J. Am. Ceram. Soc. **45**, 422 (1962).
[27]E. M. Dianov and V. M. Mashinsky, J. Lightwave Technol. **23**, 3500 (2005).
[28]M. E. Likhachev, S. S. Aleshkina, A. V. Shubin, M. Bubnov, E. Dianov, D. Lipatov, and A. Guryanov, in *European Conference on Lasers and Electro-Optics, OSA Technical Digest* (Optical Society of America, 2011), Paper No. CJ_P24.
[29]M. M. Bubnov, V. N. Vechkanov, A. N. Gur'yanov, K. V. Zotov, D. S. Lipatov, M. E. Likhachev, and M. V. Yashkov, Inorg. Mater. **45**, 444 (2009).
[30]K. Nassau, J. Shiever, and J. Krause, J. Am. Ceram. Soc. **58**, 461 (1975).
[31]J. F. MacDowell and G. H. Beall, J. Am. Ceram. Soc. **52**, 17 (1969).
[32]J. R. Simpson and J. B. MacChesney, Electron. Lett. **19**, 261 (1983).
[33]L. Dong, J. L. Cruz, J. A. Tucknott, L. Reekie, and D. N. Payne, Opt. Lett. **20**, 1982 (1995).
[34]G. W. Tasker, W. G. French, J. R. Simpson, P. Kaiser, and H. M. Presby, Appl. Opt. **17**, 1836 (1978).
[35]B. J. Cole and M. L. Dennis, "Heavy metal modified silica glass fibers doped with thulium, holmium, and thulium-sensitized-holmium high quantum efficiencies," U.S. patent 6,667,257B2 (December 23, 2003).
[36]S. Z. Yassin, M. I. Muhd, K. A. Zulkifti *et al.*, "Fabrication and characterization of solution doped gallium and barium preforms," in *2014 IEEE 5th International Conference on Photonics (ICP)* (IEEE, 2014), pp. 116-118.
[37]D. S. Gunawardena, K. A. Mat-Sharif, N. Tamchek, M.-H. Lai, N. Y. M. Omar, S. D. Emami, S. Z. Muhamad-Yasin, M. I. Zulkifli, Z. Yusoff, H. A. Abdul-Rashid, K.-S. Lim, and H. Ahmad, Appl. Opt. **54**, 5508 (2015).
[38]R. P. Tumminelli, W. C. McCollum, and E. Snitzer, J. Lightwave Technol. **8**, 1680 (1990).
[39]S. K. Mishra, "Alkali and fluorine doped optical fiber," U.S. patent 7,088,900B1 (August 8, 2006).
[40]M. E. Lines, "SiO_2-based alkali-doped optical fibe," U.S. patent 5,146,534 (September 8, 1992).
[41]J. B. MacChesney and J. R. Simpson, "Multicomponent optical fiber," U.S. patent 4,666,247 (May 19, 1987).

[42]A. Dhar, M. C. Paul, S. D. Chowdhury, M. Pal, A. Pal, and R. Sen, Phys. Status Solidi A **213**, 3039 (2016).
[43]J. B. MacChesney, J. R. Simpson, and K. L. Walker, "Doped optical fiber," U.S. patent 4,616,901 (October 14, 1986).
[44]P. C. Schultz, J. Am. Ceram. Soc. **59**, 214 (1976).
[45]P. C. Schultz, J. Am. Ceram. Soc. **57**, 309 (1974).
[46]K. Oh, A. Kilian, and T. F. Morse, J. Non-Cryst. Solids **259**, 10 (1999).
[47]G. Brambilla, V. Pruneri, and L. Reekie, Appl. Phys. Lett. **76**, 807 (2000).
[48]Y. V. Larionov, A. A. Rybaltovsky, S. L. Semjonov, M. M. Bubnov, A. N. Guryanov, M. V. Yashkov, and A. A. Umnikov, Opt. Mater. **27**, 1623 (2005).
[49]See https://patents.google.com/?q=optical+fiber&q=composition&q =MCVD &oq=optical+fiber+composition+MCVD; accessed 25 January 2018.
[50]J. MacChesney and D. DiGiovanni, J. Am. Ceram. Soc. **73**, 3537 (1990).
[51]K. Oh and U. Paek, *Silica Optical Fiber Technology for Devices and Components: Design, Fabrication, and International Standards* (Wiley, New York, 2012).
[52]A. D. Yablon, IEEE J. Sel. Top. Quantum Electron. **10**, 300 (2004).
[53]G. W. Scherer and A. R. Cooper, J. Am. Ceram. Soc. **63**, 346 (1980).
[54]U. C. Paek and C. R. Kurkjian, J. Am. Ceram. Soc. **58**, 330 (1975).
[55]Y. Hibino, F. Hanawa, and M. Horiguchi, J. Appl. Phys. **65**, 30 (1989).
[56]C.-S. Kim, Y. Han, B. H. Lee, W.-T. Han, U.-C. Paek, and Y. Chung, Opt. Commun. **185**, 337 (2000).
[57]S. Ishikawa, H. Kanamori, T. Kohgo, M. Nishimura, and Y. Yokota, in *Proceedings of Optical Fiber Communication Conference (OFC,* 1993*)*, pp. 5-6.
[58]P. Kaiser, J. Opt. Soc. Am. **64**, 475 (1974).
[59]E. J. Friebele, G. H. Sigel, and D. L. Griscom, Appl. Phys. Lett. **28**, 516 (1976).
[60]Y. Hibino, H. Hanafusa, and S. Sakaguchi, Jpn. J. Appl. Phys., Part 1 **24**, 1117 (1985).
[61]Y. Hayashi, Y. Okuda, H. Mitera, and K. Kato, Jpn. J. Appl. Phys., Part 2 **33**, L233 (1994).
[62]L. Skuja, J. Non-Cryst. Solids **239**, 16 (1998).
[63]G. H. Sigel and M. J. Marrone, J. Non-Cryst. Solids **45**, 235 (1981).
[64]E. J. Friebele, D. L. Griscom, and M. J. Marrone, J. Non-Cryst. Solids **71**, 133 (1985).
[65]R. Tohmon, Y. Shimogaichi, S. Munekuni, Y. Ohki, Y. Hama, and K. Nagasawa, Appl. Phys. Lett. **54**, 1650 (1989).
[66]A. V. Amossov and A. O. Rybaltovsky, J. Non-Cryst. Solids **179**, 75 (1994).
[67]H. Imai, K. Arai, H. Imagawa, H. Hosono, and Y. Abe, Phys. Rev. B **38**, 12772 (1988).
[68]P. Yasaka and J. Kaewkhao, "Luminescence from lanthanides-doped glasses and applications: A review," in *Proceeding of 4th ICICI-BME* (2015).
[69]M. H. V. Werts, Sci. Prog. **88**, 101 (2005).
[70]G. Blasse, J. Alloys Compd. **192**, 17 (1993).
[71]Q. Tan, J. Li, and X. Zeng, Crit. Rev. Environ. Sci. Technol. **45**, 749 (2015).
[72]R.-J. Xie, N. Hirosaki, Y. Li, and T. Takeda, Materials **3**, 3777 (2010).
[73]J. Qiu, Q. Jiao, D. Zhou, and Z. Yang, J. Rare Earths **34**, 341 (2016).
[74]*The Rare Earth Elements: Fundamentals and Applications*, edited by D. A. Atwood (John Wiley & Sons, West Sussex, UK, 2012).
[75]M. G. Mayer, Phys. Rev. **60**, 184 (1941).
[76]W. J. Miniscalco, "Optical and electronic properties of rare earth ions in glasses," in *Rare Earth Doped Fiber Lasers and Amplifiers*, edited by M. J. F. Digonnet (Marcel Dekker, New York, 1993), Chap. 2, pp. 19-133.
[77]V. M. Goldschmidt, T. Barth, and G. Lunde, *Skrifter Norske Videnskaps-Akad. Oslo, I: Mat. Naturv. Kl. No. 7* (Wiley, 1925).
[78]A. L. Allred, J. Inorg. Nucl. Chem. **17**, 215 (1961).
[79]S. G. Wang and W. H. E. Schwarz, J. Phys. Chem. **99**, 11687 (1995).
[80]E. A. Quadrelli, Inorg. Chem. **41**, 167 (2002).
[81]C. Clavaguéra, J.-P. Dognon, and P. Pyykkö, Chem. Phys. Lett. **429**, 8 (2006).
[82]S. Hüfner, *Optical Spectra of Transparent Rare Earth Compounds* (Academic Press, New York, 1978).
[83]B. G. Wybourne, *Spectroscopic Properties of Rare Earths* (John Wiley & Sons, New York, 1965).
[84]R. Tilley, *Understanding Solids: The Science of Materials* (John Wiley & Sons, West Sussex, UK, 2004), Chap. 1, pp. 3–18.
[85]B. R. Judd, *Operator Techniques in Atomic Spectroscopy* (McGraw Hill, New York, 1963).
[86]B. Henderson and G. F. Imbusch, *Optical Spectroscopy of Inorganic Solids* (Oxford University Press, Oxford, UK, 1989).
[87]J. Jensen and A. R. Mackintosh, *Rare Earth Magnetism: Structures and Excitations* (Clarendon Press, Oxford, UK, 1991).
[88]G. H. Dieke and H. M. Crosswhite, Appl. Opt. **2**, 675 (1963).
[89]R. Reisfeld, A. Patra, G. Panczer, and M. Gaft, Opt. Mater. **13**, 81 (1999).
[90]W. Gao, H. Zheng, Q. Han, E. He, F. Gao, and R. Wang, J. Mater. Chem. C **2**, 5327 (2014).
[91]N. Kojima, K. Tsushima, and I. Tsujikawa, J. Phys. Soc. Jpn. **49**, 1449 (1980).
[92]J. García Solé, L. E. Bausá, and D. Jaque, *An Introduction to the Optical Spectroscopy of Inorganic Solids* (John Wiley & Sons, West Sussex, UK, 2005), Chap. 6.
[93]Y. Tang, C. Huang, S. Wang, H. Li, and J. Xu, Opt. Express **20**, 17539 (2012).
[94]T. S. McComb, R. A. Sims, C. C. C. Willis, P. Kadwani, V. Sudesh, L. Shah, and M. Richardson, Appl. Opt. **49**, 6236 (2010).
[95]V. Sudesh, T. S. McComb, R. A. Sims, L. Shah, M. Richardson, and J. Stryjewski, Proc. SPIE **7325**, 73250B (2009).
[96]P. F. Moulton, G. A. Rines, E. V. Slobodtchikov, K. F. Wall, G. Frith, B. Samson, and A. L. G. Carter, IEEE J. Sel. Top. Quantum Electron. **15**, 85 (2009).
[97]R. Kitamura, L. Pilon, and M. Jonasz, Appl. Opt. **46**, 8118 (2007).
[98]G. A. Newburgh, J. Zhang, and M. Dubinskii, Laser Phys. Lett. **14**, 125101 (2017).
[99]P. Zhou, H. Xiao, J. Leng, J. Xu, Z. Chen, H. Zhang, and Z. Liu, J. Opt. Soc. Am. B **34**, A29 (2017).
[100]Y. Wang, J. Yang, C. Huang, Y. Luo, S. Wang, Y. Tang, and J. Xu, Opt. Express **23**, 2991 (2015).
[101]D. Creeden, B. R. Johnson, G. A. Rines, and S. D. Setzler, Opt. Express **22**, 29067 (2014).
[102]S. D. Jackson, Opt. Commun. **230**, 197 (2004).
[103]J. Y. Allain, M. Monerie, and H. Poignant, Electron. Lett. **26**, 166 (1990).
[104]S. G. Grubb, K. W. Bennett, R. S. Cannon, and W. F. Humer, Electron Lett. **28**, 1243 (1992).
[105]P. R. Barber, C. J. Mackechnie, R. D. T. Lauder, H. M. Pask, A. C. Tropper, D. C. Hanna, S. D. Butterworth, M. J. McCarthy, J.-L. Archanbault, and L. Reekie, "All solid state blue room temperature thulium-doped upconversion fiber laser," in OSA Technical Digest Series, *Compact Blue-Green Lasers* (1994), Paper No. CFA3.
[106]F. Duclos and P. Urquhart, J. Opt. Soc. Am. B **12**, 709 (1995).
[107]R. Paschotta, N. Moore, W. A. Clarkson, A. C. Tropper, D. C. Hanna, and G. Mazé, IEEE J. Sel. Top. Quantum Electron. **3**, 1100 (1997).
[108]R. M. El-Agmy, Laser Phys. **20**, 1990 (2010).
[109]J. Y. Allain, M. Monerie, and H. Poignant, Electron. Lett. **25**, 1660 (1989).
[110]M. L. Dennis, J. W. Dixon, and I. Aggarwal, Electron. Lett. **30**, 136 (1994).
[111]E. Desurvire, *Erbium-Doped Fiber Amplifiers: Principles and Applications* (John Wiley & Sons, New York, 1994).
[112]M. J. F. Digonnet, *Rare-Earth-Doped Fiber Lasers and Amplifiers*, 2nd ed. (CRC Press, Boca Raton, FL, 2001).
[113]P. C. Becker, N. A. Olsson, and, and J. R. Simpson, *Erbium-Doped Fiber Amplifiers: Fundamentals and Technology* (Academic Press, San Diego, CA, 1999).
[114]R. S. Quimby, Appl. Opt. **30**, 2546 (1991).
[115]A. Lidgard, J. R. Simpson, and P. C. Becker, Appl. Phys. Lett. **56**, 2607 (1990).
[116]D. P. Bour, N. A. Dinkel, D. B. Gilbert, K. B. Fabian, and M. G. Harvey, IEEE Photonics Technol. Lett. **2**, 153 (1990).
[117]J. J. Coleman, IEEE J. Sel. Top. Quantum Electron. **6**, 1008 (2000).
[118]J. F. Massicott, R. Wyatt, B. J. Ainslie, and S. P. Craig-Ryan, Electron. Lett. **26**, 1038 (1990).
[119]E. Desurvire, C. R. Giles, J. R. Simpson, and J. L. Zyskind, Opt. Lett. **14**, 1266 (1989).
[120]M. Dubinskii, J. Zhang, and V. Ter-Mikirtychev, Proc. SPIE **7325**, 73250A (2009).
[121]J. Zhang, V. Fromzel, and M. Dubinskii, Opt. Express **19**, 5574 (2011).
[122]P. R. Morkel and R. I. Laming, Opt. Lett. **14**, 1062 (1989).
[123]M. C. Farries, IEEE Photonics Technol. Lett. **3**, 619 (1991).
[124]J. Nilsson, P. Blixt, B. Jaskorzynska, and J. Babonas, J. Lightwave Technol. **13**, 341 (1995).
[125]Y. O. Barmenkov, A. V. Kir'yanov, A. D. Guzmán-Chávez, J.-L. Cruz, and M. V. Andrés, J. Appl. Phys. **106**, 083108 (2009).

[126]T. J. Whitley, C. A. Millar, R. Wyatt, M. C. Brierley, and D. Szebesta, Electron. Lett. **27**, 1785 (1991).
[127]J. Y. Allain, M. Monerie, and H. Poignant, Electron. Lett. **28**, 111 (1992).
[128]J. Stark, Ann. Phys. **348**, 965 (1914).
[129]J. H. Van Vleck, J. Phys. Chem. **41**, 67 (1937).
[130]M. J. Weber, J. A. Paisner, S. S. Sussman, W. M. Yen, L. A. Riseberg, and C. Brecher, J. Lumin. **12-13**, 729 (1976).
[131]H. Steinkemper, S. Fischer, M. Hermle, and J. C. Goldschmidt, New J. Phys. **15**, 053033 (2013).
[132]L. Zhang, T. Xue, D. He, M. Guzik, and G. Boulon, Opt. Express **23**, 1505 (2015).
[133]J. O. White, IEEE J. Quantum Electron. **45**, 1213 (2009).
[134]J. O. White, M. Dubinskii, L. D. Merkle, I. Kudryashov, and D. Garbuzov, J. Opt. Soc. Am. B **24**, 2454 (2007).
[135]P. Lacovara, H. K. Choi, C. A. Wang, R. L. Aggarwal, and T. Y. Fan, Opt. Lett. **16**, 1089 (1991).
[136]N. P. Barnes and B. M. Walsh, IEEE J. Quantum Electron. **35**, 101 (1999).
[137]J. Koetke and G. Huber, Appl. Phys. B **61**, 151 (1995).
[138]S. A. Payne, L. L. Chase, L. K. Smith, W. L. Kway, and W. F. Krupke, IEEE J. Quantum Electron. **28**, 2619 (1992).
[139]E. Desurvire, J. W. Sulhoff, J. L. Zyskind, and J. R. Simpson, IEEE Photonics Technol. Lett. **2**, 653 (1990).
[140]C. Zhang, J. Sun, and S. Jian, Opt. Commun. **288**, 97 (2013).
[141]A. V. Kir'yanov and N. N. Il'ichev, Laser Phys. Lett. **8**, 305 (2011).
[142]B. R. Judd, Phys. Rev. **127**, 750 (1962).
[143]G. S. Ofelt, J. Chem. Phys. **37**, 511 (1962).
[144]W. F. Krupke, Phys. Rev. **145**, 325 (1966).
[145]M. J. Weber, Phys. Rev. **171**, 283 (1968).
[146]W. F. Krupke, IEEE J. Quantum Electron. **7**, 153 (1971).
[147]M. J. Weber and T. E. Varitimos, J. Appl. Phys. **42**, 4996 (1971).
[148]W. F. Krupke, IEEE J. Quantum Electron. **10**, 450 (1974).
[149]C. K. Jørgensen and R. Reisfeld, J. Less-Common Met. **93**, 107 (1983).
[150]S. Tanabe, T. Ohyagi, N. Soga, and T. Hanada, Phys. Rev. B **46**, 3305 (1992).
[151]S. Tanabe and T. Hanada, J. Appl. Phys. **76**, 3730 (1994).
[152]H. Takebe, Y. Nageno, and K. Morinaga, J. Am. Ceram. Soc. **78**, 1161 (1995).
[153]Y. Nageno, N. Takebe, and K. Morinaga, J. Am. Ceram. Soc. **76**, 3081 (1993).
[154]C. K. Jørgensen, "The nephelauxetic series," in *Progress in Inorganic Chemistry*, edited by F. A. Cotton (John Wiley & Sons, New York, 1962), Vol. 4, Chap. 2, pp. 73-124.
[155]S. P. Sinha and H.-H. Schmidtke, Mol. Phys. **10**, 7 (1965).
[156]D. E. Henrie, Mol. Phys. **28**, 415 (1974).
[157]R. Reisfeld, "Glass lasers and solar applications," in *Spectroscopy of Solid-State Laser-Type Materials*, edited by B. Di Bartolo (Plenum Press, New York, 1987), pp. 343-396.
[158]M. J. Weber, Phys. Rev. **157**, 262 (1967).
[159]W. T. Carnall, P. R. Fields, and K. Rajnak, J. Chem. Phys. **49**, 4424 (1968).
[160]N. Spector, R. Reisfeld, and L. Boehm, Chem. Phys. Lett. **49**, 49 (1977).
[161]W. B. Fowler and D. L. Dexter, Phys. Rev. **128**, 2154 (1962).
[162]G. Wang, S. Xu, S. Dai, J. Yang, L. Hu, and Z. Jiang, J. Non-Cryst. Solids **336**, 102 (2004).
[163]J. T. Verdeyen, *Laser Electronics*, 3rd ed. (Prentice Hall, Englewood Cliffs, NJ, 1995), Chap. 10.
[164]G. A. Reider, *Photonics: An Introduction* (Springer, Sham, Switzerland, 2016), Chap. 6.
[165]B. M. Walsh, "Judd-Ofelt theory: Principles and practices," in *Advances in Spectroscopy for Lasers and Sensing*, edited by B. Di Bartolo and O. Forte (Springer, Dordrecht, The Netherlands, 2006), pp. 403-433.
[166]D. E. McCumber, Phys. Rev. **134**, A299 (1964).
[167]C.-H. Huang, L. McCaughan, and D. M. Gill, J. Lightwave Technol. **12**, 803 (1994).
[168]W. T. Carnall, P. R. Fields, and K. Rajnak, J. Chem. Phys. **49**, 4412 (1968).
[169]T. H. Taminiau, S. Karaveli, N. F. van Hulst, and R. Zia, Nat. Commun. **3**, 979 (2012).
[170]B. M. Walsh, N. P. Barnes, and B. Di Bartolo, J. Appl. Phys. **83**, 2772 (1998).
[171]H. Lin, E. Y. B. Pun, S. Q. Man, and X. R. Liu, J. Opt. Soc. Am. B **18**, 602 (2001).
[172]R. Reisfeld, AIMS Mater. Sci. **2**, 37 (2015).
[173]C. M. Dodson and R. Zia, Phys. Rev. B **86**, 125102 (2012).
[174]C. B. Layne, W. H. Lowdermilk, and M. J. Weber, Phys. Rev. B **16**, 10 (1977).
[175]R. Reisfeld, L. Boehm, and N. Spector, Chem. Phys. Lett. **49**, 251 (1977).
[176]R. Reisfeld and C. K. Jørgensen, "Excited state phenomena in vitreous materials," in *Handbook on the Physics and Chemistry of Rare Earths*, edited by K. A. Gschneidner, Jr. and L. Eyring (Elsevier, Amsterdam, The Netherlands, 1987), Chap. 58.
[177]K. Arai, H. Namikawa, K. Kumata, T. Honda, Y. Ishii, and T. Handa, J. Appl. Phys. **59**, 3430 (1986).
[178]See https://www.thorlabs.com/newgrouppage9.cfm?objectgroup_id=336 for details on this fiber.
[179]M. Cavillon, C. Kucera, T. W. Hawkins, N. Yu, P. Dragic, and J. Ballato, Opt. Mater. Express **8**, 744 (2018).
[180]T. R. Gosnell, Opt. Lett. **24**, 1041 (1999).
[181]N. Yu, M. Cavillon, C. Kucera, T. Hawkins, J. Ballato, and P. Dragic, in *CLEO 2018, OSA Technical Digest* (Optical Society of America, 2018), Paper No. STu3K.6.
[182]S. J. Lee, L. A. Vazquez-Zuniga, H. Kim, and Y. Jeong, "Thermal characteristics of ytterbium-doped phosphosilicate fiber amplifiers," in *17th Opto-Electronics and Communications Conference, Technical Digest* (OECC, 2012), Paper No. 4C4-3.
[183]M. A. Melkoumov, I. A. Bufetov, M. M. Bubnov, K. S. Kravtsov, S. L. Semjonov, A. V. Shubin, and E. M. Dianov, "Ytterbium lasers based on P_2O_5- and Al_2O_3-doped fibers," paper presented at ECOC 2004, Paper No. Th1.3.2.
[184]X. Zou and H. Toratani, Phys. Rev. B **52**, 15889 (1995).
[185]S. Unger, A. Schwuchow, S. Jetschke, V. Reichel, A. Scheffel, and J. Kirchof, Proc. SPIE **6890**, 689016 (2008).
[186]L. Wang, D. He, S. Feng, C. Yu, L. Hu, and D. Chen, Opt. Mater. Express **5**, 742 (2015).
[187]V. D. Del Cacho, L. R. P. Kassab, S. L. de Oliveira, and N. I. Morimoto, Mater. Res. **9**, 21 (2006).
[188]L. R. P. Kassab, M. E. Fukumoto, V. D. D. Cacho, N. U. Wetter, and N. I. Morimoto, Opt. Mater. **27**, 1576 (2005).
[189]M. J. Weber, J. E. Lynch, D. H. Blackburn, and D. J. Cronin, IEEE J. Quantum Electron. **19**, 1600 (1983).
[190]Y. Qiao, L. Wen, B. Wu, J. Ren, D. Chen, and J. Qiu, Mater. Chem. Phys. **107**, 488 (2008).
[191]X. Wang, R. Zhang, J. Ren, H. Vezin, S. Fan, C. Yu, D. Chen, S. Wang, and L. Hu, J. Alloys Compd. **695**, 2339 (2017).
[192]P. D. Dragic, J. Ballato, T. Hawkins, and P. Foy, Opt. Mater. **34**, 1294 (2012).
[193]J. Körner, J. Hein, M. Tiegel, S. Kuhn, J. Buldt, F. Yue, R. Seifert, A. Herrmann, C. Rüssel, and M. C. Kaluza, Proc. SPIE **9513**, 95130S (2015).
[194]M. Tiegel, A. Herrrmann, S. Kuhn, C. Rüssel, J. Körner, D. Klöpfel, R. Seifert, J. Hein, and M. C. Kaluza, Laser Phys. Lett. **11**, 115811 (2014).
[195]K. Lu and N. K. Dutta, J. Appl. Phys. **91**, 576 (2002).
[196]F. Wang, L. Hu, W. Xu, M. Wang, S. Feng, J. Ren, L. Zhang, D. Chen, N. Ollier, G. Gao, C. Yu, and S. Wang, Opt. Express **25**, 25960 (2017).
[197]W. J. Miniscalco, J. Lightwave Technol. **9**, 234 (1991).
[198]B. J. Ainslie, J. Lighwave Technol. **9**, 220 (1991).
[199]K. Linganna, K. Suresh, S. Ju, W.-T. Han, C. K. Jayasankar, and V. Venkatramu, Opt. Mater. Express **5**, 1689 (2015).
[200]S. Berneschi, M. Bettinelli, M. Brenci, R. Dall'Igna, G. Nunzi Conti, S. Pelli, B. Profilo, S. Sebastiani, A. Speghini, and G. C. Righini, Opt. Mater. **28**, 1271 (2006).
[201]F. Chen, T. Wei, X. Jing, Y. Tian, J. Zhang, and S. Xu, Sci. Rep. **5**, 10676 (2015).
[202]A. Dhar, A. Pal, S. Das, and R. Sen, Advances in Electrical and Electronic Engineering **12**, 582 (2014).
[203]X. Wen, G. Tang, Q. Yang, X. Chen, Q. Qian, Q. Zhang, and Z. Yang, Sci. Rep. **6**, 20344 (2016).
[204]G. Turri, V. Sudesh, M. Richardson, M. Bass, A. Toncelli, and M. Tonelli, J. Appl. Phys. **103**, 093104 (2008).
[205]Y.-P. Peng, X. Yuan, J. Zhang, and L. Zhang, Sci. Rep. **4**, 5256 (2014).
[206]J. L. Doualan, S. Girard, H. Haquin, J. L. Adam, and J. Montagne, Opt. Mater. **24**, 563 (2003).
[207]M. Li, G. Bai, Y. Guo, L. Hu, and J. Zhang, J. Lumin. **132**, 1830 (2012).
[208]J. J. Koponen, L. Petit, T. Kokki, V. Aallos, J. Paul, and H. Ihalainen, Opt. Eng. **50**, 111605 (2011).
[209]S. Magne, Y. Ouerdane, M. Druetta, J. P. Goure, P. Ferdinand, and G. Monnom, Opt. Commun. **111**, 310 (1994).

[210]X. Chen, S. Li, Z. Song, W. Du, O. Wen, and N. Sawanobori, J. Opt. Soc. Am. B **23**, 2581 (2006).
[211]P. Goldner, F. Pellé, D. Meichenin, and F. Auzel, J. Lumin. **71**, 137 (1997).
[212]P. Zeil and F. Laurell, Opt. Express **19**, 13940 (2011).
[213]M. Engholm, L. Norin, C. Hirt, S. T. Fredrich-Thornton, K. Petermann, and G. Huber, Proc. SPIE **7193**, 71931U (2009).
[214]K. Tankala, A. Carter, D. P. Machewirth, J. Farroni, J. Abramczyk, and Y. Manyam, Proc. SPIE **4974**, 220 (2003).
[215]Z. Burshtein, Y. Kalisky, S. Z. Levy, P. Le Boulanger, and S. Rotman, IEEE J. Quantum Electron. **36**, 1000 (2000).
[216]C. Xia, "Concentration quenching effect in rare-earth doped glasses," thesis (University of Arizona, 2017).
[217]F. Auzel and P. Goldner, Opt. Mater. **16**, 93 (2001).
[218]L. Li, A. Schülzgen, V. L. Temyanko, M. M. Morrell, S. Sabet, H. Li, J. V. Maloney, and N. Peyghambarian, Appl. Phys. Lett. **88**, 161106 (2006).
[219]M. J. V. Bell, W. G. Quirino, S. L. Oliveira, D. F. de Sousa, and L. A. O. Nunes, J. Phys.: Condens. Matter **15**, 4877 (2003).
[220]E. Delevaque, T. Georges, M. Monerie, P. Lamouler, and J.-F. Bayon, IEEE Photonics Technol. Lett. **5**, 73 (1993).
[221]H. Lin, C. Baker, Z. Huang, S. Pidishety, Y. Feng, E. J. Friebele, A. Burdett, D. Rhonehouse, B. Shaw, J. Sanghera, and J. Nilsson, in *CLEO 2018, OSA Technical Digest* (Optical Society of America, 2018), Paper No. SW4K.5.
[222]D. Lezal, J. Pedlikova, P. Kostka, J. Bludska, M. Poulain, and J. Zavadil, J. Non-Cryst. Solids **284**, 288 (2001).
[223]M. Vermillac, H. Fneich, J.-F. Lupi, J.-B. Tissot, C. Kucera, P. Vennéguès, A. Mehdi, D. R. Neuville, J. Ballato, and W. Blanc, Opt. Mater. **68**, 24 (2017).
[224]M. C. Paul, S. Bysakh, S. Das, M. Pal, S. K. Bhadra, S. Yoo, A. J. Boyland, and J. K. Sahu, Sci. Adv. Mater. **4**, 292 (2012).
[225]S. Yoo, M. P. Kalita, A. J. Boyland, A. S. Webb, R. J. Standish, J. K. Sahu, M. C. Paul, S. Das, S. K. Bhadra, and M. Pal, Opt. Commun. **283**, 3423 (2010).
[226]K.-S. Lim, S. Yoo, M. C. Paul, H. Ahmad, M. Pal, S. K. Bhadra, and J. K. Sahu, IEEE Photonics Technol. Lett. **24**, 679 (2012).
[227]M. C. Paul, A. V. Kir'yanov, Y. O. Barmenkov, S. Das, M. Pal, S. K. Bhadra, S. Yoo, A. J. Boyland, J. K. Sahu, A. Martínez-Gamez, and J. L. Lucio-Martínez, J. Lightwave Technol. **30**, 2062 (2012).
[228]A. V. Kir'yanov, M. C. Paul, Y. O. Barmenkov, S. Das, M. Pal, S. K. Bhadra, L. E. Zarate, and A. D. Guzman-Chavez, Opt. Express **19**, 14823 (2011).
[229]I. Savelli, L. Bigot, B. Capoen, C. Gonnet, C. Chanéac, E. Burova, A. Pastouret, H. El-Hamzaoui, and M. Bouazaoui, Nanoscale Res. Lett. **12**, 206 (2017).
[230]W. Blanc, B. Dussardier, and M. C. Paul, Glass Technol. – European Journal of Glass Science and Technology Part A **50**, 79 (2009).
[231]W. Blanc, B. Dussardier, G. Monnom, R. Peretti, A.-M. Jurdyc, B. Jacquier, M. Foret, and A. Roberts, Appl. Opt. **48**, G119 (2009).
[232]C. C. Baker, E. J. Friebele, A. A. Burdett, D. L. Rhonehouse, J. Fontana, W. Kim, S. R. Bowman, L. B. Shaw, J. Sanghera, J. Zhang, R. Pattnaik, M. Dubinskii, J. Ballato, C. Kucera, A. Vargas, A. Hemming, N. Simakov, and J. Haub, Opt. Express **25**, 13903 (2017).
[233]N. A. B. Rahmat, H. A. A. Rashid, H. Y. Wong, and M. Zaman, Am. J. Appl. Sci. **14**, 150 (2017).
[234]I. Kasik, P. Peterka, J. Mrazek, and P. Honzatko, Curr. Nanosci. **12**, 277 (2016).
[235]J. Ballato, H. Ebendorff-Heidepriem, J. Zhao, L. Petit, and J. Troles, Fibers **5**, 11 (2017).
[236]G. Xue, B. Zhang, K. Yin, W. Yang, and J. Hou, Opt. Express **22**, 25976 (2014).
[237]N. Saidin, S. W. Harun, S. S. A. Damanhuri, S. M. M. Ali, H. Ahmad, A. Halder, M. C. Paul, S. Das, M. Pal, and S. K. Bhadra, Chin. Phys. Lett. **30**, 034204 (2013).
[238]T. Hu, D. D. Hudson, B. J. Eggleton, and S. D. Jackson, in *CLEO 2012, OSA Technical Digest* (Optical Society of America, 2012), Paper No. CM2N.3.
[239]R. M. Percival, D. Szebesta, and S. T. Davey, Electron. Lett. **29**, 1054 (1993).
[240]L. Dong, W. H. Loh, J. E. Caplen, J. D. Minelly, K. Hsu, and L. Reekie, Opt. Lett. **22**, 694 (1997).
[241]G. G. Vienne, J. E. Caplen, L. Dong, J. D. Minelly, J. Nilsson, and D. N. Payne, J. Lightwave Technol. **16**, 1990 (1998).
[242]A. Langar, C. Bouzidi, H. Elhouichet, and M. Férid, J. Lumin. **148**, 249 (2014).
[243]W. Zhang, J. Liu, G. Zhou, C. Xia, S. Liang, Y. Chen, and Z. Hou, Opt. Mater. Express **7**, 1708 (2017).
[244]K. Aiso, Y. Tashiro, T. Suzuki, and T. Yagi, Furukawa Rev. **20**, 41 (2001).
[245]D. Klimentov, V. V. Dvoyrin, A. Halder, M. C. Paul, S. Das, S. K. Bhadra, and I. T. Sorokina, Opt. Mater. **42**, 270 (2015).
[246]D. A. Simpson, W. E. K. Gibbs, S. F. Collins, W. Blanc, B. Dussardier, G. Monnom, P. Peterka, and G. W. Baxter, Opt. Express **16**, 13781 (2008).
[247]H. Haris, A. R. Muhammad, N. Saidin, M. S. Z. Abidin, H. Arof, M. C. Paul, and S. W. Harun, Indon. J. Electr. Eng. Comp. Sci. **8**, 457 (2017).
[248]V. V. Dvoyrin, D. Klimentov, A. Halder, M. C. Paul, M. Pal, S. K. Bhadra, A. V. Kir'yanov, and I. T. Sorokina, Proc. SPIE **8601**, 86012X (2013).
[249]P. R. Watekar, S. Ju, and W.-T. Han, IEEE Photonics Technol. Lett. **18**, 1609 (2006).
[250]Y. Jeong, S. Yoo, C. A. Codemard, J. Nilsson, J. K. Sahu, D. N. Payne, R. Horley, P. W. Turner, L. Hickey, A. Harker, M. Lovelady, and A. Piper, IEEE J. Sel. Top. Quantum Electron. **13**, 573 (2007).
[251]B. E. A. Saleh and M. C. Teich, *Fundamentals of Photonics*, 2nd ed. (John Wiley & Sons, Hoboken, New Jersey, 2007), Chap. 9, pp. 325–364.
[252]R. S. Quimby, *Photonics and Lasers: An Introduction* (John Wiley & Sons, Hoboken, New Jersey, 2006), Appendix A, pp. 495–498.
[253]See https://www.lumentum.com/en/optical-communications/products/pump-lasers for examples of these pump lasers offered by Lumentum, Milpitas, CA, USA.
[254]H. Po, E. Snitzer, R. Tumminelli, L. Zenteno, F. Hakimi, N. M. Cho, and T. Haw, "Double clad high brightness Nd fiber laser pumped by GaAlAs phased array," in *OSA Technical Digest Series* (OFC, 1989), Paper No. PD7-1
[255]E. Snitzer, H. Po, F. Hakimi, R. Tumminelli, and B. C. McCollum, "Double clad, offset core Nd fiber laser," in *OSA Technical Digest Series* (OFS, 1988), Paper No. PD5.
[256]K. Tankala, D. Guertin, J. Abramczyk, and N. Jacobson, Opt. Eng. **50**, 111607 (2011).
[257]J. Nilsson, W. A. Clarkson, R. Selvas, J. K. Sahu, P. W. Turner, S.-U. Alam, and A. B. Grudinin, Opt. Fiber Technol. **10**, 5 (2004).
[258]T. Haw, L. Zenteno, H. Po, and N. M. Cho, Proc. SPIE **1177**, 257 (1990).
[259]C. A. Codemard, A. Malinowski, and M. N. Zervas, Proc. SPIE **10083**, 1008315 (2017).
[260]D. Molin, G. Kuyt, M. Bigot-Astruc, and P. Sillard, "Recent advances in MMF technology for data networks," *Proceedings of the Optical Fiber Communications Conference* (2011), Paper No. OWJ6.
[261]D. Molin, F. Achten, M. Bigot, A. Amezcua-Correa, and P. Sillard, "WideBand OM4 multi-mode fiber for next-generation 400 Gbps data communications," in *Proceedings of the European Conference on Optical Communications* (2014), Paper No. P.1.6.
[262]S. Yoo, D. B. S. Soh, J. Kim, Y. Jung, J. Nilsson, J. K. Sahu, J. W. Lee, and K. Oh, Opt. Commun. **247**, 153 (2005).
[263]S. Kawakami and S. Nishida, IEEE J. Quantum Electron. **QE-10**, 879 (1974).
[264]T. P. Tanaka, S.-I. Onoda, and M. Sumi, Appl. Opt. **15**, 1121 (1976).
[265]J. Kim, P. Dupriez, C. Codemard, J. Nilsson, and J. K. Sahu, Opt. Express **14**, 5103 (2006).
[266]R. Khazaeinezhad, S. H. Kassani, H. Jeong, T. Nazari, D.-I. Yeom, and K. Oh, IEEE Photonics J. **7**, 1500109 (2015).
[267]L. N. Duan, X. M. Liu, L. R. Wang, D. Mao, and G. X. Wang, Laser Phys. **21**, 948 (2011).
[268]L. Dong and B. Samson, *Fiber Lasers: Basics, Technology, and Applications* (CRC Press, Boca Raton, Florida, 2017), Chap. 11, pp. 199–222.
[269]A. M. Heidt, J. S. Feehan, J. H. V. Price, and T. Feurer, J. Opt. Soc. Am. B **34**, 764 (2017).
[270]K. Nagasaka, T. H. Tuan, T. Cheng, M. Matsumoto, H. Tezuka, T. Suzuki, and Y. Ohishi, Appl. Phys. Express **10**, 032103 (2017).
[271]J. M. Dudley and J. R. Taylor, *Supercontinuum Generation in Optical Fibers* (Cambridge University Press, New York, 2010).
[272]P. Laperle, C. Paré, H. Zheng, A. Croteau, and Y. Taillon, Proc. SPIE **6343**, 63430X (2006).
[273]V. Kuhn, S. Unger, S. Jetschke, D. Kracht, J. Neumann, J. Kirchhof, and P. Weßels, J. Lightwave Technol. **28**, 3212 (2010).
[274]A. Carter, J. Farroni, K. Tankala, B. Samson, D. Machewirth, N. Jacobson, W. Torruellas, Y. Chen, M. Cheng, A. Galvanauskas, and A. Sanchez, "Robustly single-mode polarization maintaining Er/Yb Co-

doped LMA fiber for high power applications," in *OSA Technical Digest Series* (CLEO, 2007), Paper No. CTuS6.
[275]M. Steinke, D. Kracht, J. Neumann, and P. Wessels, "1.0 μm co-seeded Er:Yb fiber amplifier with 50 W output power at 1.5 μm," in *OSA Technical Digest Series* (CLEO, 2013), Paper No. CTu1K.7.
[276]P. Laperle, C. Paré, H. Zheng, and A. Croteau, Proc. SPIE **6453**, 645308 (2007).
[277]A. E. Siegman, J. Opt. Soc. Am. B **24**, 1677 (2007).
[278]A. E. Siegman, J. Opt. Soc. Am. A **20**, 1617 (2003).
[279]V. Sudeshi, T. McComb, Y. Chen, M. Bass, M. Richardson, J. Ballato, and A. E. Siegman, Appl. Phys. B **90**, 369 (2008).
[280]P. G. Yarandi, K. M. Gundu, and A. Mafi, J. Opt. Soc. Am. B **28**, 2430 (2011).
[281]F. Ai, J. Qian, J. Shi, and M. Zhang, Appl. Opt. **56**, 8169 (2017).
[282]W. Li, M. Lu, Z. Yang, H. Guo, P. Wang, and B. Peng, J. Opt. Soc. Am. B **28**, 1498 (2011).
[283]Y. Xiao, F. Brunet, M. Kanskar, M. Faucher, A. Wetter, and N. Holehouse, Opt. Express **20**, 3296 (2012).
[284]D. Jain, Y. Jung, P. Barua, S. Alam, and J. K. Sahu, Opt. Express **23**, 7407 (2015).
[285]F. Kong, T. W. Hawkins, M. Jones, J. Parsons, M. Kalichevsky-Dong, C. Dunn, and L. Dong, "Ytterbium-doped 30/400 LMA fibers with a record-low ~NA of 0.028," in *OSA Technical Digest Series* (CLEO 2016), Paper No. SM2Q.2.
[286]J. P. Koplow, D. A. Kliner, and L. Goldberg, Opt. Lett. **25**, 442 (2000).
[287]M.-J. Li, X. Chen, A. Liu, S. Gray, J. Wang, D. T. Walton, and L. A. Zenteno, J. Lighwave Technol. **27**, 3010 (2009).
[288]C.-H. Liu, G. Chang, N. Litchinitser, A. Galvanauskas, D. Guertin, N. Jacobson, and K. Tankala, *Effectively Single-Mode Chirally-Coupled Core Fiber*, OSA Technical Digest Series (ASSP, 2007), Paper No. ME2.
[289]X. Ma, C. Zhu, I.-N. Hu, A. Kaplan, and A. Galvanauskas, Opt. Express **22**, 9206 (2014).
[290]J. C. Knight, T. A. Birks, P. St, J. Russell, and D. M. Atkin, Opt. Lett. **21**, 1547 (1996).
[291]J. C. Knight, J. Opt. Soc. Am. B **24**, 1661 (2007).
[292]W. J. Wadsworth, R. M. Percival, G. Bouwmans, J. C. Knight, P. St, and J. Russell, Opt. Express **11**, 48 (2003).
[293]B. Zintzen, T. Langer, J. Geiger, D. Hoffman, and P. Loosen, Opt. Express **15**, 16787 (2007).
[294]K. P. Hansen, C. B. Olausson, J. Broeng, D. Noordegraaf, M. D. Maack, T. T. Alkeskjold, M. Laurila, T. Nikolajsen, P. M. W. Skovgaard, M. H. Sørensen, M. Denninger, C. Jakobsen, and H. Simonsen, Opt. Eng. **50**, 111609 (2011).
[295]J. Limpert, T. Schreiber, S. Nolte, H. Zellmer, A. Tünnermann, R. Iliew, F. Lederer, J. Broeng, G. Vienne, A. Petersson, and C. Jakobsen, Opt. Express **11**, 818 (2003).
[296]O. Schmidt, J. Rothhardt, T. Eidam, F. Röser, J. Limpert, A. Tünnermann, K. P. Hansen, C. Jakobsen, and J. Broeng, Opt. Express **16**, 3918 (2008).
[297]L. Dong, J. Li, and X. Peng, Opt. Express **14**, 11512 (2006).
[298]L. Dong, "Advanced Optical Fibers for High Power Fiber Lasers," in *Advances in Optical Fiber Technology: Fundamental Optical Phenomena and Applications* , edited by M. Yasin (InTech, London, UK, 2015), Chap. 7, pp. 221–252.
[299]J. W. Nicholson, J. M. Fini, A. M. DeSantolo, E. Monberg, F. DiMarcello, J. Fleming, C. Headley, D. J. DiGiovanni, S. Ghalmi, and S. Ramachandran, Opt. Express **18**, 17651 (2010).
[300]C. A. Balanis, *Advanced Engineering Electromagnetics* (John Wiley & Sons, New York, 1989), Chap. 9, pp. 470–542.
[301]A. L. Cauchy, Bull. Sci. Math. **14**, 6 (1830).
[302]A. L. Cauchy, *Mémoire Sur la Dispersion de la Lumière* (Calve, Prague, 1836).
[303]W. Sellmeier, Ann. Phys. **219**, 272 (1871).
[304]G. Ghosh, Appl. Opt. **36**, 1540 (1997).
[305]I.-I. Oprea, H. Hesse, and K. Betzler, Opt. Mater. **26**, 235 (2004).
[306]M. Englert, P. Hartmann, and S. Reichel, Proc. SPIE **9131**, 91310H (2014).
[307]B. Tatian, Appl. Opt. **23**, 4477 (1984).
[308]G. Ghosh, *Handbook of Thermo-Optic Coefficients of Optical Materials with Applications* (Academic Press, San Diego, CA, 1998), Chap. 2, pp. 5–114.
[309]P. A. Tick and P. L. Bocko, "Optical fiber materials," in *Optical Materials*, a Series of Advances, edited by S. Musikant (Marcel Dekker, New York, 1990), Vol. 1, Chap. 2, pp. 147–260.
[310]See https://refractiveindex.info for a very nice refractive index calculator for a wide range of materials.
[311]C. R. Hammond, Opt. Quantum Electron. **10**, 163 (1978).
[312]J. W. Fleming, Appl. Opt. **23**, 4486 (1984).
[313]P. Dragic, M. Cavillon, and J. Ballato, Int. J. Appl. Glass Sci. **9**, 421–427 (2018).
[314]D. J. DiGiovanni, J. B. MacChesney, and T. Y. Kometani, J. Non-Cryst. Solids **113**, 58 (1989).
[315]G. G. Vienne, W. S. Brocklesby, R. S. Brown, Z. J. Chen, J. D. Minelly, J. E. Roman, and D. N. Payne, Opt. Fiber Technol. **2**, 387 (1996).
[316]M. E. Likhachev, M. M. Bubnov, K. V. Zotov, D. S. Lipatov, M. V. Yashkov, and A. N. Guryanov, Opt. Lett. **34**, 3355 (2009).
[317]P. D. Dragic, C. Ryan, C. J. Kucera, M. Cavillon, M. Tuggle, M. Jones, T. W. Hawkins, A. D. Yablon, R. Stolen, and J. Ballato, Opt. Lett. **40**, 5030 (2015).
[318]G. P. Agrawal, *Nonlinear Fiber Optics*, 2nd ed. (Academic Press, 1995).
[319]E. Garmire, New J. Phys. **19**, 011003 (2017).
[320]A. Kobyakov, M. Sauer, and D. Chowdhury, Adv. Opt. Photonics **2**, 1 (2010).
[321]R. W. Boyd, K. Rzążewski, and P. Narum, Phys. Rev. A **42**, 5514 (1990).
[322]T. C. Zhu, H. J. Maris, and J. Tauc, Phys. Rev. B **44**, 4281 (1991).
[323]R. W. Boyd, *Nonlinear Optics* (Academic Press, San Diego, CA, 1992).
[324]R. G. Smith, Appl. Opt. **11**, 2489 (1972).
[325]C. Barnard, P. Myslinski, J. Chrostowski, and M. Kavehrad, IEEE J. Quantum Electron. **30**, 1817 (1994).
[326]S. K. Turitsyn, A. E. Bednyakova, M. P. Fedoruk, A. I. Latkin, A. A. Fotiadi, A. S. Kurkov, and E. Sholokhov, Opt. Express **19**, 8394 (2011).
[327]J. Bai and E. Towe, J. Opt. Soc. Am. B **31**, 2809 (2014).
[328]See https://www.thorlabs.com/catalogpages/1074.pdf for the software package offered by Thorlabs, Newton, NJ, USA.
[329]See https://www.rp-photonics.com/software.html for the software package offered by RP Photonics, Bad Dürrheim, Germany.
[330]A. Safaai-Jazi, C. K. Jen, and G. W. Farnell, IEEE Trans. Ultrason. Ferroelectr. Freq. Control **UFFC-33**, 59 (1986).
[331]C. K. Jen, Proc. IEEE Ultrason. Symp. **2**, 1128 (1985).
[332]C. K. Jen and N. Goto, IEEE J. Lightwave Technol. **7**, 2018 (1989).
[333]C. K. Jen, J. E. B. Oliveira, N. Goto, and K. Abe, Electron. Lett. **24**, 1419 (1988).
[334]S. Herstrøm, L. Grüner-Nielsen, and B. Pálsdóttir, Opt. Lett. **34**, 3689 (2009).
[335]N. Shibata, Y. Azuma, T. Horiguchi, and M. Tateda, Opt. Lett. **13**, 595 (1988).
[336]N. Shibata, K. Okamoto, and Y. Azuma, J. Opt. Soc. Am. B **6**, 1167 (1989).
[337]P. D. Dragic, P.-C. Law, and Y.-S. Liu, Microw. Opt. Technol. Lett. **54**, 2347 (2012).
[338]A. Hadjifotou and G. A. Hill, IEE Proc. J. Optoelectron. **133**, 256 (1986).
[339]M. Hildebrandt, S. Büsche, P. Weßels, M. Frede, and D. Kracht, Opt. Express **16**, 15970 (2008).
[340]P. D. Dragic, J. Ballato, S. Morris, and T. Hawkins, Opt. Mater. **35**, 1627 (2013).
[341]S. Wang, W. Zheng, Y. Deng, S. Yan, J. Xu, and Y. Tang, Laser Phys. **25**, 085101 (2015).
[342]F. Beier, C. Hupel, S. Kuhn, S. Hein, J. Nold, F. Proske, B. Sattler, A. Liem, C. Jauregui, J. Limpert, N. Haarlammert, T. Schreiber, R. Eberhardt, and A. Tünnermann, Opt. Express **25**, 14892 (2017).
[343]N. Platonov, R. Yagodkin, J. De La Cruz, A. Yusim, and V. Gapontsev, Proc. SPIE **10512**, 105120E (2018).
[344]Y. Xu, Q. Fang, X. Cui, B. Hou, S. Fu, Z. Xie, and W. Shi, Proc. SPIE **10512**, 105122S (2018).
[345]V. R. Supradeepa, Opt. Express **21**, 4677 (2013).
[346]J. O. White, M. Harfouche, J. Edgecumbe, N. Satyan, G. Rakuljic, V. Jayaraman, C. Burgner, and A. Yariv, Appl. Opt. **56**, B116 (2017).
[347]J. E. Masnik, J. Kieffer, and J. D. Bass, J. Am. Ceram. Soc. **76**, 3073 (1993).
[348]C. Krischer, J. Acoust. Soc. Am. **48**, 1086 (1970).
[349]P.-C. Law and P. D. Dragic, Opt. Express **18**, 18852 (2010).
[350]J. Galbraith and J. W. Zwanziger, J. Non-Cryst. Solids **433**, 82 (2016).
[351]R. Su, P. Zhou, X. Wang, R. Tao, and X. Xu, High Power Laser Sci. Eng. **2**, e3 (2014).
[352]J. Geng, Q. Wang, Z. Jiang, T. Luo, S. Jiang, and G. Czarnecki, Opt. Lett. **36**, 2293 (2011).
[353]A. Flores and I. Dajani, "Kilowatt-class, all-fiber amplifiers for beam combining," SPIE Newsroom (2016).
[354]K. Shiraki, M. Ohashi, and M. Tateda, Electron. Lett. **31**, 668 (1995).
[355]J. Cui, H. Dang, K. Feng, W. Yang, T. Geng, Y. Hu, Y. Zhang, D. Jiang, X. Chen, and J. Tan, Photonics Res. **5**, 233 (2017).

[356]M. Ohashi and M. Tateda, J. Lightwave Technol. **11**, 1941 (1993).
[357]A. Evert, T. Hawkins, R. Stolen, P. Dragic, R. Rice, and J. Ballato, Opt. Fiber Technol. **19**, 432 (2013).
[358]J. Hansryd, F. Dross, M. Westlund, P. A. Andrekson, and S. N. Knudsen, J. Lighwave Technol. **19**, 1691 (2001).
[359]A. Liu, Opt. Express **15**, 977 (2007).
[360]N. Yoshizawa, T. Horiguchi, and T. Kurashima, Electron. Lett. **27**, 1100 (1991).
[361]E. Lucas, L. Lombard, Y. Yaouën, S. Bordais, and G. Canat, Appl. Opt. **53**, 4413 (2014).
[362]J. E. Rothenberg, P. A. Thielen, M. Wickham, and C. P. Asman, Proc. SPIE **6873**, 68730O (2008).
[363]P. D. Dragic, "Brillouin suppression by fiber design," in *IEEE Photonics Society Summer Topicals 2010*, IEEE Technical Digest (IEEE, 2010), Paper No. TuC3.2.
[364]A. Mangognia, C. Kucera, J. Guerrier, J. Furtick, T. Hawkins, P. D. Dragic, and J. Ballato, Opt. Mater. Express **3**, 511 (2013).
[365]P. D. Dragic, C.-H. Liu, G. C. Papen, and A. Galvanauskas, "Optical fiber with an acoustic guiding layer for stimulated Brillouin scattering suppression," in *CLEO/QELS 2005*, OSA Technical Digest (Optical Society of America, 2005), p. 1984.
[366]M.-J. Li, X. Chen, J. Wang, A. B. Ruffin, D. T. Walton, S. Li, D. A. Nolan, S. Gray, and L. A. Zenteno, "Fiber designs for reducing stimulated Brillouin scattering," in *OFC-NFOEC 2006*, OSA Technical Digest (Optical Society of America, 2006), Paper No. OTuA4.
[367]S. Gray, D. T. Walton, X. Chen, J. Wang, M.-J. Li, A. Liu, A. B. Ruffin, J. A. Demeritt, and L. A. Zenteno, IEEE J. Sel. Top. Quantum Electron. **15**, 37 (2009).
[368]M. D. Mermelstein, M. J. Andrejco, J. Fini, C. Headley, and D. J. DiGiovanni, Proc. SPIE **7580**, 75801G (2010).
[369]L. Dong, J. Lightwave Technol. **21**, 3156 (2010).
[370]P. Dragic, J. Lightwave Technol. **29**, 967 (2011).
[371]J. Ballato and P. Dragic, J. Am. Ceram. Soc. **96**, 2675 (2013).
[372]J. Ballato and P. Dragic, Materials **7**, 4411 (2014).
[373]J. Ballato, M. Cavillon, and P. Dragic, Int. J. Appl. Glass Sci. **9**, 263 (2018).
[374]P. Dragic, T. Hawkins, P. Foy, S. Morris, and J. Ballato, Nat. Photonics **6**, 627 (2012).
[375]P. D. Dragic, C. Kucera, J. Ballato, D. Litzkendorf, J. Dellith, and K. Schuster, Appl. Opt. **53**, 5660 (2014).
[376]P. Dragic, K. Kucera, J. Furtick, J. Guerrier, T. Hawkins, and J. Ballato, Opt. Express **21**, 10924 (2013).
[377]M. Cavillon, J. Furtick, C. J. Kucera, C. Ryan, M. Tuggle, M. Jones, T. W. Hawkins, P. Dragic, and J. Ballato, J. Lightwave Technol. **34**, 1435 (2016).
[378]C. Ryan, J. Furtick, C. J. Kucera, R. Stolen, J. Ballato, and P. Dragic, Int. J. Appl. Glass Sci. **6**, 387 (2015).
[379]J. Ballato, T. Hawkins, P. Foy, B. Kokuoz, R. Stolen, C. McMillen, M. Daw, Z. Su, T. M. Tritt, M. Dubinskii, J. Zhang, T. Sanamyan, and M. J. Matthewson, J. Appl. Phys. **105**, 053110 (2009).
[380]M. E. Lines, J. Appl. Phys. **62**, 4363 (1987).
[381]F. L. Galeener, J. Non-Cryst. Solids **71**, 373 (1985).
[382]F. L. Galeener and G. Lucovsky, Phys. Rev. Lett. **37**, 1474 (1976).
[383]F. L. Galeener, Phys. Rev. B **19**, 4292 (1979).
[384]M. Heck, V. Bock, R. G. Krämer, D. Richter, T. A. Goebel, C. Matzdorf, A. Liem, T. Schreiber, A. Tünnermann, and S. Nolte, Proc. SPIE **10512**, 105121I (2018).
[385]D. Nodop, C. Jauregui, F. Jansen, J. Limpert, and A. Tünnermann, Opt. Lett. **35**, 2982 (2010).
[386]J. M. Fini, M. D. Mermelstein, M. F. Yan, R. T. Bise, A. D. Yablon, P. W. Wisk, and M. J. Andrejco, "Suppression of stimulated Raman scattering in a cladding pumped amplifier with an Yb-doped filter fiber," in *CLEO 2006*, OSA Technical Digest (Optical Society of America, 2006), Paper No. CTuQ1.
[387]C. A. Codemard, N. T. Vukovic, J. S. Chan, P. J. Almeida, J. R. Hayes, M. N. Petrovich, C. Baskiotis, A. Malinowski, and M. N. Zervas, IEEE J. Sel. Top. Quantum Electron. **24**, 0901509 (2018).
[388]X. Ma, I.-N. Hu, and A. Galvanauskas, Opt. Express **19**, 22575 (2011).
[389]P. D. Dragic, Opt. Commun. **250**, 403 (2005).
[390]T. T. Alkeskjold, Proc. SPIE **7580**, 758012 (2010).
[391]C. A. Codemard, P. Dupriez, Y. Jeong, J. K. Sahu, M. Ibsen, and J. Nilsson, Opt. Lett. **31**, 2290 (2006).
[392]Y. Feng, L. Zhang, and H. Jiang, Proc. SPIE **9344**, 93440U (2015).
[393]T. Yao, A. V. Harish, J. K. Sahu, and J. Nilsson, Appl. Sci. **5**, 1323 (2015).
[394]Q. Xiao, P. Yan, D. Li, J. Sun, X. Wang, Y. Huang, and M. Gong, Opt. Express **24**, 6758 (2016).
[395]G. E. Walrafen and J. Stone, Appl. Spectrosc. **29**, 337 (1975).
[396]F. L. Galeener, J. C. Mikkelsen, R. H. Geils, and W. J. Mosby, Appl. Phys. Lett. **32**, 34 (1978).
[397]P. D. Dragic and J. Ballato, Electron. Lett. **49**, 895 (2013).
[398]T. Kato, Y. Suetsugu, and M. Nishimura, Opt. Lett. **20**, 2279 (1995).
[399]Z. Zhao, H. Xuan, H. Igarashi, S. Ito, K. Kakizaki, and Y. Kobayashi, Opt. Express **23**, 29764 (2015).
[400]M. Leigh, W. Shi, J. Zong, Z. Yao, S. Jiang, and N. Peyghambarian, Appl. Phys. Lett. **92**, 181108 (2008).
[401]M. J. Munroe, M. Y. Hamamoto, and D. A. Dutton, Proc. SPIE **7195**, 71952N (2009).
[402]C. Xu, L. Mollenauer, and X. Liu, Electron. Lett. **38**, 1578 (2002).
[403]R. Su, P. Zhou, P. Ma, H. Lü, and X. Xu, Appl. Opt. **52**, 7331 (2013).
[404]K. Petermann, *Laser Diode Modulation and Noise* (Kluwer, Dordrecht, Netherlands, 1988).
[405]G. D. Goodno, S. J. McNaught, J. E. Rothenberg, T. S. McComb, P. A. Thielen, M. G. Wickham, and M. E. Weber, Opt. Lett. **35**, 1542 (2010).
[406]S. J. McNaught, P. A. Thielen, L. N. Adams, J. G. Ho, A. M. Johnson, J. P. Machan, J. E. Rothenberg, C.-C. Shih, D. M. Shimabukuro, M. P. Wacks, M. E. Weber, and G. D. Goodno, IEEE J. Sel. Top. Quantum Electron. **20**, 0901008 (2014).
[407]M. R. Zunoubi, B. Anderson, S. A. Naderi, T. J. Madden, and I. Dajani, Proc. SPIE **10083**, 100830S (2017).
[408]B. M. Anderson, N. A. Naderi, and A. Flores, "Nonlinear characterization of a Kolowatt-class amplifier based on laser gain competition," in *CLEO 2018*, OSA Technical Digest (Optical Society of America, 2018), Paper No. SW4K.3.
[409]R. Adair, L. L. Chase, and S. A. Payne, Phys. Rev. B **39**, 3337 (1989).
[410]K. Nakajima and M. Ohashi, IEEE Photonics Technol. Lett. **14**, 492 (2002).
[411]R. Adair, L. L. Chase, and S. A. Payne, J. Opt. Soc. Am. B **4**, 875 (1987).
[412]A. V. Smith, B. T. Do, G. R. Hadley, and R. L. Farrow, IEEE Sel. Top. Quantum Electron. **15**, 153 (2009).
[413]N. Kuzuu, K. Yoshida, H. Yoshida, T. Kamimura, and N. Kamisugi, Appl. Opt. **38**, 2510 (1999).
[414]R. L. Farrow, D. A. V. Kliner, G. R. Hadley, and A. V. Smith, Opt. Lett. **31**, 3423 (2006).
[415]C. D. Brooks and F. Di Teodoro, Opt. Commun. **280**, 424 (2007).
[416]O. Schmidt, J. Rothardt, F. Roser, S. Linke, T. Schreiber, K. Rademacher, J. Limpert, S. Ermeneux, P. Yvernault, F. Salin, and A. Tünnermann, Opt. Lett. **32**, 1551 (2007).
[417]S. Desmoulins and F. Di Teodoro, Opt. Express **16**, 2431 (2008).
[418]C. Jauregui, T. Eidam, J. Limpert, and A. Tünnermann, Opt. Express **19**, 3258 (2011).
[419]A. V. Smith and J. J. Smith, Opt. Express **19**, 10180 (2011).
[420]A. V. Smith and J. J. Smith, "Review of models of mode instability in fiber amplifiers," https://pdfs.semanticscholar.org/023b/8b994407852d360f1ad6ae4312bc9fca02d1.pdf
[421]C. Ye, L. Petit, J. J. Koponen, I.-N. Hu, and A. Galvanauskas, IEEE J. Sel. Top. Quantum Electron. **20**, 0903512 (2014).
[422]L. Dong and B. Samson, *Fiber Lasers: Basics, Technology, and Applications* (CRC Press, Boca Raton, 2017), Chap. 3, p. 50.
[423]T. Eidam, C. Wirth, C. Jauregui, F. Stutzki, F. Jansen, H.-J. Otto, O. Schmidt, T. Schreiber, J. Limpert, and A. Tünnermann, Opt. Express **19**, 13218 (2011).
[424]L. Dong, Opt. Express **21**, 2642 (2013).
[425]C. Shi, H. Zhang, X. Wang, P. Zhou, and X. Xu, High Power Laser Sci. Eng. **6**, e16 (2018).
[426]J. P. Leidner and J. R. Marciante, Proc. SPIE **10512**, 105121Z (2018).
[427]Z. Li, Z. Huang, X. Xiang, X. Liang, H. Lin, S. Xu, Z. Yang, J. Wang, and F. Jing, Photonics Res. **5**, 77 (2017).
[428]F. Kong, G. Gu, T. W. Hawkins, M. Jones, J. Parsons, M. T. Kalichevsky-Dong, B. Pulford, I. Dajani, and L. Dong, Proc. SPIE **10083**, 10083311 (2017).
[429]M. Kanskar, J. Zhang, J. Koponen, O. Kimmelma, V. Aallos, I.-N. Hu, and A. Galvanauskas, Proc. SPIE **10512**, 105120F (2018).
[430]P. Dragic, M. Cavillon, and J. Ballato, Opt. Mater. Express **7**, 3654 (2017).
[431]P. Dragic, M. Cavillon, C. Kucera, J. Parsons, T. Hawkins, and J. Ballato, "Tailoring the thermo-optic coefficient in silica optical fibers," in *OFS-26*, OSA Technical Digest 2018 (Optical Society of America, 2018), Paper No. TuE82.

[432]L. Dong, Opt. Express **24**, 19841 (2016).
[433]D. C. Brown and H. J. Hoffman, IEEE J. Quantum Electron. **37**, 207 (2001).
[434]P. D. Dragic, M. Cavillon, A. Ballato, and J. Ballato, Int. J. Appl. Glass Sci. **9**, 278 (2017).
[435]P. D. Dragic, M. Cavillon, A. Ballato, and J. Ballato, Int. J. Appl. Glass Sci. **9**(3), 307 (2018).
[436]M. B. Volf, *Mathematical Approach to Glass* (Elsevier, Amsterdam, 1988).
[437]M. Cavillon, C. Kucera, T. Hawkins, J. Dawson, P. D. Dragic, and J. Ballato, Int. J. Appl. Glass Sci. **9**(4), 447 (2018).
[438]P. D. Dragic, Electron. Lett. **45**, 256 (2009).
[439]P. D. Dragic, Int. J. Appl. Glass Sci. **1**, 330 (2010).
[440]P. D. Dragic, J. Non-Cryst. Solids **355**, 403 (2009).
[441]P. D. Dragic, J. Ballato, S. Morris, and T. Hawkins, J. Opt. Soc. Am. B **30**, 244 (2013).
[442]A. Bertholds and R. Dändliker, J. Lightwave Technol. **6**, 17 (1988).
[443]P. Richet, Chem. Geol. **62**, 111 (1987).
[444]A. Winkelmann and O. Schott, Ann. Phys. Chem. **51**, 730 (1894).
[445]S. English and W. E. S. Turner, J. Am. Ceram. Soc. **10**, 551 (1927).
[446]F. P. Hall, J. Am. Ceram. Soc. **13**, 182 (1930).
[447]P. Gilard and L. Dubrul, Verre Silic. Ind. **5**, 122 (1934).
[448]H. Doweidar, Phys. Chem. Glass **42**, 158 (2001).
[449]M. Cavillon, J. Ballato, and P. D. Dragic, Opt. Lett. **42**, 3650 (2017).
[450]T. Hosaka, Y. Sasaki, K. Okamoto, and J. Noda, Electron. Commun. Jpn. **68**, 37 (1985).
[451]K. Mochizuki, Y. Namihira, and Y. Ejiri, Appl. Opt. **21**, 4223 (1982).
[452]D. Grobnic, S. J. Mihailov, J. Ballato, and P. D. Dragic, Optica **2**, 313 (2015).
[453]P. D. Dragic, S. W. Martin, A. Ballato, and J. Ballato, Int. J. Appl. Glass Sci. **7**, 3 (2016).
[454]V. I. Kovalev and R. G. Harrison, Opt. Lett. **31**, 161 (2006).
[455]A. Ballato, P. D. Dragic, S. W. Martin, and J. Ballato, Int. J. Appl. Glass Sci. **7**, 11 (2016).
[456]J. Ballato and A. Ballato, Appl. Phys. Lett. **111**, 221901 (2017).
[457]P. Dragic, J. Ballato, A. Ballato, S. Morris, T. Hawkins, P.-C. Law, S. Ghosh, and M. C. Paul, Opt. Mater. Express **2**, 1641 (2012).
[458]A. V. Dotsenko, L. B. Glebov, and V. A. Tsekhomsky, *Physics and Chemistry of Photochromic Glasses* (CRC Press, Boca Raton, Florida, 1997).
[459]N. A. Papunashvili, V. D. Ryabtseva, and Y. L. Chibalashvili, Sov. J. Glass Phys. Chem. **9**, 229 (1983).
[460]S. Tammela, M. Söderlund, J. Koponen, V. Philippov, and P. Stenius, Proc. SPIE **6116**, 61160G (2006).
[461]C. A. Millar, S. R. Mallinson, B. J. Ainslie, and S. P. Craig, Electron. Lett. **24**, 590 (1988).
[462]M. M. Broer, D. M. Krol, and D. J. DiGiovanni, Opt. Lett. **18**, 799 (1993).
[463]G. R. Atkins and A. L. G. Carter, Opt. Lett. **19**, 874 (1994).
[464]R. Paschotta, J. Nilsson, P. R. Barber, J. E. Caplen, A. C. Tropper, and D. C. Hanna, Opt. Commun. **136**, 375 (1997).
[465]J. J. Koponen, M. J. Söderlund, S. K. T. Tammela, and H. Po, Proc. SPIE **5990**, 599008 (2005).
[466]J. J. Koponen, M. J. Söderlund, H. J. Hoffman, and S. K. T. Tammela, Opt. Express **14**, 11539 (2006).
[467]J. Koponen, M. Söderlund, H. J. Hoffman, D. A. V. Kliner, J. P. Koplow, and M. Hotoleanu, Appl. Opt. **47**, 1247 (2008).
[468]M. Hotoleanu, J. Koponen, T. Kokki, and M. Laurila, *Experimental Verification of Spatial Distribution of Photodarkening in Large Mode Area Ytterbium Doped Fibers*, OSA Technical Digest Series (CLEO, 2008), Paper No. CFS3.
[469]J. J. Montiel i Ponsoda, M. Söderlund, J. Koplow, J. Koponen, A. Iho, and S. Honkanen, Proc. SPIE **7195**, 71952D (2009).
[470]J. Koponen, M. Söderlund, H. J. Hoffman, D. Kliner, and J. Koplow, Proc. SPIE **6453**, 64531E (2007).
[471]S. Taccheo, H. Gebavi, A. Monteville, O. Le Goffic, D. Landais, D. Mechin, D. Tregoat, B. Cadier, T. Robin, D. Milanese, and T. Durrant, Opt. Express **19**, 19340 (2011).
[472]M. N. Zervas, F. Ghiringhelli, M. K. Durkin, and I. Crowe, Proc. SPIE **7914**, 79140L (2011).
[473]K. Shimakawa, N. Nakagawa, and T. Itoh, Appl. Phys. Lett. **95**, 051908 (2009).
[474]S. Jetschke, S. Unger, U. Röpke, and J. Kirchhof, Opt. Express **15**, 14838 (2007).
[475]L. Dong, J. L. Archambault, L. Reekie, P. St, J. Russell, and D. N. Payne, Appl. Opt. **34**, 3436 (1995).
[476]P. Laperle, L. Desbiens, H. Zheng, M. Drolet, A. Proulx, and Y. Taillon, Proc. SPIE **7580**, 75801Y (2010).
[477]T. Kitabayashi, M. Ikeda, M. Nakai, T. Sakai, K. Himeno, and K. Ohashi, *Population Inversion Factor Dependence of Photodarkening of Yb-Doped Fibers and its Suppression by Highly Aluminum Doping*, OSA Technical Digest Series (OFC, 2006), Paper No. OThC5.
[478]S. Jetschke and U. Röpke, Opt. Lett. **34**, 109 (2009).
[479]P. Laperle, L. Desbiens, K. Le Foulgoc, M. Drolet, P. Deladurantaye, A. Proulx, and Y. Taillon, Proc. SPIE **7195**, 71952C (2009).
[480]A. V. Shubin, M. V. Yashkov, M. A. Melkumov, S. A. Smirnov, I. A. Bufetov, and E. M. Dianov, *Photodarkening of Aluminosilicate and Phosphosilicate Yb-Doped Fibers*, OSA Technical Digest Series (CLEO, Europe, 2007), Paper No. CJ3-1-THU.
[481]R. Peretti, A.-M. Jurdyc, B. Jacquier, C. Gonnet, A. Pastouret, E. Burov, and O. Cavani, Opt. Express **18**, 20455 (2010).
[482]R. Peretti, C. Gonnet, and A.-M. Jurdyc, Proc. SPIE **8257**, 825705 (2012).
[483]R. Peretti, C. Gonnet, and A.-M. Jurdyc, J. Appl. Phys. **112**, 093511 (2012).
[484]S. Jetschke, M. Leich, S. Unger, A. Schwuchow, and J. Kirchhof, Opt. Express **19**, 14473 (2011).
[485]H. Li, L. Zhang, R. Sidharthan, D. Ho, X. Wu, N. Venkatram, H. Sun, T. Huang, and S. Yoo, J. Light Technol. **35**, 2535 (2017).
[486]S. Jetschke, S. Unger, A. Schwuchow, M. Leich, J. Fiebrandt, M. Jäger, and J. Kirchhof, Opt. Express **21**, 7590 (2013).
[487]J. Jasapara, M. Andrejco, D. DiGiovanni, and R. Windeler, *Effect of Heat and H2 Gas on the Photo-Darkening of Yb3+ Fibers*, OSA Technical Digest Series (CLEO, 2006), Paper No. CTuQ5.
[488]M. Engholm, L. Norin, and D. Åberg, Opt. Lett. **32**, 3352 (2007).
[489]M. Engholm and L. Norin, Opt. Express **16**, 1260 (2008).
[490]M. Engholm, P. Jelger, F. Laurell, and L. Norin, Opt. Lett. **34**, 1285 (2009).
[491]P. Jelger, M. Engholm, L. Norin, and F. Laurell, J. Opt. Soc. Am. B **27**, 338 (2010).
[492]N. Zhao, Y. Wang, J. Li, C. Liu, J. Peng, H. Li, N. Dai, L. Yang, and J. Li, Appl. Phys. A **122**, 75 (2016).
[493]S. Jetschke, S. Unger, A. Schwuchow, M. Leich, and M. Jäger, Opt. Express **24**, 13009 (2016).
[494]G. Chen, Y.-B. Wang, L. Xie, Y.-B. Xing, H.-Q. Li, Z.-W. Jiang, J.-G. Peng, N.-L. Dai, and J.-Y. Li, *Self-Bleaching Phenomenon Observed in the Ce/Yb Co-Doped Silica Fiber*, OSA Technical Digest Series (CLEO, 2013), Paper No. CM4I.5.
[495]S. Rydberg and M. Engholm, Opt. Express **21**, 6681 (2013).
[496]S. Wang, F. Lou, C. Yu, Q. Zhou, M. Wang, S. Feng, D. Chen, L. Hu, W. Chen, M. Guzik, and G. Boulon, J. Mater. Chem. C **2**, 4406 (2014).
[497]D. S. McClure and Z. Kiss, J. Chem. Phys. **39**, 3251 (1963).
[498]A. D. Guzman Chávez, A. V. Kir'yanov, Y. O. Barmenkov, and N. N. Il'ichev, Laser Phys. Lett. **4**, 734 (2007).
[499]T. Arai, K. Ichii, K. Okada, T. Kitabayashi, S. Tanigawa, and M. Fujimaki, Fujikura Giho **115**, 6 (2008).
[500]T. Arai, K. Ichii, S. Tanigawa, and M. Fujimaki, Proc. SPIE **7914**, 79140K (2011).
[501]T. Deschamps, H. Vezin, C. Gonnet, and N. Ollier, Opt. Express **21**, 8382 (2013).
[502]S. Yoo, C. Basu, A. J. Boyland, C. Sones, J. Nilsson, J. K. Sahu, and D. Payne, Opt. Lett. **32**, 1626 (2007).
[503]E. J. Friebele and D. L. Griscom, *Color Centers in Glass Optical Fiber Waveguides* (Proc. Mat. Res. Symp., 1986), Vol. 61, p. 319.
[504]T. E. Tsai, M. A. Saifi, E. J. Friebele, D. L. Griscom, and U. Österberg, Opt. Lett. **14**, 1023 (1989).
[505]L. J. Poyntz-Wright, M. E. Fermann, and P. St. J. Russell, Opt. Lett. **13**, 1023 (1988).
[506]C. G. Carlson, K. E. Keister, P. D. Dragic, A. Croteau, and J. G. Eden, J. Opt. Soc. Am. B **27**, 2087 (2010).
[507]Y.-S. Liu, T. C. Galvin, T. Hawkins, J. Ballato, L. Dong, P. R. Foy, P. D. Dragic, and J. G. Eden, Opt. Express **20**, 14494–14507 (2012).
[508]P. D. Dragic, C. G. Carlson, and A. Croteau, Opt. Express **16**, 4688 (2008).
[509]P. D. Dragic, IEEE Photonics Technol. Lett. **20**, 1760 (2008).
[510]K. E. Mattsson, Opt. Express **19**, 19797 (2011).
[511]Y. W. Lee, S. Sinha, M. J. F. Digonnet, R. L. Byer, and S. Jiang, Electron. Lett. **44**, 14 (2008).

[512]S. Jetschke, S. Unger, M. Leich, and J. Kirchhof, Appl. Opt. **51**, 7758 (2012).
[513]J. K. Sahu, S. Yoo, A. J. Boyland, C. Basu, M. P. Kalita, A. Webb, C. L. Sones, J. Nilsson, and D. N. Payne, *488 nm Irradiation Induced Photodarkening Study of Yb-Doped Aluminosilicate and Phosphosilicate Fibers*, OSA Technical Digest Series (CLEO, 2008), Paper No. JTuA27.
[514]S. Suzuki, H. A. McKay, X. Peng, L. Fu, and L. Dong, Opt. Express **17**, 9924 (2009).
[515]S. Jetschke, S. Unger, A. Schwuchow, M. Leich, V. Reichel, and J. Kirchhof, Proc. SPIE **6873**, 68731G (2008).
[516]S. Jetschke, S. Unger, A. Schwuchow, M. Leich, and J. Kirchhof, Opt. Express **16**, 15540 (2008).
[517]T. Deschamps, N. Ollier, H. Vezin, and C. Gonnet, J. Chem. Phys. **136**, 014503 (2012).
[518]B. Schaudel, P. Goldner, M. Prassas, and F. Auzel, J. Alloys Comp. **300-301**, 443 (2000).
[519]L. Giacomazzi, L. Martin-Samos, A. Alessi, M. Valant, K. C. Gunturu, A. Boukenter, Y. Ouerdane, S. Girard, and N. Richard, Opt. Mater. Express **8**, 385 (2018).
[520]S. S. Aleshkina, M. E. Likhachev, D. S. Lipatov, O. I. Medvedkov, K. K. Bobkov, and A. N. Guryanov, Proc. SPIE **9728**, 97281C (2016).
[521]S. S. Aleshkina, A. E. Levchenko, O. I. Medvedkov, K. K. Bobkov, M. M. Bubnov, D. S. Lipatov, A. N. Guryanov, and M. E. Likhachev, IEEE Photonics Technol. Lett. **30**, 127 (2018).
[522]Y. Li, K. Peng, H. Zhan, S. Liu, L. Ni, Y. Wang, J. Yu, X. Wang, J. Wang, F. Jing, and A. Lin, Opt. Fiber Technol. **41**, 7 (2018).
[523]F. Beier, C. Hupel, J. Nold, S. Kuhn, S. Hein, J. Ihring, B. Sattler, N. Haarlammert, T. Schreiber, R. Eberhardt, and A. Tünnermann, Opt. Express **24**, 6011 (2016).
[524]H.-J. Otto, N. Modsching, C. Jauregui, J. Limpert, and A. Tünnermann, Opt. Express **23**, 15265 (2015).
[525]B. Ward, Opt. Express **24**, 3488 (2016).
[526]K. K. Bobkov, M. M. Bubnov, S. S. Aleshkina, and M. E. Likhachev, Laser Phys. Lett. **14**, 015102 (2017).
[527]N. Zhao, Y. Liu, M. Li, J. Li, J. Peng, L. Yang, N. Dai, H. Li, and J. Li, Opt. Express **25**, 18191 (2017).
[528]S. Sugiyama, Y. Fujimoto, M. Murakami, H. Nakano, T. Sato, and H. Shiraga, Electron. Lett. **49**, 148 (2013).
[529]Y. Fujimoto, S. Sugiyama, M. Murakami, H. Nakano, T. Sato, and H. Shiraga, *Suppression Mechanism by Ca Additive of Photodarkened Effect in Yb-Doped Silica Glass Fiber*, OSA Technical Digest Series (CLEO, 2013), Paper No. CM4I.6.
[530]Y. Sakaguchi, Y. Fujimoto, M. Masuda, N. Miyanaga, and H. Nakano, J. Non-Cryst. Solids **440**, 85 (2016).
[531]K. Schuster, S. Grimm, A. Kalide, J. Dellith, M. Leich, A. Schwuchow, A. Langner, G. Schötz, and H. Bartelt, Opt. Mater. Express **5**, 887 (2015).
[532]I. Manek-Hönninger, J. Boullet, T. Cardinal, F. Guillen, S. Ermeneux, M. Podgorski, R. Bello Doua, and F. Salin, Opt. Express **15**, 1606 (2007).
[533]R. Piccoli, T. Robin, T. Brand, U. Klotzbach, and S. Taccheo, Opt. Express **22**, 7638 (2014).
[534]H. Gebavi, S. Taccheo, D. Tregoat, A. Monteville, and T. Robin, Opt. Mater. Express **2**, 1286 (2012).
[535]A. Jolly, C. Vinçont, Ch. Pierre, and J. Boullet, Appl. Phys. B **123**, 227 (2017).
[536]G. D. Goodno, L. D. Book, and J. E. Rothenberg, Opt. Lett. **34**, 1204–1206 (2009).
[537]W. S. Brocklesby, A. Mathieu, R. S. Brown, and J. R. Lincoln, Opt. Lett. **18**, 2105 (1993).
[538]G. Frith, A. Carter, B. Samson, J. Faroni, K. Farley, K. Tankala, and G. E. Town, Proc. SPIE **7580**, 75800A (2010).
[539]A. Sincore, J. D. Bradford, J. Cook, L. Shah, and M. C. Richardson, IEEE Sel. Top. Quantum Electron. **24**, 0901808 (2018).
[540]J.-F. Lupi, M. Vermillac, W. Blanc, F. Mady, M. Benabdesselam, B. Dussardier, and D. R. Neuville, Opt. Lett. **41**, 2771 (2016).
[541]J.-F. Lupi, M. Vermillac, W. Blanc, F. Mady, M. Benabdesselam, B. Dussardier, and D. R. Neuville, Opt. Mater. **72**, 106 (2017).
[542]J. E. Townsend, S. B. Poole, and D. Payne, Electron Lett. **23**, 329 (1987).
[543]D. J. DiGiovanni and J. B. MacChesney, "Sol-gel doping of optical fiber preform," U.S. patent 5,123,940 (June 23, 1992).
[544]F. Wu, G. Puc, P. Foy, E. Snitzer, and G. H. Sigel, Mater. Res. Bull. **28**, 637 (1993).
[545]F. Wu, D. Machewirth, E. Snitzer, and G. H. Sigel, J. Mater. Res. **9**, 2703 (1994).
[546]P. A. Tick, N. F. Borrelli, L. K. Cornelius, and M. A. Newhouse, J. Appl. Phys. **78**, 6367 (1995).
[547]B. N. Samson, P. A. Tick, and N. F. Borrelli, Opt. Lett. **26**, 145–147 (2001).
[548]B. N. Samson, L. R. Pinckney, J. Wang, G. H. Beall, and N. F. Borelli, Opt. Lett. **27**, 1309 (2002).
[549]M. J. Dejneka, J. Non-Cryst. Solids **239**, 149 (1998).
[550]M. J. Dejneka, Mater. Res. Soc. Bull. **23**, 57 (1998).
[551]A. Halder, S. K. Bhadra, S. Bysakh, S. M. C. Paul, and S. Das, Curr. Nanosci. **12**, 309 (2016).
[552]A. Dhar, I. Kašík, B. Dussardier, O. Podrazky, and V. Matějec, Int. J. Appl. Ceram. Technol. **9**, 341 (2012).
[553]A. Dhar, S. Das, P. H. Reddy, S. H. Siddiki, D. Dutta, M. Pal, A. V. Kir'yanov, and M. C. Paul, Phys. Status Solidi A. **214**, 1600655 (2017).
[554]J. Mrázek, I. Kašík, J. Boháček, J. Proboštová, J. Aubrecht, O. Podrazký, J. Cajzl, and P. Honzátko, Proc. SPIE **9507**, 950703 (2015).
[555]M. Vermillac, J.-F. Lupi, F. Peters, M. Cabié, P. Vennéguès, C. Kucera, T. Neisius, J. Ballato, and W. Blanc, J Am. Ceram. Soc. **100**, 1814 (2017).
[556]C. Kucera, K. B. Kokuoz, D. Edmondson, D. Griese, M. Miller, A. James, W. Baker, and J. Ballato, Opt. Lett. **34**, 2339 (2009).
[557]T. Lindstrom, E. Garber, D. Edmonson, T. Hawkins, Y. Chen, G. Turri, M. Bass, and J. Ballato, Opt. Mater. Express **2**, 1520 (2012).
[558]K. Schuster, S. Unger, C. Aichele, F. Lindner, S. Grimm, D. Litzkendorf, J. Kobelke, J. Bierlich, K. Wondraczek, and H. Bartelt, Adv. Opt. Technol. **3**, 447 (2014).
[559]M. Cavillon, "Molten core fabrication of intrinsically low nonlinearity glass optical fibers," PhD Dissertation (Clemson University, 2018).
[560]D. Darwich, R. Dauliat, R. Jamier, A. Benoit, J.-L. Auguste, S. Grimm, J. Kobelke, A. Schwuchow, K. Schuster, and P. Roy, "Relevance of the REPUSIL process for the production of LMA thulium-doped fibers," in *Advanced Photonics 2016* (IPR, NOMA, Sensors, Networks, SPPCom, SOF), OSA Technical Digest (online) (Optical Society of America, 2016), Paper No. Tu3D.3.
[561]J. Ballato and E. Snitzer, Appl. Opt. **34**, 6848 (1995).
[562]J. Ballato, C. McMillen, T. W. Hawkins, P. Foy, R. Stolen, R. Rice, L. Zhu, and O. Stafsudd, Opt. Mater. Express **2**, 153 (2012).
[563]J. Ballato, T. W. Hawkins, P. Foy, B. Yazgan-Kokuoz, C. McMillen, L. Burka, S. Morris, R. Stolen, and R. Rice, Opt. Fiber Technol. **16**, 399 (2010).
[564]A. C. Peacock, U. J. Gibson, and J. Ballato, Adv. Phys. X **1**, 114 (2016).
[565]E. M. Dianov, Proc. SPIE **8601**, 86010H (2013).
[566]M. A. Melkumov, V. Mikhailov, A. M. Hegai, K. I. Riumkin, P. S. Westbrook, D. J. DiGiovanni, and E. M. Dianov, Electron. Lett. **53**, 1661 (2017).